

AD-A069 726

EXTRANUCLEAR LABS INC PITTSBURGH PA

F/G 14/2

STUDIES OF THE BALLOON-BORNE MASS SPECTROMETER PROBLEM. (U)

AUG 78 M W SIEGEL, W L FITE

F19628-77-C-0183

UNCLASSIFIED

AFGL-TR-78-0220

NL

1 OF 2

AD A069726



LEVEL

9/2

AFGL-TR-78-0220

STUDIES OF THE BALLOON-BORNE MASS SPECTROMETER PROBLEM

M. W. Siegel
W. L. Fite

Extranuclear Laboratories, Inc.
P.O. Box 11512
250 Alpha Drive
Pittsburgh, PA 15238

August 30, 1978

Final Report
1 July 1977 - 30 August 1978

DDC
RECEIVED
JUN 12 1979
C

Approved for public release; distribution unlimited.

DDC FILE COPY

AD A 069726

AIR FORCE GEOPHYSICS LABORATORY
AIR FORCE SYSTEMS COMMAND
UNITED STATES AIR FORCE
HANSCOM AFB, MASSACHUSETTS 01731

79 06 11 006

Qualified requestors may obtain additional copies from the Defense Documentation Center. All others should apply to the National Technical Information Service.

REPORT DOCUMENTATION PAGE		READ INSTRUCTIONS BEFORE COMPLETING FORM
1. REPORT NUMBER (18) AFGL-TR-78-0220 ✓	2. GOVT ACCESSION NO.	3. RECIPIENT'S CATALOG NUMBER (9)
4. TITLE (and Subtitle) (6) Studies of the Balloon-Borne Mass Spectrometer Problem.	5. TYPE OF REPORT & PERIOD COVERED Scientific - Final rept. 1 Jul 1977-30 Aug 1978.	
7. AUTHOR(s) (10) M.W./Siegel, W.L./Fite	8. CONTRACT OR GRANT NUMBER(s) (15) F19628-77-C-0183 <i>new</i>	
9. PERFORMING ORGANIZATION NAME AND ADDRESS Extranuclear Laboratories, Inc. P.O. Box 11512 (250 Alpha Drive) Pittsburgh, PA 15238	10. PROGRAM ELEMENT, PROJECT, TASK AREA & WORK UNIT NUMBERS (16) 6210JF (17) 03 (16) 66870240	
11. CONTROLLING OFFICE NAME AND ADDRESS Air Force Geophysics Laboratory Hanscom AFB, MA 01730 Contract Monitor: Mr. Alan D. Bailey/LKB	12. REPORT DATE (11) 30 Aug 1978	
14. MONITORING AGENCY NAME & ADDRESS (if different from Controlling Office)	13. NUMBER OF PAGES (12) 127 p.	
	15. SECURITY CLASS. (of this report) Unclassified	
15a. DECLASSIFICATION/DOWNGRADING SCHEDULE		
16. DISTRIBUTION STATEMENT (of this Report) Approved for public release; distribution unlimited.		
17. DISTRIBUTION STATEMENT (of the abstract entered in Block 20, if different from Report)		
18. SUPPLEMENTARY NOTES		
19. KEY WORDS (Continue on reverse side if necessary and identify by block number) Ion Sampling Stratosphere Positive Ions Balloon Negative Ions Mass Spectrometer		
20. ABSTRACT (Continue on reverse side if necessary and identify by block number) The project involved theoretical studies of the ion sampling problem for balloon-borne mass spectrometric apparatus in the stratosphere, manufacturing of standard, special, and prototype apparatus, construction of a vacuum system and ancillary apparatus for testing and experimentation, and described experimental work. Appendices to the report include a literature survey and instructions for the deliverable manufactured items.		

388370

Smec

CONTENTS

		<u>Page</u>
Section -	Report Documentation Page	i
-	Table of Contents	1
-	List of Figures	2
I	Introduction	3
II	Cumulative Narrative Recapitulation	5
III	Apparatus and Experiment Design Considerations	7
IV	The Mass Spectrometer and Ion Optics	55
V	Ancillary Apparatus	77
VI	Experimental Program and Results	94
VII	Conclusion and Recommendations	114
	References 1-28	117
	Appendix I: Deliverable Items	118
	Appendix II: Literature Search (Annotated Bibliography)	121

Accession For	
NTIS GRA&I	<input checked="" type="checkbox"/>
DDC TAB	<input type="checkbox"/>
Unannounced	<input type="checkbox"/>
Justification	<input type="checkbox"/>
By _____	
Distribution/	
Availability Codes	
Dist	Avail and/or special
A	

FIGURES

		<u>Page</u>
FIGURE 1.	Probe Characteristic in Classical Plasma . . .	14
2.	Probe Characteristic in Negative Ion Dominated Plasma	18
3.	Electric Field, Charge Density, and Current Density.	22
4.	Resistive Disk Ion Optical Elements.	45
5.	Two Dimensional Model of Resistive Disk. . .	49
6.	Electric Field near Conducting and Resistive Surfaces	53
7.	Vacuum System (Mechanical)	56
8.	Vacuum System (Schematic).	58
9.	RF Feedthrough for use at approximately one torr	60
10.	Perfluorotributylamine Test Spectrum	63
11.	Resolved and Integral Spectral Mode Test Spectra.	65
12.	Transmission vs. Resolution: Data	67
13.	Transmission vs. Resolution: Graph.	70
14.	API Spectrum	72
15.	Microwave Discharge Spectrum	74
16.	API Source Assembly (Mechanical)	78
17.	Corona Discharge Source (Schematic).	81
18.	Estimated Ion Density vs. Position	84
19.	External Ion Collection Array.	86
20.	Potentials for External Ion Collection Array	89
21.	"Outside" Movable Langmuir Probe	92
22.	Pressure, Density, Temperature vs. Altitude.	95
23.	Aperture Diameter vs. Pressure and Altitude.	97
24.	Inside vs. Outside Pressure.	100
25.	Mass Spectrum with Prototype External Array.	103
26.	Mass Spectrum of Corona Discharge Source . .	106
27.	"Outside" Probe Characteristic	109
28.	"Inside" Probe Characteristic.	111

I - INTRODUCTION

This contract involved five interrelated technical tasks:

(1) a theoretical study and literature search to characterize the atmospheric ion sampling problem;

(2) modification and augmentation of one of EL's existing vacuum chambers to make it suitable for experimental studies to further characterize the stratospheric ion sampling problem;

(3) construction of specially modified items in EL's normal product line, for use in connection with the experimental studies, and for eventual delivery to AFGL:

(4) construction of prototype items for use in connection with the experimental studies, and where suitable, for delivery to AFGL;

(5) additional experimental studies aimed at studying optimization of the function of deliverable items as they might be incorporated in an AFGL planned flight package.

Because of the intimate way in which theoretical studies, experimental studies, manufacturing, prototype development, and optimization tests are interwoven in this project, this report (with appropriate appendices) will also serve as an instruction manual for the specialized delivered apparatus. Appendix I lists the delivered items and provides a brief description of each in reference to EL's standard instruction manuals and drawing numbers.

II - CUMULATIVE NARRATIVE RECAPITULATION

The following section summarizes information provided in previous reports connected with this contract. These consist of Status Report #1, covering the period July 1 through September 30, 1977 and Design Evaluation Report #1, covering the period July 1 through November 30, 1977.

The objectives of the contracted work were summarized as:

To identify and quantify the sampling problems predictably attendant to the sampling of ambient ions in the stratosphere using balloon-borne mass spectrometric apparatus. To establish design criteria and parameters for such apparatus. To design and fabricate a test facility for such apparatus, including ion collection array (if desirable) with in-flight ionizer for stratospheric neutral species, sampling aperture mechanism, ion focusing lens, and quadrupole mass filter with entrance fringe field separation device (ELFS).

The literature survey was undertaken, with the conclusion that the best information available on these subjects usually traces back to the AFGL effort. Where non-AFGL workers are involved, they seem to have excellent professional communications with the AFGL group, as evidenced by the fact that several times during the course of the contract we were provided with preprints of forthcoming articles which had been sent to AFGL long before they would have been available to us in the journals. Thus we feel the literature survey will be of little additional value to AFGL, except insofar as it confirms that AFGL is already well informed on the subject. Furthermore, the information collected was of only minimal value to EL in its performance. Most of the relevant theoretical considerations in the literature appear to have ignored parameter regimes of stratospheric interest. These considerations were taken up, to the best of our ability, by EL personnel and reported in the Design Evaluation Report. Appendix II is an Annotated Bibliography summarizing the results of the literature survey.

The Design Evaluation Report is summarized as follows:

The test facility and program are described by brief discussion and supported by schematic diagrams, block diagrams, photographs and design drawings. Assumptions concerning the neutral constituents and expected absolute ionization levels in the altitude range of interest are explicitly stated. Charged particle dynamics and general considerations of sampling in a sheathless plasma are reviewed from an intuitive point of view. A more formal review of classical plasma physics and probe characteristics is then given, and is followed by an approximate formal treatment considering modifications due to collisions in the sheath. It is concluded that under the anticipated conditions approximately equal diffusion currents of positive and negative ions, $j_+ \sim e D^{1/2} R^{3/2} n_0^{3/2}$ (where D is the mean diffusion constant characteristic of ions, R is the recombination rate, and n_0 is the ion density far from the probe), reach the instrument surface, and a small conduction current component proportional to the difference in positive and negative ion mobilities adds to or subtracts from the diffusion current to make the net signed current to the floating package equal zero. The ion current through a sampling aperture is shown to be larger due to ion trapping by the bulk gas flow. Modifications to this treatment due to balloon package charging or an external ion collection array are treated, and it is shown that since strong fields can decouple ion motion from the bulk gas flow, the net effect of an external ion collection array is not expected to be a dramatic improvement. The likelihood of balloon charging due to photoelectron emission is considered, and shown to be a significant possibility at upper stratosphere altitudes. The magnitude of the possible effect is estimated, and its importance evaluated in different configurations. Possible countermeasures to unwanted charging are considered. In an Appendix design considerations for an external ion collection device are discussed.

III - APPARATUS AND EXPERIMENT DESIGN CONSIDERATIONS

The material in Section III is comprised of relevant sections of the previously referenced and summarized Design Evaluation Report, edited to conform to the format of this Final Report, and with redundant information omitted for brevity.

1. Assumptions

Ion sampling is to be attempted in the stratosphere, defined as the altitude range 20-40 Km. The corresponding pressure range is approximately 38-0.61 torr. The pressure at the middle of this range (35 Km) is approximately 7.3 torr, with a corresponding mean-free-path for neutral molecules of 1.5×10^{-3} cm. Where "typical" values must be assumed, 35 Km values will be used. The temperature in this altitude range is only slowly varying, between about 215 K and 270 K, and the 35 Km value of 240 K is assumed. The corresponding neutral particle density is approximately 1.6×10^{17} cm⁻³. Reference 1 is a convenient source of this data. Figure 22 presents this information in graphical form.

In this altitude regime, the relative concentrations of the major neutral components N₂, O₂, Ar, CO₂ are substantially the same as at ground level. H₂O and He are present at about the 6 ppm level. The concentrations of atomic oxygen, NO, and O₂ (A ¹Δ_g) may increase with altitude by several orders of magnitude in the 20-50 Km range, but even at the upper end none exceeds 1 ppm. During the day ozone peaks at about 10 ppm at about 35 Km, dropping off by a factor of three towards 50 Km, and we assume a similar drop toward 20 Km.

The thermal electron concentration is essentially zero: all electrons released by ion pair producing radiation rapidly attach to form negative ions. According to information provided by AFGL, expected total ion concentrations (of either sign) are of the order of 10⁴ cm⁻³(2). Other authors report lower values, i.e., 10³ or even 10² cm⁻³(3).

2. Charged Particle Dynamics

In a bulk medium (such as the stratosphere) in which ionization is occurring, at equilibrium we can expect to find essentially equal concentrations of positive ions and electrons plus negative ions. The spatial

extent over which significant departures from net charge neutrality can occur is given by the Debye length*

$$\lambda = \sqrt{\frac{\epsilon_0 kT}{ne^2}}$$

where n is the charge density of either sign.

The Debye length at temperatures and ion densities of interest is the order of 1-10 cm, and is thus large compared with sampling aperture sizes, but small compared with the balloon and instrument package. This means that under some circumstances sampled ions may not be characteristic of the bulk medium, a situation to be avoided.

Equilibrium requires that the net current to the entire floating package must be zero, for were this not the case charge would be accumulating and equilibrium would not then exist. When a floating probe is immersed in a plasma dominated by positive ions and electrons, equilibrium is attained when the probe acquires sufficient negative charge that at the surface the (reduced) diffusion velocity of the electrons equals the (increased) diffusion velocity of the positive ions. Under these circumstances, the sampling of positive ions will be enhanced, and the sampling of negative ions impeded; furthermore the ions, sampled from the positive ion-rich plasma sheath, might not be characteristic of the bulk medium. On the other hand, in the stratospheric plasma, characterized by equal concentrations of positive and negative ions (assumed for the time being of equal mobility), there is no net charge accumulation, no sheath, and no sampling bias. Identifying the factors which detract from the exactness of this last statement, and finding techniques for compensating for them, is one goal of this work.

3. General Considerations of Sampling in a Sheathless Plasma

Primary ionization due to cosmic rays, solar ultraviolet, etc., will yield mostly N_2^+ , O_2^+ , N^+ , O^+ , and low energy (few eV) electrons.

*Some definitions of the Debye length have a somewhat different constant multiplier, but we are concerned with the order of magnitude only. See Reference 4.

Ion-molecule reactions, with rate constants as high as several times $10^{-9} \text{ cm}^3 \text{ sec}^{-1}$, at the ambient neutral particle densities of several times 10^{17} cm^{-3} , will lead to terminal positive ions within a few times 10^{-8} sec when major neutral species are involved, and correspondingly longer when trace neutral species are involved; however, even when trace species at the part-per-billion level are important, terminal reactions will occur within the order of 1 second.

Similarly, the electrons produced by primary ionization will be rapidly thermalized and attached to form terminal negative ions. The details depend on the details of the secondary electron energy spectrum, which in turn depends on the primary ionization mechanisms. Nevertheless, order-of-magnitude estimates are straightforward. The slowest processes are of greatest relevance to the following discussion; electrons above a few eV can participate in dissociative attachment processes and can be rapidly lost. Slower electrons ($\sim 1 \text{ eV}$) must be thermalized before they can be lost by three-body attachment.

The order-of-magnitude of the thermalization time is estimated as follows. Assuming thermalization proceeds by elastic collisions, the electron energy is degraded approximately as⁽⁵⁾

$$E_n = E_0 \left(1 - \frac{2m}{M}\right)^n$$

where E_n is the electron energy after n collisions, E_0 is the initial energy, and m and M are the electron and gas molecule masses. To degrade the electron energy by a factor of 50 (from 1 eV to thermal) in air ($M \sim 30$) requires

$$n \approx \frac{\ln \frac{E}{E_0}}{\ln \left(1 - \frac{2m}{M}\right)}$$

The mean time required for n collisions is

$$t_n \approx \sqrt{\frac{m}{2}} \sum_{i=0}^n \frac{\lambda_i}{E_i^{1/2}}$$

where λ_i is the mean free path for electrons of energy E_i . To the extent that λ_e , this electron mean free path, can be taken as constant, i.e., to

the extent that the elastic cross section is energy independent between thermal energy and about 1 eV, the sum is given by

$$t_n = \lambda_e \sqrt{\frac{m}{2}} \frac{1}{E_0^{1/2}} \frac{1 - \alpha^{n+1}}{1 - \alpha}$$

where $\alpha = (1 - \frac{2m}{M})^{-1/2}$. The relevant cross sections for air are the order of 10^{-15} cm², so at a density of 1.5×10^{17} cm⁻³ we have

$$\lambda_e = \frac{1}{n\sigma} \approx 6.6 \times 10^{-3} \text{ cm}$$

and

$$\frac{1 - \alpha^{n+1}}{1 - \alpha} \approx 2.8 \times 10^5$$

giving

$$t_n \approx 3 \times 10^{-5} \text{ sec}$$

Rate constants for three body attachment of thermal electrons are the order of 10^{-30} cm⁶ sec⁻¹(6), which at the ambient density give a thermal electron lifetime of the order of 4×10^{-5} sec, so a few times 10^{-4} is an upper bound on the lifetime of an electron produced by primary ionization. Terminal negative ions will then be reached with rate constants characteristic of ion-molecule reactions, i.e., 10^{-9} cm³ sec⁻¹, and as in the case of positive ions the time scale will be of the order of 1 second if the terminal ions are due to part-per-billion trace species and much faster for major species.

In contrast to these time scales, we need to consider the lifetimes of terminal ions against loss by recombination, and by diffusion to nearby surfaces, e.g., the instrument package. The relationship between the primary ionization rate (S ion pair $\text{cm}^{-3} \text{sec}^{-1}$), the rate constant for recombination ($R \sim 10^{-7}$ cm³ sec⁻¹ typically)(7), and the negative and positive ion densities ($n_+ = n_- \equiv n_0$) in the bulk of the stratosphere is

$$\frac{dn_0}{dt} = 0 = S - Rn_0^2$$

For n_0 in the range of $10^2 - 10^4 \text{ cm}^{-3}$ (the upper end of this range corresponding to ion densities expected by AFGL), it follows that the primary ionization rate is in the range 10^{-3} to $10 \text{ cm}^{-3} \text{ sec}^{-1}$. Because of the square root relationship between ion density and ionization rate in a recombination-limited situation, large changes in S produce relatively small changes in n_0 .

The time scale for recombination is given by

$$\tau_R = (n_0 R)^{-1}$$

with a range of 10^5 to 10^3 for n_0 in the range 10^2 to 10^4 cm^{-3} . Because these times are long with respect to estimated times for obtaining terminal ions it follows that the vast majority of ions in the stratosphere will be the terminal ions characteristic of the neutral gas mixture, irrespective of the actual degree of ionization.

This does not necessarily mean that sampled ions will be representative of the bulk, however; if there is a strong bias towards observing ions produced very near the instrument, then sampling may yield ion spectra characteristic of a too-early stage of the ion-molecule reaction sequence. We now show that this is not the case, i.e., that we can in principle expect to obtain a valid sample. To do this, we need to consider the time scale characteristic of diffusion.

The diffusion constant ($D \approx \lambda v/3$)⁽⁸⁾ for ions at the altitude of interest will be of the order of $5 \text{ cm}^2/\text{sec}$, and the corresponding diffusion time associated with distance ℓ will be

$$\tau_D = \frac{\ell^2}{D}$$

Ions will thus be observed from distances such that $\tau_D \lesssim \tau_R$; ions produced at greater distances from the sampling device will tend to be lost to recombination before they can be collected. If we choose the value $\tau_D \approx \tau_R \approx 10^3 \text{ sec}$, corresponding to $n_0 \approx 10^4 \text{ cm}^{-3}$, we obtain

$$\ell \approx 70 \text{ cm}$$

Two points are apparent: the distance is a "comfortable" one, in that it indicates good altitude resolution can be expected, and on the other hand is sufficiently small for the time involved (70 cm/1000 sec = 0.7 mm/sec) that the air speed will presumably wash out any very local fluctuations. Furthermore, a majority of the ions sampled will come from spatial regions far enough from the instrument that problems due to normal outgassing should not be too severe.

It is of interest to compare the distance-of-origin weighting function for this diffusion and recombination limited case to the corresponding weighting under collisionless conditions such as those prevalent at high satellite altitudes. Under collisionless conditions, a source volume element contribute ion current to a sampling aperture as the inverse square of the distance to that element (a solid angle consideration), while the volume of a shell of any given thickness increases as the square of the distance from the sampling aperture. These two effects thus cancel, and in purely collisionless sampling, ions are observed with equal weight from all distances. In contrast, under the present circumstances, current originating in a given volume element is attenuated by recombination as $\exp(-t/\tau_R)$, where t is the time an ion requires to travel from its origin to the sampling aperture. Since $t = \ell^2/D$, we have

$$P(\ell) = \text{const} \times e^{-\ell^2/D\tau_R}$$

where the constant provides the required normalization. There is thus a gaussian distance weighting, with 68% of the observed ions originating within distance

$$\ell_0 = \sqrt{D\tau_R} = \sqrt{\frac{D}{n_0 R}} \approx 70 \text{ cm}$$

of the sampling aperture.

Finally, it is of interest to inquire as to what fraction of the ions are likely to be non-terminal, i.e., ions which are born so close

to the sampling aperture that they reach it before the ion-molecule reaction chain is complete. Certainly, from considerations given above, 1 second is adequate for terminal ions due to part-per-billion impurities. In such a case

$$\ell_{\min}^2 = D \times 1 \text{ sec} \approx 5 \text{ cm}^2$$

$$\ell_{\min} \approx 2.2 \text{ cm}$$

From standard error function tables, we determine that in this case about 2.4% of the collected ions originate within the hemisphere of radius ℓ_{\min} , or 97.6% of the collected ions may be assumed to be terminal ions.

4. Review of Plasma Physics and Probe Characteristics

The following discussion is definitely inappropriate to the balloon/stratosphere problem, in that it makes the following assumptions:⁽⁹⁾

1. The probe dimensions are much smaller than the mean free path of the plasma particles (the mean free path for ions will be $\approx 1 \mu\text{m}$, small even compared with the aperture dimension);
2. The sheath thickness is much less than the probe dimensions (the sheath thickness, $\approx 10 \text{ cm}$, is fairly small compared to the dimensions of the entire balloon and instrument package, but is not small compared to relevant dimensions of the sampling apparatus).

The theory, however, is simple and well developed for these conditions, so we present the "classical" picture first, and use it as a starting point for further discussion.

If a probe is immersed in this conventional positive ion-electron plasma, the current-voltage characteristic is as represented in Figure 1. For explanatory purposes some simplifications have been made, e.g., complete saturation is never actually attained, but this picture is adequate for our purposes. Since the net current to a floating probe (such as the balloon and instrument package) is zero, the potential at which the probe current is zero is referred to as the floating potential, ϕ_f .

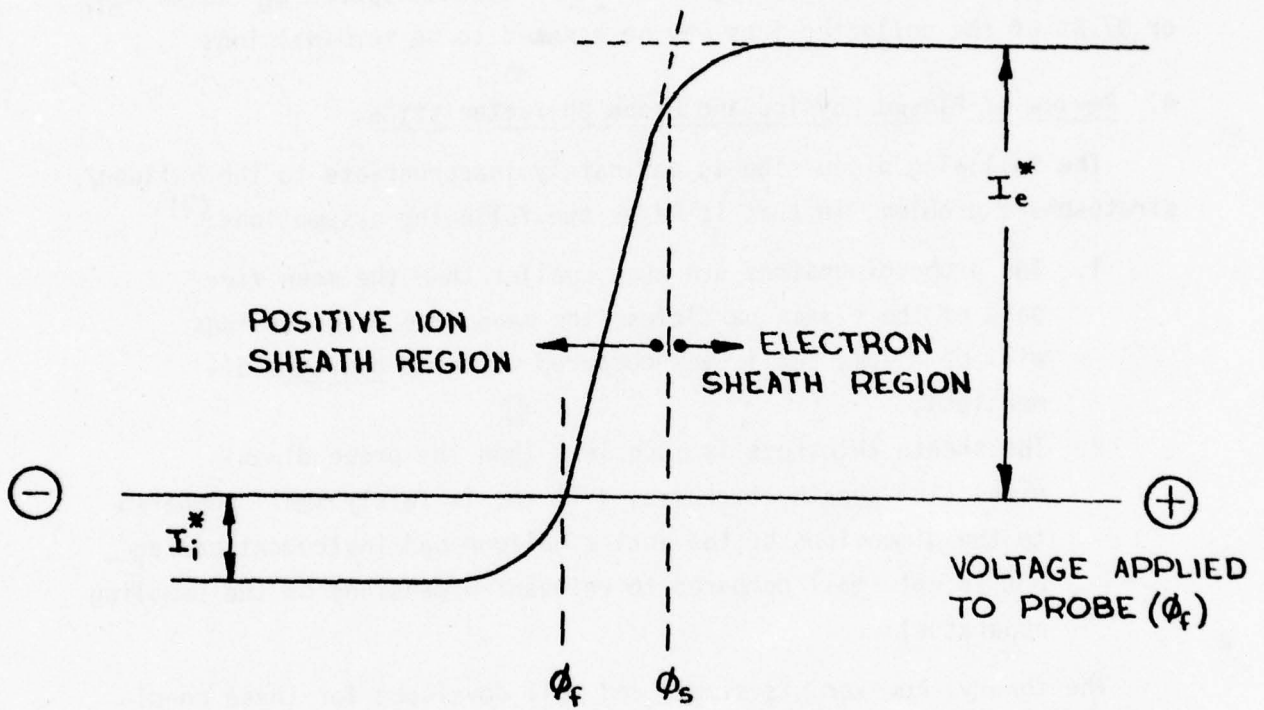


FIGURE 1

Figure 1: Probe Characteristic in Classical Plasma

A schematic representation of probe current versus applied voltage in an electron-dominated plasma. I_e^+ and I_i^+ represent the saturation currents of electrons and positive ions; ϕ_f is the "floating" potential, i.e., the potential which an isolated probe will eventually acquire; ϕ_s is the "plasma" or "space" potential, at which the net current is $I_e^* - I_i^*$, i.e., both ions and electrons reach the surface with their thermal velocities. The floating probe is surrounded by a positive ion sheath.

At sufficiently negative probe voltages, collected current is due primarily to positive ions, and the saturation current is given by

$$I_i^* = Aen\bar{c}_i/4$$

where A is the probe area, e the electron charge, n the bulk charge density of either sign, and $\bar{c}_i = (8kT/\pi m_i)^{1/2}$ is the mean thermal speed (relative to any mass velocity of the flow) of ions of mass m_i . When ions of more than one mass are present, appropriate summation is of course required.

At sufficiently positive probe voltages, collected current is due primarily to electrons, and the saturation current is similarly given by

$$I_e^* = Aen\bar{c}_e/4$$

with similar definitions of the terms.

The qualifier "primarily" appears in both of the above definitions because in the high energy tail of the Maxwell velocity distribution there are always some particles which can overcome any retarding potential.

The extrapolated potential ϕ_s in Figure 1 is referred to as the plasma potential or space potential. At this potential ions and electrons reach the probe unimpeded, the excess of electron current being due to the higher thermal velocity of electrons. Clearly the net current collected at potential ϕ_s is

$$I(\phi_s) = I_e^* - I_i^*$$

which by convention is positive when electrons are collected.

If $\phi_p < \phi_s$, the probe must be surrounded by an electron sheath. This is just a consequence of Gauss' Law. In the sheath, which represents a transition region between the probe potential ϕ_p and the space potential ϕ_s , there must be an electric field of such sign as to repel electrons when $\phi_p < \phi_s$, and to repel positive ions when $\phi_p > \phi_s$. The functional form of the electric field strength vs distance from the

probe is not easy to calculate, but its spatial extent is always of the order of the Debye length. Taking too local a point of view of this situation can lead to confusion: the existence of a positive ion sheath is sometimes misconstrued by beginning students as implying that electrons will be attracted rather than repelled, whereas in reality the positive ion sheath is the result of an electric field which attracts positive ions and repels electrons.

Consider now a positive ion-negative ion plasma (with essentially no free electrons) and only one species of positive ion, characterized by m_+ and one species of negative ion, characterized by m_- . As sketched in Figure 6, there are now saturation currents.

$$I_+^* = Aen\bar{c}_+/4$$

and

$$I_-^* = Aen\bar{c}_-/4$$

which in this case are comparable, since m_+ and m_- are comparable, and much smaller than I_e^* in the previous example. In Figure 2 we show the situation for $m_+ < m_-$, so the space potential is below the floating potential, and a floating probe will be surrounded by a negative ion sheath (in contrast to the positive ion sheath surrounding a floating probe in an electron dominated plasma).

In this case the spatial extent of the sheath is still the Debye length, but the potential difference ($\phi_f - \phi_s$) is small, so the electric field strength is correspondingly small.

While the details of the derivation are beyond the scope of this work, the well known result is⁽⁹⁾

$$\phi_s - \phi_f = \frac{kT}{e} \ln \frac{I_e^*}{I_i^*} = \frac{kT}{2e} \ln \frac{m_i}{m_e}$$

in the electron dominated case or

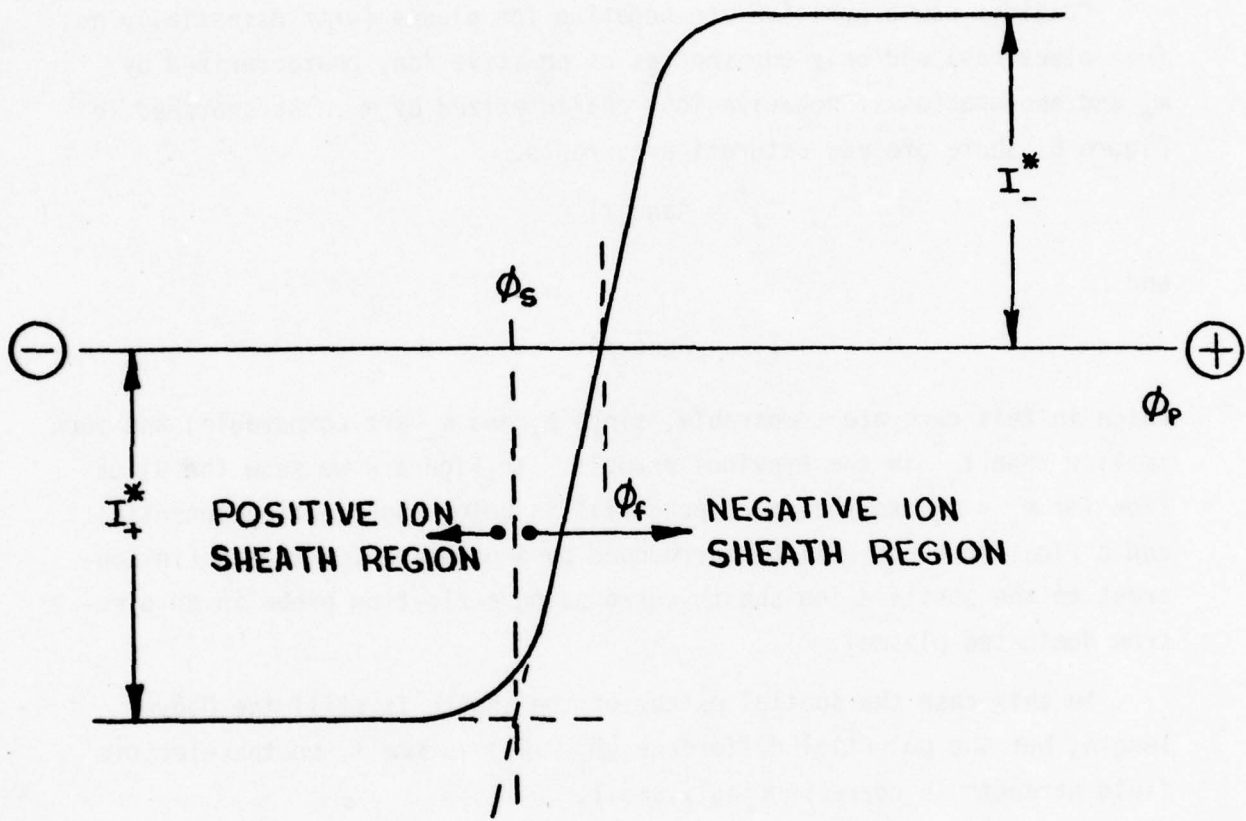


FIGURE 2

Figure 2: Probe Characteristic in Negative Ion Dominated Plasma

Defined quantities are analogous to Figure 1, but I_+^* and I_-^* are comparable, in contrast to $I_i^* \ll I_e^*$; the small difference between ion currents is due to differing mobilities, and whether I_+^* or I_-^* is larger depends on the ion species involved; in this example I_+^* is the larger, and the floating probe is surrounded by a negative ion sheath.

$$\phi_s - \phi_f = \frac{kT}{e} \ln \frac{I_-^*}{I_+^*} = \frac{kT}{2e} \ln \frac{m_+}{m_-}$$

in the negative ion dominated case.

Putting in typical numbers, it is easily seen that in the electron dominated case, for $m_i \approx 50$, $(\phi_s - \phi_f) \approx +6 kT \approx +0.15$ volt, whereas in the negative ion case with say a factor of two difference in m_+ and m_- , $\{\phi_s - \phi_f\} \approx 0.3 kT \approx 0.0008$ volt.

Extension of this treatment to include several ion species of each sign is clearly straightforward.

5. Modifications Due to Collisions

As was mentioned at the outset, the treatment of the previous section assumes that the mean free path of ions is large compared to the Debye length, and we know this will not be the case in the stratosphere. Unfortunately probe theory is not so well developed in the relevant case, and we must proceed largely on the basis of our own intuition.

If the sampling aperture is imbedded in a surface whose radius of curvature and linear extent are fairly large compared to the Debye length, we can approach the problem in a planar geometry. In the discussion below we adopt the normal sign convention for currents, i.e., positive current is the direction of positive ion motion, and opposite to the direction of negative ion motion.

Consider a plasma of one species each of positive and negative ions; if an initially uncharged object is immersed in this plasma, one or the other species (say the positive ions) may at first diffuse to it preferentially, imparting (in this case) a positive charge whose field then decreases the rate of collection of positive ions and increases the rate of collection of negative ions until, in the steady state, equal fluxes of positive and negative ions reach the object. The two current components are then

$$j_+ = e\mu_+ E n_+ - e D_+ \frac{dn_+}{dz}$$

and

$$j_- = e\mu_- E n_- + eD_- \frac{dn_-}{dz}$$

The choice of signs in these equations is made clear by reference to Figure 3. The charge densities $n_+(z)$ and $n_-(z)$ both approach n_0 at large values of z , and j_+ , j_- , and E are all zero there. At $z = 0$, j_+ is negative and j_- is positive, meaning ions of both signs enter the surface; at large z both currents approach zero. Furthermore at $z = 0$ we know $j_+ + j_- = 0$.

Conservation of charge requires that the continuity equations

$$\nabla \cdot j_+ = \frac{dj_+}{dz} = eS - eRn_+n_-$$

and

$$\nabla \cdot j_- = \frac{dj_-}{dz} = -eS + eRn_+n_-$$

hold everywhere, and by adding these we obtain

$$\nabla \cdot (j_+ + j_-) = 0 \text{ or } j_+ + j_- = \text{constant}$$

everywhere. It follows that $j_+ + j_- = 0$ everywhere, since it is zero at $z = 0$ and at large values of z , and has zero derivative.

By noting that Gauss' Law, $\nabla \cdot D = \rho$, requires

$$\frac{dE}{dz} = \frac{e(n_+ - n_-)}{\epsilon_0}$$

and by making use of the Einstein Relation⁽¹⁰⁾

$$D = \frac{\mu kT}{e}$$

we can write two coupled integro-differential equations in the functions n_+ and n_- :

$$-\frac{\epsilon_0 kT}{e^2} n_+'' + n_+' \int_0^z (n_+ - n_-) dz + (n_+ - n_-) n_+ = \frac{\epsilon_0}{e\mu_+} (S - Rn_+n_-)$$

$$-\frac{\epsilon_0 kT}{e^2} n_-'' + n_-' \int_0^z (n_+ - n_-) dz - (n_+ - n_-) n_- = \frac{\epsilon_0}{e\mu_-} (S - Rn_+n_-)$$

where the prime indicates differentiation with respect to z .

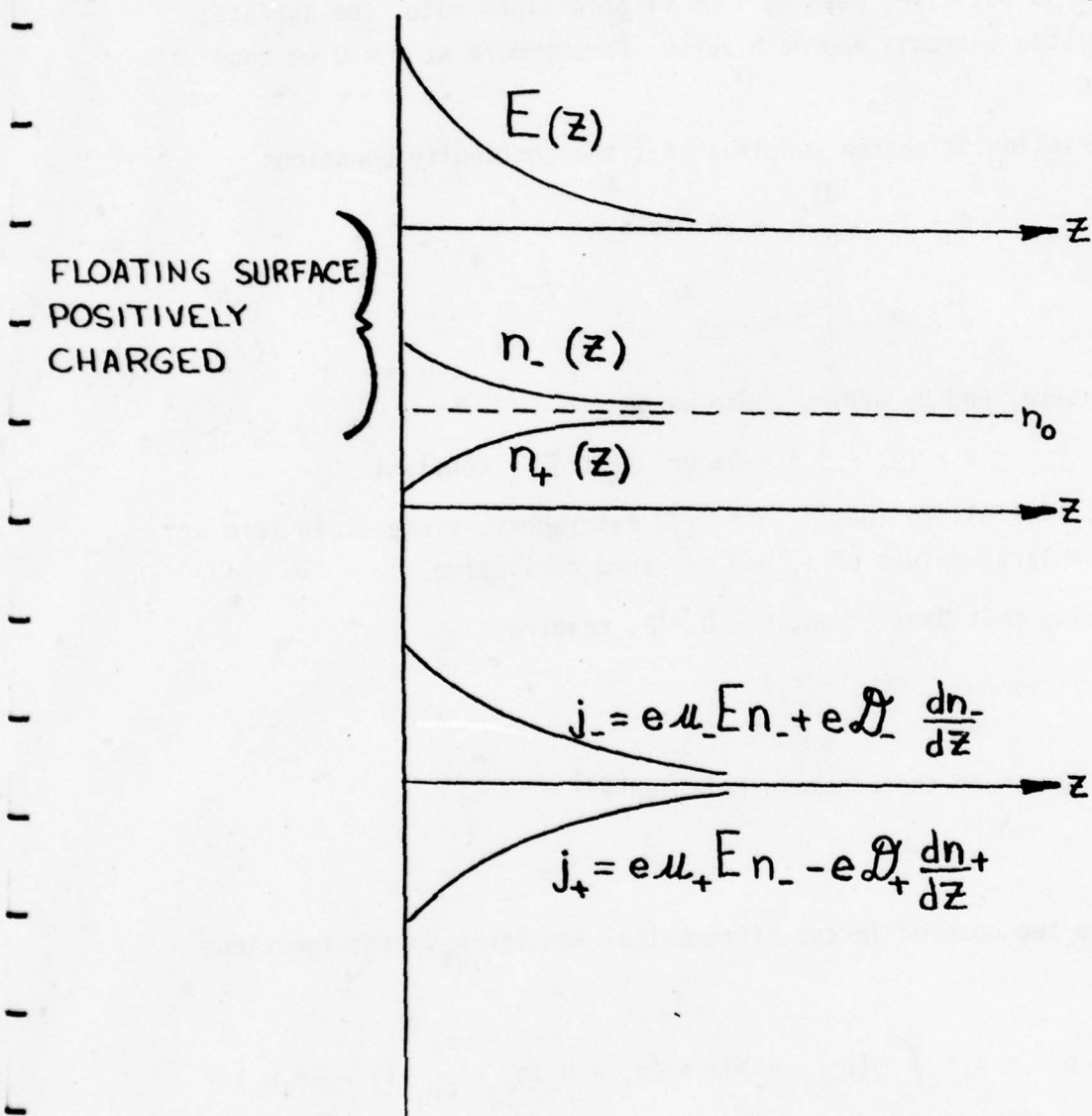


FIGURE 3

Figure 3: Electric Field, Charge Density, and Current Density

Adjacent to a plasma boundary wall, an electric field results in a charge imbalance whose sign is appropriate to impede the charge carriers with the higher thermal speed. This figure serves to define the sign conventions used in the rate equations developed in the text.

If both equations are divided through by n_0^2 , then the Debye length

$$\lambda = \sqrt{\frac{\epsilon_0 kT}{e^2 n_0}}$$

appears as a characteristic length for the problem, and the equations can be written in a dimensionless form

$$-\lambda^2 \alpha_+'' + \alpha_+' \int_0^z (\alpha_+ - \alpha_-) dz + (\alpha_+ - \alpha_-) \alpha_+ = \frac{\epsilon_0}{e \mu_+ n_0^2} (S - R n_+ n_-)$$

$$-\lambda^2 \alpha_-'' - \alpha_-' \int_0^z (\alpha_+ - \alpha_-) dz - (\alpha_+ - \alpha_-) \alpha_- = \frac{\epsilon_0}{e \mu_- n_0^2} (S - R n_+ n_-)$$

where

$$\alpha_+ = \frac{n_+}{n_0} \quad \text{and} \quad \alpha_- = \frac{n_-}{n_0}$$

If we write

$$n_+ = n_0 (1 - f)$$

and

$$n_- = n_0 (1 + g)$$

where f and g are dimensionless functions of z , then by noting

$$S = n_0^2 R$$

we obtain some simplification on the right hand side:

$$\lambda^2 f'' + f' \int_0^z (f+g) dz - (f+g)(1-f) = \frac{\epsilon_0 R}{e \mu_+} (f - g + fg)$$

$$-\lambda^2 g'' + g' \int_0^z (f+g) dz + (f+g)(1+g) = \frac{\epsilon_0 R}{e \mu_-} (f - g + fg)$$

Since we expect the positive and negative ion mobilities to be comparable, it is useful to define a mean mobility μ and a small parameter δ by

$$\frac{1}{\mu_+} = \frac{1-\delta}{\mu} \quad \text{and} \quad \frac{1}{\mu_-} = \frac{1+\delta}{\mu}$$

Then by forming the sum and difference of the two equations we obtain

$$\lambda^2(f'' - g'') + (f' + g') \int_0^z (f+g) dz + (f+g)^2 = \frac{2\epsilon_0 R}{\mu e} (f - g - fg)$$

$$\lambda^2(f'' + g'') + (f' - g') \int_0^z (f+g) dz + (f-g)^2 = -\frac{2\delta}{\mu} \frac{\epsilon_0 R}{e} (f - g + fg)$$

By defining

$$x = f + g \quad \text{and} \quad y = f - g$$

so

$$fg = \frac{x^2 - y^2}{4}$$

and

$$f = \frac{x + y}{2} \quad \text{and} \quad g = \frac{x - y}{2}$$

we obtain

$$\lambda^2 y'' + x' \int_0^z x dz = \frac{2}{\mu} \frac{\epsilon_0 R}{e} \left(y + \frac{x^2}{4} - \frac{y^2}{4} \right) - x^2$$

$$\lambda^2 x'' + y' \int_0^z x dz = -\frac{2\delta}{\mu} \frac{\epsilon_0 R}{e} \left(y + \frac{x^2}{4} - \frac{y^2}{4} \right) + 2x - xy$$

In the limiting case of equal mobilities ($\delta = 0$), we require equal densities n_+ and n_- at all locations (not just in the bulk), i.e.,

$$f = -g \quad f + g = x = 0$$

in which case the two equations become

$$\lambda^2 y'' = \frac{2}{\mu} \frac{\epsilon_0 R}{e} \left(y - \frac{y^2}{4} \right)$$

and

$$0 = 0$$

The nontrivial equation is now a familiar one, immediately recognized (by analogy with the anharmonic oscillator problem) as having no analytical solution. But as long as we can reasonably expect y to be small (the conditions for validity of this expectation will be discussed below), the solution is obtained by inspection:

$$y = A \exp\left(-\sqrt{\frac{2Rn_0 e}{\mu kT}} z\right)$$

where the scaling length in the exponent is obtained from

$$\frac{2\epsilon_0 R}{\mu e} \frac{1}{\lambda^2} = \frac{2\epsilon_0 R}{\mu e} \frac{e^2 n_0}{\epsilon_0 kT}$$

A characteristic length for diffusion/recombination is thus defined by

$$\lambda_0 = \sqrt{\frac{\mu kT}{2Rn_0 e}} = \sqrt{\frac{D}{2Rn_0}}$$

where λ_0 is to be carefully distinguished from the Debye length, λ . It follows that

$$f = \frac{A}{2} e^{-z/\lambda_0} = -g$$

so

$$n_+ = n_- = n_0 \left(1 - \frac{A}{2} e^{-z/\lambda_0}\right)$$

Evaluating the constant A is somewhat less than straightforward, requiring physical intuition rather than mathematical technique. Physically realistic choices must be in the range $0 < A \leq 2$. Obviously $A < 0$ implies

an increasing charge density toward the wall, and $A = 0$ implies a constant charge density to the wall, both of which are physically unrealistic because diffusion requires charge flow into the wall. $A > 2$ allows negative charge densities, which are meaningless. The "traditional" choice is $A = 2$, which makes $n_+ = n_- = 0$ at the wall, but this is objectionable on the grounds that it makes sense for continuous fluids, but not necessarily in a molecular picture. The choice $A = 2$ will also cause problems when the effects of nonzero $-s$ (different mobilities for positive and negative ions) are considered.

We adopt the following argument as expedient, yielding a solution which is certainly of the right qualitative sort and which will give a result which can differ from reality only by a constant multiplier of order unity.

In our picture, adjacent to the wall the primary ionization rate is effectively reduced by a factor of two, half the primary ions and electrons being almost instantly lost to the wall. Thus in the absence of diffusion from the bulk toward the wall, the charge density near the wall would be

$$n(z = 0) = \sqrt{\frac{S}{2R}} = \frac{\sqrt{2}}{2} n_0$$

The corresponding value of A is given by solution of

$$\left(1 - \frac{A}{2}\right) = \frac{\sqrt{2}}{2}$$

or

$$A = 0.586$$

For any choice of A the diffusion current to the wall (a negative current of positive ions balanced by a positive current of negative ions) is

$$j_0 = eDn'(z=0) = eDn_0 \frac{A}{2\lambda_0}$$

or

$$j_0 = 2^{-1/2} e D^{1/2} R^{1/2} n_0^{3/2} A$$

Before continuing to determine the effect of $\delta \neq 0$, we investigate the range of validity of the solution for $\delta = 0$. We approximated the solution to

$$\lambda_0^2 y'' = y - \frac{y^2}{4}$$

by neglecting the term in y^2 , which gave

$$y = Ae^{-z/\lambda_0}$$

A complete solution is obtained in the form

$$y = \sum_{n=1}^{\infty} A_n e^{-nz/\lambda_0}$$

$$y' = \sum_{n=1}^{\infty} -\frac{n}{\lambda_0} A_n e^{-nz/\lambda_0}$$

$$y'' = \sum_{n=1}^{\infty} \frac{n^2}{\lambda_0^2} A_n e^{-nz/\lambda_0}$$

which gives

$$\sum_{n=1}^{\infty} n^2 A_n e^{-nz/\lambda_0} = \sum_{n=1}^{\infty} A_n e^{-nz/\lambda_0} - \frac{1}{4} \sum_{i,j} A_i A_j e^{-(i+j)z/\lambda_0}$$

where implicitly terms with $i = j$ are counted only once. Equating terms with equal exponents gives

$$-4(n^2-1)A_n = \sum_{i+j=n} A_i A_j$$

A_1 is arbitrary, replacing A in the single-exponential solution. The other coefficients are then given by

$$-4 (2^2 - 1) A_2 = A_1 A_1 \quad \longrightarrow \quad A_2 = -0.0833 A_1^2$$

$$-4 (3^2 - 1) A_3 = 2A_1 A_2 \quad \longrightarrow \quad A_3 = 5.21 \times 10^{-3} A_1^3$$

$$-4 (4^2 - a) A_4 = 2A_1 A_3 + A_2 A_2 \quad \longrightarrow \quad A_4 = -2.89 \times 10^{-4} A_1^4$$

.etc.

We thus have (with $n_+ = n_- \equiv n$)

$$n = n_0 \left(1 - \frac{A}{2} \left(e^{-z/\lambda_0} - 0.0833 A e^{-z/\lambda_0} + 5.21 \times 10^{-3} A^2 e^{-3z/\lambda_0} \dots \right) \right)$$

Our prior obsession with obtaining a value of A other than 2 was partly due to desiring some assurance that this series would not blow up; clearly the value 0.586 chosen above gives this guarantee. It is clear from inspection of this series that at $z = 0$, where the approximation is worst, the error (for $A = 0.586$) due to retaining only the first term is no more than about 4%.

We can now use the approximate solution

$$y = A e^{-z/\lambda_0}$$

to determine an iteratively corrected solution in the case $\delta \neq 0$. The relevant equation is then

$$\lambda^2 x'' + y' \int_0^z x \, dz = - \frac{2\epsilon_0 \delta R}{e\mu} \left(y + \frac{x^2}{4} - \frac{y^2}{4} \right) + 2x - xy$$

or

$$\lambda^2 x'' - \frac{A}{\lambda_0} e^{-z/\lambda_0} \int_0^z x \, dz = \frac{-2\epsilon_0 \delta R}{e\mu} A e^{-z/\lambda_0} + 2x - x A e^{-z/\lambda_0}$$

if we neglect terms in x^2 and y^2 .

We adopt the trial solution

$$x = B e^{-\sqrt{2}z/\lambda}$$

(note again the distinction between λ and λ_0) which recommends itself via the obvious approximation

$$\lambda^2 x'' = 2x$$

Carrying out the differential and integral operations then gives

$$\frac{B}{\sqrt{2}} \frac{\lambda}{\lambda_0} (1 - e^{-2z/\lambda}) = \frac{2\epsilon_0 \delta R}{e\mu} + B e^{-\sqrt{2}z/\lambda}$$

For larger values of z , we thus have

$$B = \frac{\sqrt{2}\lambda_0}{\lambda} \frac{2\epsilon_0 \delta R}{e\mu} = 2 \sqrt{\frac{\epsilon_0 R}{e\mu}} \delta$$

It then follows that

$$n_+ \approx n_0 \left(1 - \frac{A}{2} e^{-z/\lambda_0} - \sqrt{\frac{\epsilon_0 R}{e\mu}} \delta e^{-\sqrt{2}z/\lambda} \right)$$

$$n_- \approx n_0 \left(1 - \frac{A}{2} e^{-z/\lambda_0} + \sqrt{\frac{\epsilon_0 R}{e\mu}} \delta e^{-\sqrt{2}z/\lambda} \right)$$

and

$$\frac{dE}{dz} = \frac{e}{\epsilon_0} (n_+ - n_-) = -2 n_0 \delta \sqrt{\frac{eR}{\epsilon_0 \mu}} e^{-\sqrt{2}z/\lambda}$$

Integrating this equation from 0 to z gives

$$E = 2 n_0 \delta \sqrt{\frac{eR}{\epsilon_0 \mu}} \frac{\lambda}{2} (e^{-\sqrt{2}z/\lambda} - 1)$$

This is, of course, the electric field due to the space charge alone; it is clear that the constant term (coefficient $\times (-1)$) is the electric field due to the charge on the wall, and the actual total electric field in space is just

$$E = 2 n_0 \delta \sqrt{\frac{eR}{\epsilon_0 \mu}} \frac{\lambda}{\sqrt{2}} e^{-\sqrt{2}z/\lambda}$$

It is instructive to estimate the size of the electric field at the wall. If we assume (as we have previously)

$$n_0 \approx 10^4 \text{ cm}^{-3}$$

$$R \approx 10^{-7} \text{ cm}^3 \text{ sec}^{-1}$$

$$\mu \approx 250 \text{ cm}^2 \text{ volt}^{-1} \text{ sec}^{-1}$$

$$\lambda \approx 3.8 \text{ cm}$$

then

$$E_0 \approx 1.4 \times 10^{-3} \delta \text{ volt cm}^{-1}$$

Since

$$\delta \approx \frac{\mu_+ - \mu_-}{\mu_+ + \mu_-}$$

and is assumed small (perhaps 10%), it follows that the electric field is less than 1 mV/cm, which is small even compared to patch fields due to contact potential inhomogeneities.

The corresponding net charge density on the surface is estimated via

$$E = \frac{\sigma}{\epsilon_0} \rightarrow \sigma \approx 10^{-16} \text{ coul cm}^{-2}$$

If we denote the small conduction or mobility component of the total flux to the wall by

$$\Delta j_{\pm} = e\mu E n_{\pm}$$

and the major diffusion component by

$$j_{\pm} = eDn_{\pm}' = 2^{-1/2} eD^{1/2} R^{1/2} n_0^{3/2} A$$

then it follows that at the wall

$$\frac{\Delta j_{\pm}}{j_{\pm}} = \frac{2(1 - \frac{A}{2})}{A} \delta$$

which is clearly trouble if $A = 2$, but for the value $A = 0.586$ gives

$$\frac{\Delta j_{\pm}}{j} = 2.41 \delta$$

It thus obviously follows that the conduction current to a floating probe due to an imbalance in negative and positive ion mobilities (or diffusion constants) is generally an order-of-magnitude less than the diffusion current.

At the conclusion of this section we re-emphasize the apparent lack of previous consideration of this problem by plasma physics experts, and note that we look forward to having our crude attempts at theoretical analysis examined, corrected, and completed by these experts.

6. Modifications Due to Balloon Package Charging or External Array

It is apparent that the floating package, in the absence of external charging mechanisms (such as the photoelectric effect) should present little difficulty. The ion current of either sign to the skin of the package will be diffusion limited, and the expected magnitude of the current flux is (omitting the constant coefficient)

$$j_{\pm} \sim e D^{1/2} R^{1/2} n_0^{3/2}$$

which evaluates to about 10^{-16} amps cm^{-2} , or about 10^3 ions $\text{cm}^{-2} \text{sec}^{-1}$ of either sign.

This is, of course, the flux to the skin in the absence of aerodynamic collection. In the vicinity of the sampling aperture, bulk flow will carry many more than 10^3 ions cm^{-2} (of aperture) sec^{-1} into the mass spectrometer vacuum. If we assume a 10^4 liter/sec cryogenic pumping capacity, and a working pressure of 10^{-5} torr (obtained by choice of aperture size), then we will collect about 100 torr $\text{cm}^3 \text{sec}^{-1}$ of gas. At an external pressure of 7 torr (35 Km), this will amount to about 14 $\text{cm}^3 \text{sec}^{-1}$ of the external gas. If the ion density in the vicinity of the aperture is about $n_0/\sqrt{2}$, then the bulk flow will carry about 10^5 ions sec^{-1} through the aperture.

With a counting detection system, even if the total system transmission (from aperture to pulse preamplifier) is as poor as 1%, the signal-to-noise level should be sufficient to obtain the required analysis with entirely reasonable integrating times. We expect the total system transmission to be considerably better than 1%.

This treatment of course assumes that the aerodynamic perturbation does not seriously modify the ion density (or spectrum) in the bulk of the sampled volume. Since the extent of the aerodynamic perturbation (pressure reduction in the vicinity of the aperture) is comparable to the aperture diameter, and thus occupies a few mm^3 at most, while the effective sampled volume is of the order of a cubic meter, this approximation should be a good one.

We now want to consider the effect of additional electric fields, both natural (balloon charging) and imposed (the external array) on the sampling problem. We have found that a formal mathematical approach, an extension of that used in considering the diffusion-limited problem, generates difficulties which will require additional time to resolve. For the present, we will thus restrict the discussion to a qualitative (or at best, semi-quantitative) one, with the hope that a more rigorous treatment will be obtained by future workers.

As in previous sections, for purposes of discussion we will take the sign of any excess charge on the package as being positive, so that the electric field points away from the package. This convention is useful in part because it simplifies the discussion, and in part because it is the actual case when charging is due to photoelectron emission. Such a field will have the following effects:

1. enhance the motion of negative ions toward the package;
2. inhibit the motion of positive ions toward the package;
3. decrease the product n_+n_- , and so increase the ion current leaving any volume element;
4. change the mean speed of ions relative to their purely thermal speeds, and thus influence ion-molecule reaction rates.

To obtain a feeling for the size of relevant effects, let us first treat the electric field, through its perturbation of the ion velocity distribution ($\Delta v = \mu E$), as a perturbation on the diffusion constant. Using the relation

$$D_0 \approx \lambda_i v_0 / 3$$

for the "field free" diffusion constant, where λ_i is the ion mean free path, and combining it with the Einstein relation, we obtain a position-dependent diffusion "constant"

$$D_{\pm} \equiv D_0 \left(1 \mp \frac{e \lambda_i E}{kT} \right)$$

Since the spatial extent of the electric field will be the order of the Debye length (λ), we can average D_{\pm} over this distance to obtain

$$\langle D_{\pm} \rangle \sim D_0 \left(1 \mp \frac{e \lambda_i \phi}{\lambda kT} \right)$$

where ϕ is the potential difference between the instrument package and the bulk plasma. Since the ion mean free path is the order of 10^{-4} cm, and the Debye length is the order of 1 cm, we can estimate that this picture will have some validity so long as

$$10^{-4} \frac{e \phi}{kT} \lesssim 1$$

which at the ambient temperature means

$$\phi \gtrsim 200 \text{ volts}$$

We can thus roughly estimate that the positive ion flux will be reduced to about zero, and the negative ion flux will about double, when the potential of the instrument with respect to the atmosphere is the order of a few hundred volts. The details are clearly very much more complicated than this, but the object of this exercise is simply to estimate at what point worry is appropriate, or at what magnitude of bias voltage an external array might have some effect.

At much less than a few hundred volts, diffusion effects will continue to dominate mobility effects, and both positive and negative ions should reach the vicinity of the sampling aperture with relatively minor enhancement or inhibition. At much more than a few hundred volts, the current reaching the instrument should be determined by mobility (or conduction) considerations.

To qualitatively understand this high field region, we propose a simple and highly artificial picture in which the potential falls linearly from the imposed value of ϕ_0 at the surface to zero at a distance of one Debye length:

$$\begin{aligned}\phi(z) &= \phi_0 - \frac{\phi_0}{\lambda} z & z \leq \lambda \\ &= 0 & z \geq \lambda\end{aligned}$$

The corresponding electric field is constant, with a discontinuity at $z = \lambda$:

$$\begin{aligned}E(z) &= \frac{\phi}{\lambda} & z \leq \lambda \\ &= 0 & z > \lambda\end{aligned}$$

With a constant electric field, and neglecting diffusion, the continuity equations become

$$\begin{aligned}e\mu E n_+' &= eS - eR n_+ n_- \\ e\mu E n_-' &= -eS + eR n_+ n_-\end{aligned}$$

where we assume $\mu_+ = \mu_- \equiv \mu$. Since the sum of these equations gives zero on the right hand side, it follows that

$$n_+' = -n_-'$$

so we can write

$$n_{\pm} = n_0 (1 \mp f)$$

The remaining differential equation is then easily solved to give the exact result:

$$n_{\pm} = n_0 \left(1 \mp \frac{\mu E}{n_0 R} \frac{1}{z} \right)$$

or

$$n_{\pm} = n_0 \left(1 \mp \frac{\mu \phi}{n_0 R} \frac{1}{\lambda z} \right)$$

The term with the position dependence is not really independent of n_0 , because λ depends on $n_0^{-1/2}$.

This mathematically exact result (for this artificial model) is clearly unphysical for small z , because it allows n_{+} to become negative. To estimate the corresponding current, we evaluate

$$j_{\pm} = e \mu E n_{\pm}$$

at the location where $n_{+} = 0$ or $n_{-} = 2n_0$:

$$j_{-} = 2e \mu \frac{\phi}{\lambda} n_0$$

$$\approx 10^{-12} \phi \text{ amp cm}^{-2}$$

with ϕ in volts. This can clearly be several orders of magnitude larger than the diffusion current ($\sim 10^{-16}$ amp cm^{-2}) reaching the floating package.

However the increased ion flux to the package does not imply a corresponding increase in current through the sampling aperture, because in the strong field case the ion motion is decoupled from the bulk gas flow, and the bulk gas flow is responsible for most of the ion current through the aperture in the low or zero field case. At the beginning of this section, we allowed for a bulk gas flow of $14 \text{ cm}^3 \text{ sec}^{-1}$ at 7 torr, and the corresponding aperture area (using P (liter sec^{-1}) $\approx 10 A$ (cm^2)) is about $1.4 \times 10^{-3} \text{ cm}^2$. It follows that the high-field current through the aperture in this picture is about 10^{-15} amp per volt of bias, or, at a few hundred volts, a few tens times the diffusion bulk flow current of 10^{-14} amp.

As a general conclusion, then, we would expect an "external array" to be more trouble than it is worth; it will probably result in not much of an increase in ion signal, while the strong fields required will modify reaction rates, result in the collection of ions before terminal reactions

have occurred, and enhance ion sampling from regions close to the instrument package at the expense of ions originating in the relatively clean atmosphere far from the package. These conclusions, of course, require experimental testing as part of the laboratory development work connected with this project.

Additional thoughts on this subject, as well as experimental design proposals, are discussed by W. L. Fite in Section III.9.

7. Balloon Charging Evaluation

Whether or not natural charging is likely to produce severe problems, and what if anything can be done to compensate, is discussed in light of the conclusions reached in the previous section. We consider two cases, one in which we treat only a spherical conducting package, and the other in which we discuss effects due to differential charging between the balloon and the gondola.

Photoelectrons are considered to be the major contributor to instrument package charging. Photoelectrons are ejected from solid surfaces with a maximum energy

$$E_m = h\nu - \phi_0$$

where $h\nu$ is the photon energy (~ 6.2 eV @ 200nm) and ϕ_0 is the work function of the material (~ 5 eV for ferrous metals). The distribution of electron energies below E_m is approximately linear with zero intercept.⁽¹¹⁾ Thus in the balloon environment, especially at the higher altitudes (above the ozone layer), ultraviolet radiation may release significant numbers of photoelectrons at energies of order-of-magnitude 1 eV.

We have previously estimated (III.3) that it requires the order of 10^5 collisions to thermalize a 1 eV electron. The distance the electron travels while undergoing thermalization determines the spatial extent of the problem, since thermal electrons are rapidly lost to recombination or attachment followed by recombination. Negative ion formation by resonance attachment of high energy electrons is negligible until the electron energy reaches several eV.

In the random walk approximation the electron travels a distance

$$d \sim n^{1/2} \lambda_e$$

where n is the number of collisions and λ_e is the mean free path. We have already shown $\lambda_e \sim 10^{-2}$ cm, so

$$d \sim 3 \text{ cm}$$

Thus if a significant number of photoelectrons are released from the sampling instrument, they can have a serious effect on ion densities and perhaps even on ion species just in the region where ion sampling will occur.

The solar ultraviolet flux on the upper atmosphere is about 8×10^{10} photons $\text{cm}^{-2} \text{sec}^{-1} \text{A}^{-1}$ at 200 nm, and drops rapidly to about 2.5×10^8 at 100 nm.⁽¹²⁾ Since the photon flux above 2000 Å will be relatively ineffective in producing photoelectrons, and the photon flux below 100 nm is relatively weak, we start with an order-of-magnitude estimate of 3×10^{13} photons $\text{cm}^{-2} \text{sec}^{-1}$ incident on the upper atmosphere and capable of ejecting photoelectrons. We will consider only the worse case, above the ozone layer, and note that at the upper stratosphere altitudes the electron mean free path is an order of magnitude greater than the 10^{-2} cm used above, so the spatial extent of the perturbation may be as great as 30 cm.

Typical photoelectron quantum yields are the order of 10^{-3} ,⁽¹¹⁾ so we can expect about 3×10^{10} photoelectrons $\text{cm}^{-2} \text{sec}^{-1}$, or an electron current density of about 3×10^{-9} amp cm^{-2} leaving the instrument surface. This may be compared with the previously derived estimated of about 10^{-16} amp cm^{-2} of ion flux of either sign reaching the instrument by diffusion. The instrument package must then acquire sufficient positive charge to raise its potential to the point where the equivalent of the photoelectron current is returned as a slow electron or negative ion current.

We have previously estimated that in the high field approximation

$$j_- = 2e\mu n_0 \phi / \lambda \cong 10^{-12} \phi \text{ amp cm}^{-2}$$

if the current is returned as negative ions at an altitude where $\mu \approx 250 \text{ cm}^2 \text{ volt}^{-1} \text{ sec}^{-1}$. At the higher altitudes, where the pressure is a factor of 10 lower, μ is correspondingly increased; thus j_- may reach $\sim 10^{-11} \phi \text{ amp cm}^{-2}$. In this altitude range (middle to upper stratosphere), a photoelectron current of $3 \times 10^{-9} \text{ amp cm}^{-2}$ may thus lead to an instrument package potential of order-of-magnitude 300 to 3000 volts, if this picture is valid.

We can be sure that the picture is not totally valid, because the electron mobility is about 1000 times the negative ion mobility, and many photoelectrons will be returned to the instrument surface very rapidly. To investigate the extreme of this possibility, we ignore the surrounding plasma and ask the nature of the electron cloud surrounding an irradiated metal sphere in an atmosphere which thermalizes the electron velocity, but has no propensity to remove electrons by recombination or attachment. For simplicity, we assume photoelectrons are monoenergetic and ejected only normal to the surface.

The motion of the outgoing electrons under these conditions is given by

$$m \frac{dv}{dt} + \frac{c}{\lambda} v = eE$$

where c is the mean thermal speed of the gas molecules, λ is the electron mean free path (assumed constant over this energy range), and c/λ is obviously related to the definition of mobility.

If we substitute $-d\phi/dr$ for E and divide through by mv we obtain

$$\frac{dv}{dr} = \frac{e}{mv} \frac{d\phi}{dr} - \frac{c}{\lambda}$$

Solutions are available only when one or the other of the two right hand terms dominates:

$$v = v_0 \left(1 - \frac{2e(\phi - \phi_0)}{mv_0^2} \right)^{1/2}$$

or

$$v = v_0 - \frac{c}{\lambda} (r - r_0)$$

where the initial conditions provide constants v_0 (the initial velocity, corresponds to $\sim 1\text{eV}$), ϕ (the potential of the instrument package relative to zero in the bulk plasma), and r_0 (the radius of the spherical package).

The spatial extent of the charge cloud can be estimated from the second limiting case, which gives $v = 0$ at some r_{max} defined by

$$r_{\text{max}} - r_0 = \frac{\lambda v_0}{c}$$

A typical numerical value for $r_{\text{max}} - r_0$, taking $\lambda \sim 10^{-2}\text{ cm}$, $v_0 \sim 6 \times 10^7\text{ cm sec}^{-1}$ at 1 eV , and $c \sim 5 \times 10^4\text{ cm sec}^{-1}$, is 10 cm , which is a number we have previously derived as the thermalization distance for electrons.

It is interesting (however obvious) to note that in the absence of collisions the potential the sphere acquires is equal to the kinetic energy of the electrons released, at least in the case where the photon flux is low enough that space charge does not have to be considered. We will proceed to show that under collision-dominated conditions, much higher potentials are possible.

We are given (or have estimated) a photon flux sufficient to eject $j_0 \sim 3 \times 10^{-9}\text{ amp cm}^{-2}$. In this picture, with no losses, this photocurrent is thermalized in $\sim 10\text{ cm}$, and then, under the influence of the field established, returns to the instrument package. The returning current follows the mobility equation ($dv/dr = 0$), so we have at the surface

$$j_0 = \mu n_i \Big|_{r=r_0} = \frac{Q}{4\pi\epsilon_0 r_0^2}$$

where n_i is the electron density associated with the incoming current, and Q is the (positive) charge on the sphere. Since the total charge in the cloud surrounding the sphere must be at Q , and most of it is associated with the incoming current (because of the higher velocity of the outgoing electrons), we can estimate (very roughly)

$$en_i \Big|_{r=r_0} \approx \frac{Q}{\frac{4}{3}\pi(r_{\text{max}}^3 - r_0^3)}$$

which gives

$$\phi = \frac{Q}{4\pi\epsilon_0 r} = \sqrt{\frac{j_0}{3\epsilon_0 \mu} (r_{\max}^3 - r_0^3)}$$

If we take r_0 as 100 cm, $(r_{\max} - r_0) = 10$ cm, $j_0 = 3 \times 10^{-9}$ amp cm^{-2} , and $\mu = 10^7$ cm^2 volt sec^{-1} (for electrons in the upper stratosphere) we conclude

$$\phi \approx 20 \text{ volts}$$

Obviously this estimate is very crude, the model leaving much to be desired and the approximations leaving even more to be desired, but we believe the result is at least of the right order-of-magnitude.

It may seem somewhat puzzling that while in the absence of collisions, at least for small photon fluxes where space charge can be neglected, the sphere acquires only the potential required to stop the photoelectrons at "infinity", while when collisions are considered, a higher potential is reached. When a friction-like force aids the retarding field in slowing down the departing electrons, a lower potential would seem sufficient to return the slow electrons. But it must be remembered that in the collisionless case the returning electrons arrive with the same speed they had when they left, while in the collisional case they arrive with a much lower speed determined by the field strength. In the collisional case the potential must rise to a value sufficiently high to produce an electric field which can return the required current. The mechanism for building this stronger electric field is the space charge cloud close to the sphere; the field there is similar to that in a concentric sphere capacitor with a fairly small spacing between the inner and outer spheres.

It is important to examine how our estimate of ϕ depends on r_0 , since we need to consider the effect of a small gondola (~ 1 meter diameter) suspended under a large balloon ($\sim 10^5$ ft^3 , or ~ 15 meter diameter). For $(r_{\max} - r_0) \ll r_0$ we have

$$r_{\max}^3 - r_0^3 = 3r_0^2 \Delta r$$

where Δr is $(r_{\max} - r_0)$. It follows that the potential to which a floating object is raised, in this picture, increases linearly with its radius, and the balloon might reach ~ 300 volts.

If the balloon and gondola are connected by an insulating cable, then the influence of the higher balloon potential on sampling at the gondola location will be negligible, because of the shielding effect of the electron cloud and the plasma. If on the other hand they are connected by a conducting cable, then their (assumed conducting) surfaces will have to come to the same potential. This means that there will be a net flow of negative charge through space from the balloon to the gondola, returned through the connecting cable as an electron flow from gondola to balloon. Thus in the case of the balloon and gondola connected by a conducting cable the electric fields surrounding the two will be coupled, while in the case of an insulating cable they will be essentially independent. The latter case seems preferable, although it appears imperative to test this interpretation experimentally. An interesting configuration would be a conducting cable with an insulating break in it which could be shorted by a ground-commanded switch.

8. Effects of Gondola Charging

In the previous section we assumed that photoelectrons are returned to the instrument as electrons. However, the lifetime of thermal electrons against negative ion formation in the stratosphere is sufficiently small ($\sim 10^{-4}$ sec) that the current returning to the gondola will consist primarily of negative ions. Because negative ion mobilities are the order of 10^3 times smaller than electron mobilities, a correspondingly higher electric field will be required to return the photocurrent, and above the ozone layer the gondola potential could reach tens of kilovolts rather than the tens of volts appropriate for electrons.

Under these circumstances there may be considerable difficulty in collecting positive ions, and we would speculate that the failure of previous attempts to observe stratospheric ions may be related to this phenomena.

Furthermore the negative ions observed will be uncharacteristic of those in the bulk of the stratosphere, because ion formation and destruction mechanisms in the photoelectron sheath will be very different from those prevailing in the bulk.

If these speculations are valid, and if no countermeasures are taken, then we would expect valid data collection to be possible in the lower stratosphere, but not in the upper stratosphere. However, it is possible to envision several countermeasures which could be easily incorporated into the flight package. One simple countermeasure is to treat the surface so that it has a sufficiently high work function that the emitted photocurrent will be negligible. Another, more interesting, method has been proposed to counter the satellite charging problem. This is to "anchor" the instrument potential to the plasma potential by extending a boom equipped with a thermionic emitter of electrons or positive ions, as is appropriate for the specific sign of the accumulated excess charge. In this case a positive ion emitter would be appropriate. Since the expected magnitude of the photocurrent is $\sim 3 \times 10^{-9}$ amp cm^{-2} and the gondola may present an effective area of about 3×10^4 cm^2 , an ion emission current of about 10^{-4} amp may be anticipated. In a vacuum, alkali-metal aluminosilicate thermionic emitters can easily support the required current from a square centimeter or less of hot surface,⁽¹³⁾ but whether more sophisticated techniques may be required in an air environment is not known to us. The incorporation of thermionic electrons and positive ion emitters on the instrument would make possible a number of experiments to test these ideas.

9. Design Considerations for an External Ion Collection Device*

At first glance the mass spectrometric analysis of ambient ions in the stratosphere appears to be no problem. The plasma, consisting only of positive and negative ions at the ambient gas temperature, should form no

*This subsection was prepared independently by W. L. Fite, and the details of some of the assumptions are slightly different from those used in Sections III. 1-8. The essential assumptions, and the conclusions, are comparable.

sheaths. The plasma densities (of the order of 10^3 ions/cm³) are sufficient that even if electrons were present and had an elevated temperature, the sheaths would still probably cause no problems, based on experience with sampling from flowing afterglow systems.

However, balloon flights to date have apparently not been able to successfully measure the ion mass spectra and presumably the problem is getting the ions from the ambient gas into the high vacuum of a mass spectrometer.

These notes summarize some considerations relevant to the sampling problem.

i. Idea of Sampling Scheme Here Considered

The sampling scheme here considered is one in which electrostatic fields are set up to draw ions from the ambient plasma toward an aperture. Because of the limitations of geometry of electrodes, it is envisaged at some point as the ions approach the aperture, they will have to leave the region of the field and enter a field free space, where gas flow will carry them on through the aperture.

With regard to the manner of setting up the electric fields, it is envisaged that conducting electrodes will not be used, because field lines terminate on them at right angles. Instead, consideration is given to using resistive electrodes, which provide a field component directed toward the aperture.

The scheme considered is shown conceptually in Figure 4. In configuration (a), the resistive material is tapered to provide an electric field above it which increases as the aperture is approached. Current density limitations in the tapered resistive material require that it terminate at some inner radius, where a mesh hemisphere can both terminate the field and allow passage of gas through it. Inside the hemisphere, the region is field free and aerodynamics carry the ions on in to the aperture. In configuration (b) the resistive material is not tapered. Since there is no increase, the inner radius of the resistive material can be made smaller

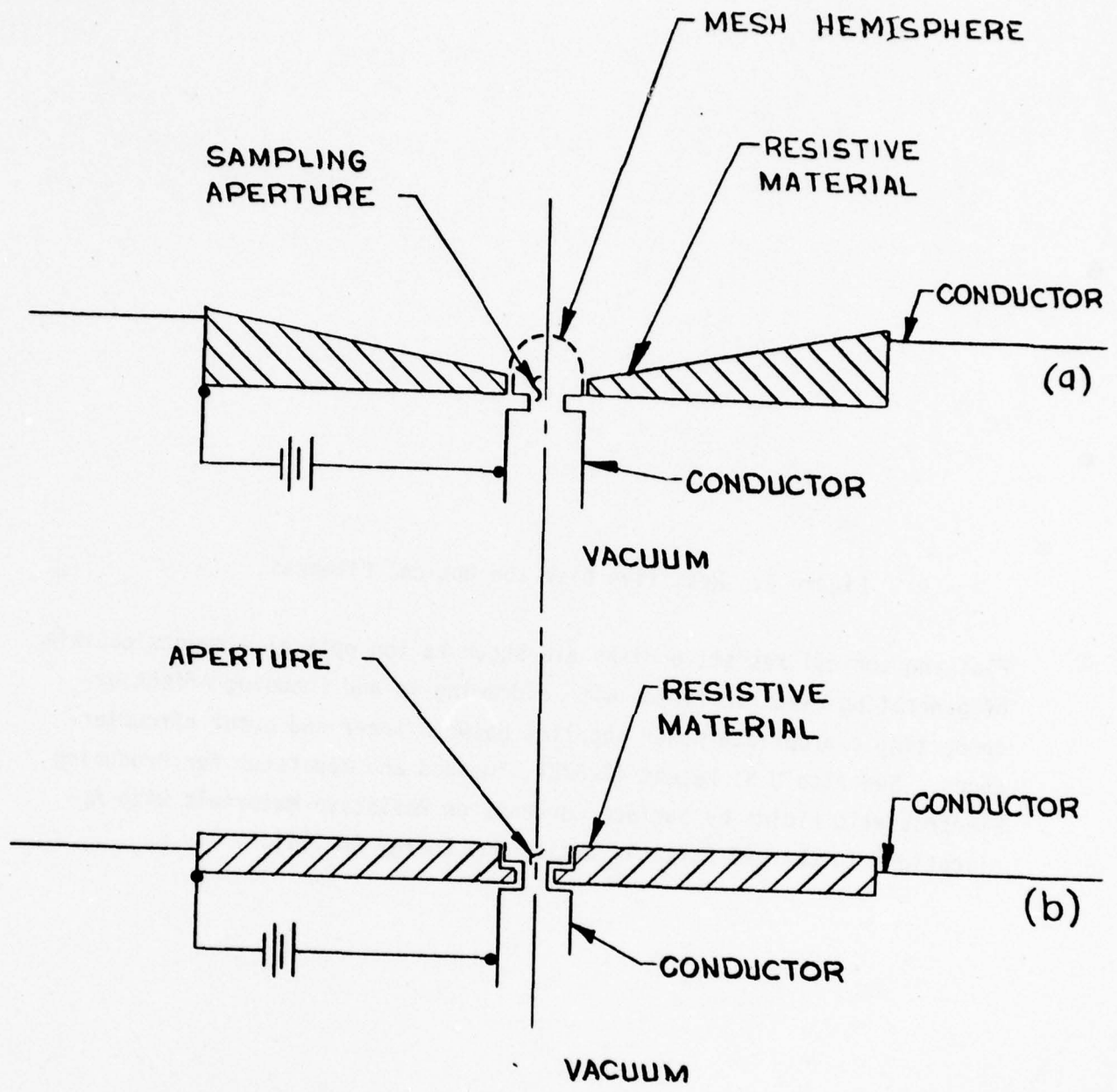


FIGURE 4

Figure 4: Resistive Disk Ion Optical Elements

Flat and conical resistive disks are shown as ion optical elements capable of generating electric fields with a drawing-in and focusing effect by connecting appropriate power supplies between inner and outer circumferences. See also U.S. Patent 4126781, "Method and Apparatus for Producing Electrostatic Fields by Surface Currents on Resistive Materials with Applications to Charged Particle Optics and Energy Analysis".

without encountering current density problems. The field free region can be made as small as the aperture itself.

The two problems considered here are: motion of ions after they enter the field free region and the improvements in extraction fields by going to resistive lenses.

ii. Motion of Ions in Gases

Ions moving through a gas under influence of an electric field, E , have a drift velocity, \bar{v} , given by

$$\bar{v} = \mu E = \frac{e\lambda}{mc} E \quad (1)$$

where μ is the mobility, e , and m the charge and mass of the ions, λ is the mean free path of ions in the gas, and c is the mean thermal speed of the gas molecules.

To crude approximation, one can estimate the stopping distance of a group of ions with initial drift velocity, v_0 , by considering that

$$m\dot{\bar{v}} = eE - \frac{mc}{\lambda} \bar{v} \quad (2)$$

which combines the acceleration due to an electric field and the drag by the gas. This formula reduces to Equation (1) when there is no acceleration. Setting $E = 0$ in Equation 2,

$$m \frac{d\bar{v}}{dt} = m\bar{v} \frac{d\bar{v}}{dx} = - \frac{mc}{\lambda} \bar{v}$$
$$\frac{d\bar{v}}{dx} = - \frac{c}{\lambda}$$

or

$$\bar{v} = \bar{v}_0 - \frac{c}{\lambda} x \quad (3)$$

where v_0 is the velocity of an ion initially, after it enters the field free region. The stopping distance, L , which is the value of x at which $v = 0$ is

$$L = \lambda \bar{v}_0 / c$$

Thermal speeds of molecules at stratospheric temperatures are of the order of 4×10^4 cm/sec. At stratospheric pressures of the order of 1 torr the mean free path is of the order of 4×10^{-3} cm and the mobility of ions is of the order of 10^3 cm² volt⁻¹ sec⁻¹. For reasonable fields of less than 10^3 volts/cm, and velocities of ions as they leave the field free region of the order of 10^6 cm/sec, stopping distances of the order of 25 mean free paths are involved, i.e., less than 1 mm.

Since both the mobility (and therefore v_0) and the mean free path decreases linearly as the gas pressure increases, and since these are in Equation (1), the stopping distance decreases as the square of the pressure.

For all intents and purposes, the ions can be considered stopped within the ambient gas as soon as they enter the field free regions, and move with the gas.

iii. Resistive Lenses

We here consider the effects of making the field electrodes of resistive rather than conducting materials.

For simplicity of mathematics and some guidance, we consider a two dimensional situation as shown in Figure 5. A current flows within the resistive material to provide a continuously varying linear potential along the surface of the material.

Using fourier analysis, the potential in the upper half plane must be of the form

$$\phi = \int_{-\infty}^{\infty} A(k) \cos kx e^{-ky} dk \quad (5)$$

Setting $y = 0$ and using the boundary conditions from the figure, the amplitudes can be evaluated to yield

$$\phi = \frac{2v_0}{\pi L} \int_0^{\infty} \frac{1 - \cos kL}{k^2} \cos kx e^{-ky} dk \quad (6)$$

$$= \frac{4v_0}{\pi L} \int_0^{\infty} \frac{\sin^2 \frac{kL}{2}}{k^2} \cos kx e^{-ky} dk \quad (7)$$

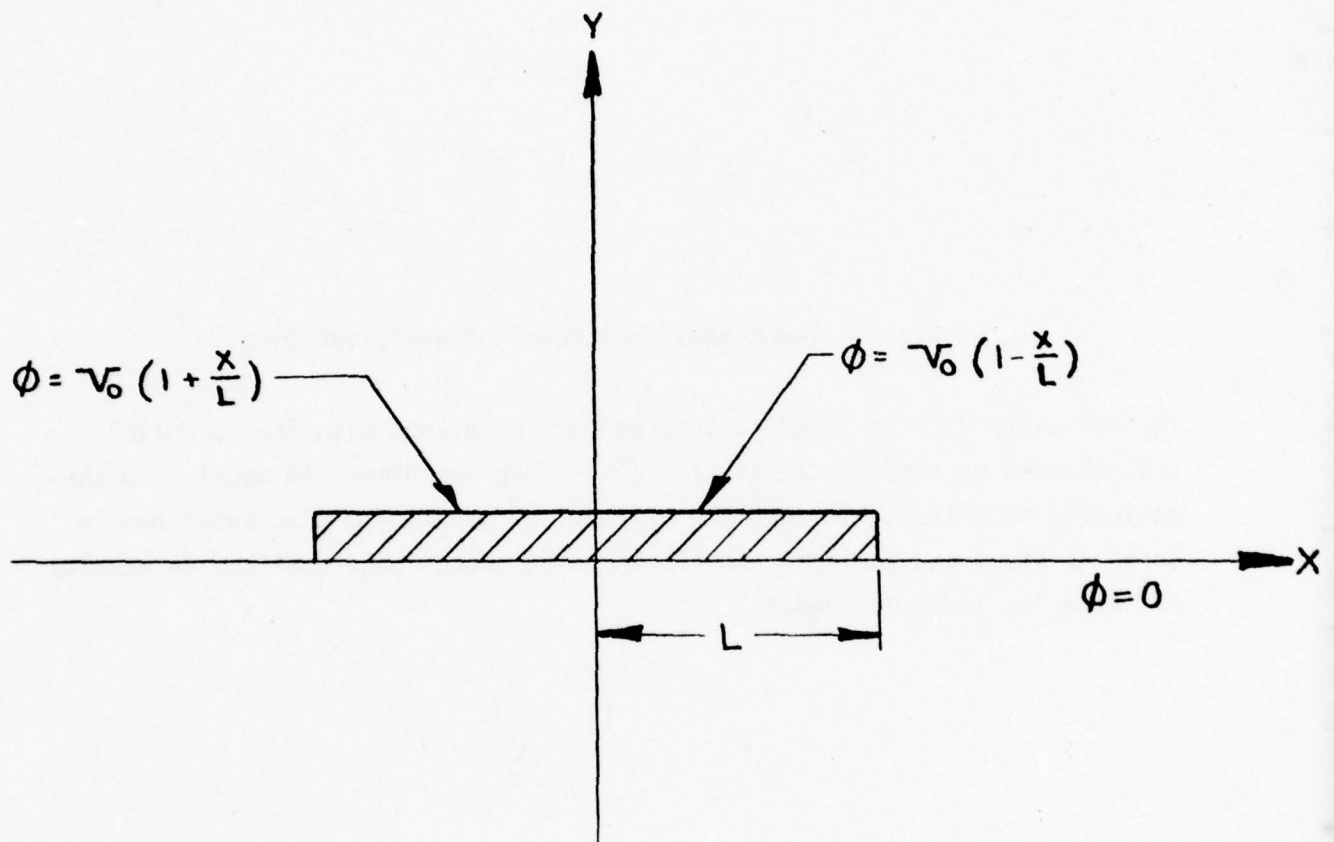


FIGURE 5

Figure 5: Two Dimensional Model of Resistive Disk

The resistive disk is imbedded in a conducting plane, with the potential distribution as shown; note $\phi(-x) = \phi(x)$. The two dimension model is mathematically more tractable than the cylindrical model, yielding solutions in terms of sines and cosines rather than Bessel functions; qualitative results are expected to be analogous.

These integrals cannot be evaluated in closed form. However, their derivatives with respect to x and y can be. They are

$$E_x = -\frac{d\phi}{dx} = \frac{4V_0}{\pi L} \left[\tan^{-1} \frac{x}{y} - \frac{1}{2} \tan^{-1} \left(\frac{2xy}{y^2 + \frac{L^2}{4} - x^2} \right) \right] \quad (8)$$

$$E_y = -\frac{d\phi}{dy} = \frac{V_0}{\pi L} \ln \left[\frac{(y^2 + (L+x)^2) \cdot (y^2 + (L-x)^2)}{(x^2 + y^2)^2} \right] \quad (9)$$

These expressions are found in Gradshteyn and Ryzhik, Tables of Integrals, Series and Products. (Formulas 3.949.2 and 3.949.3)

Several features of these integrals are noteworthy. First, is the fact that although the current in the resistive material is parallel to the surface, the electric field normal to the surface at the surface locations, $y = 0$, in general is not equal to zero. Equation (9) indicates that E_y vanishes when the argument of the logarithm is unity, a condition which is satisfied when $x = L/\sqrt{2}$. E_y increases as x increases beyond this point. As x decreases from this point toward the origin E_y is negative and increases to infinity at $x = 0$.

The implication of this is that near the surface the field is not parallel to the surface, as would seem to be implied by Maxwell's third equation, but in addition having a grounded plane adjacent to the resistive material causes surface charges to be located on the surface producing the perpendicular field component. Thus, using a resistive material helps in transporting ions under drifting conditions toward the origin, since there is a parallel component of field; however, the total field lines do terminate on the resistive material and would deposit some of the ions on the resistive material.

This may be contrasted with the situation if the resistive material were replaced by a conducting material. In this situation all field lines terminate on the surface and do so with field lines normal to the surface.

It appears that it would be preferable to use a resistive material rather than a conductor because if there were an aperture or slit at $x = 0$ through which the ions were to pass, the parallel field component with the resistive material would assist the air flow in carrying ions to the aperture, whereas a conducting material would not.

Figure 6 shows qualitatively the situation comparing conducting and resisting materials. The resistive material provides field lines which are more conducive to guiding ions toward the aperture at the center.

The problem here considered is of course only a two-dimensional problem. Setting up the problem in three dimensions with cylindrical symmetry about an axis normal to a flat surface of a flight package is straightforward to do. Solving the problem, however, is a task requiring extensive computer calculations.

It is felt that carrying out the calculations is not justified at this point, and that with the insight provided by the two-dimensional problem, can turn directly to experiment.

The principal points of insight are: (1) Using resistive material will help, but will not provide an ideal solution to shaping of field lines; and (2) since it will only help it is probably not worthwhile to go to extensive shaping and difficult machining of the resistive material. The first step appears to be to use a flat resistive material shape, i.e., an annulus. The material to be used in the experiments is ceramically bonded carbon with a resistivity of approximately 10^5 ohm-cm, which is manufactured by the Stackpole Carbon Company.

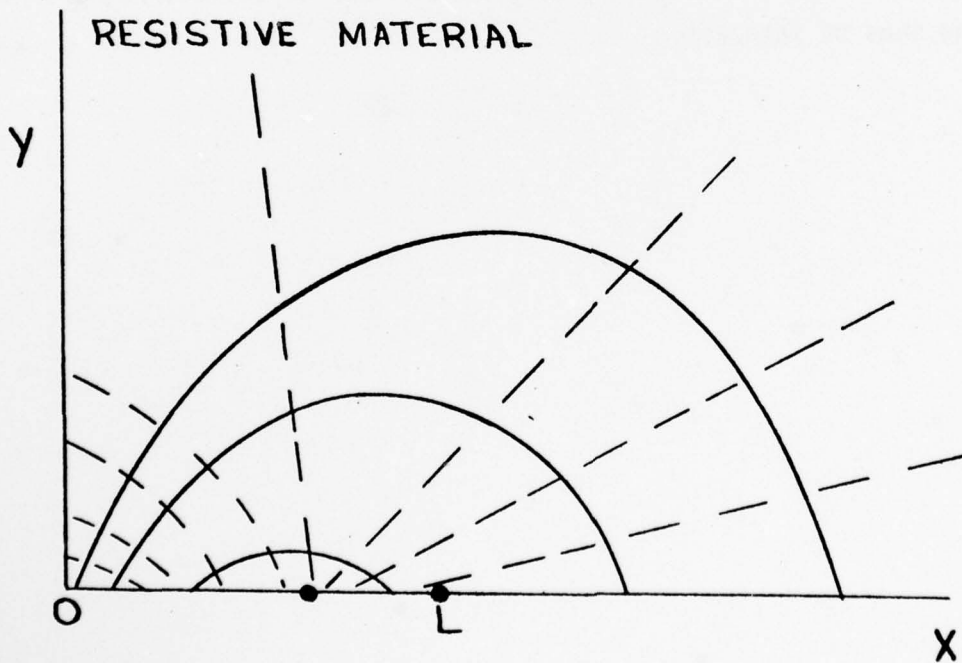
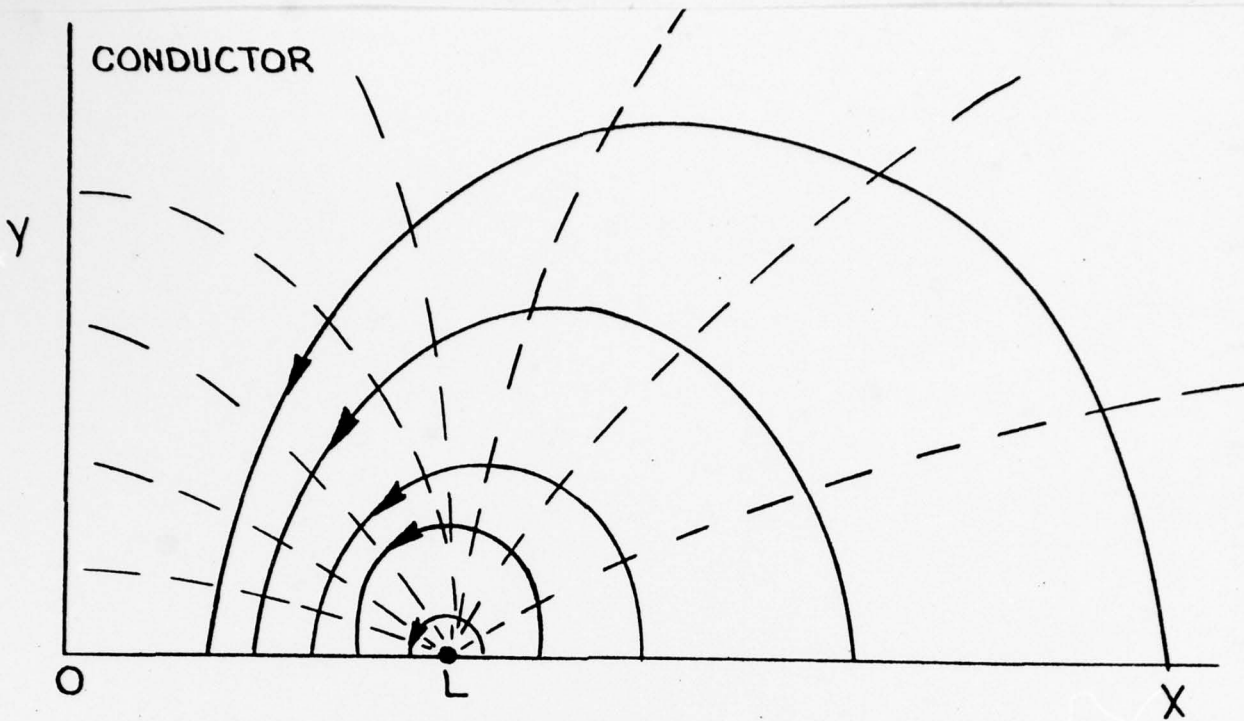


FIGURE 6




Figure 6: Electric Fields Near Conducting and Resistive Surfaces

This illustrates the possible advantage of a resistive disk with radial current flow in directing ions toward a sampling aperture, in contrast to the situation with a conducting disk which tends to collect rather than direct the ions of interest.

IV - THE MASS SPECTROMETER AND ION OPTICS

Reference is made to Figure 7 (EL drawing number D1623) which is an assembly drawing for the inner vacuum system housing the ion optics, quadrupole, and multiplier. This apparatus is installed in a larger vacuum chamber evacuated to a pressure simulating the stratosphere, as shown in Figure 8. These two figures show most of the deliverable items in a form depicting their interrelation. The multiplier and its mounting hardware are not deliverables and have not been shipped.

This apparatus is disassembled into three parts for shipping: (1) the quadrupole in its vented case with ion optics attached to the entrance plate; (2) the quadrupole housing which is the inner vacuum chamber containing the quadrupole, topped by a larger diameter chamber into which the ion optics project and closed by a flange containing the sampling aperture; and (3) a mating tube in which a multiplier can be mounted and through which the assembly can be evacuated.

The "quick-disconnect" feedthroughs for the quadrupole RF have been blanked off for delivery. AFGL may choose to make RF connections in a number of ways. One possibility is to bring RF leads to the appropriate locations by insulated wires in the high vacuum. Another is to use an arrangement similar to that sketched in Figure 9, whereby the RF leads use the quick disconnects by passing them through the simulated stratospheric vacuum, sheathed by an atmospheric pressure jacket to prevent electrical breakdown. This was the arrangement actually used during our tests. The original feedthrough shown in Figure 7 proved unsatisfactory due to RF breakdown.

Several field modifications were made during testing, and are noted on the design drawing. These include:

- (1) modifications to the aperture holding flange to improve ion collection and transmission;
- (2) modifications to ELFS mounting to improve ion entrance conditions;
- (3) venting of quadrupole case to improve vacuum pumping.

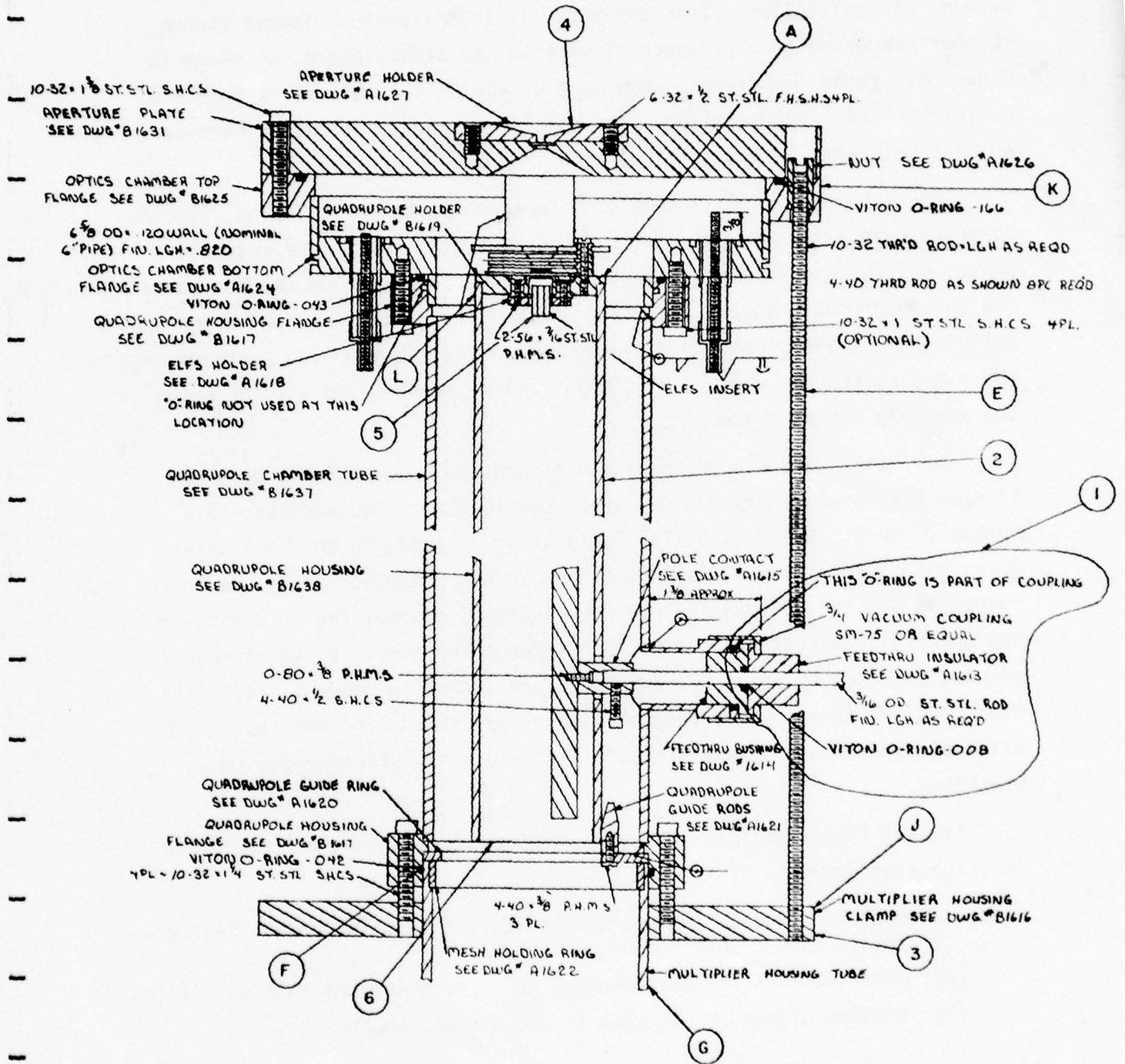


FIGURE 7




Figure 7: Vacuum System (Mechanical)

This part of EL Drawing D1623 shows the quadrupole mass filter, ion collection optics/electron impact ionizer, vacuum housing, and sampling aperture. The apparatus is installed in the vacuum chamber which simulates the stratosphere, as shown in Figure 8.

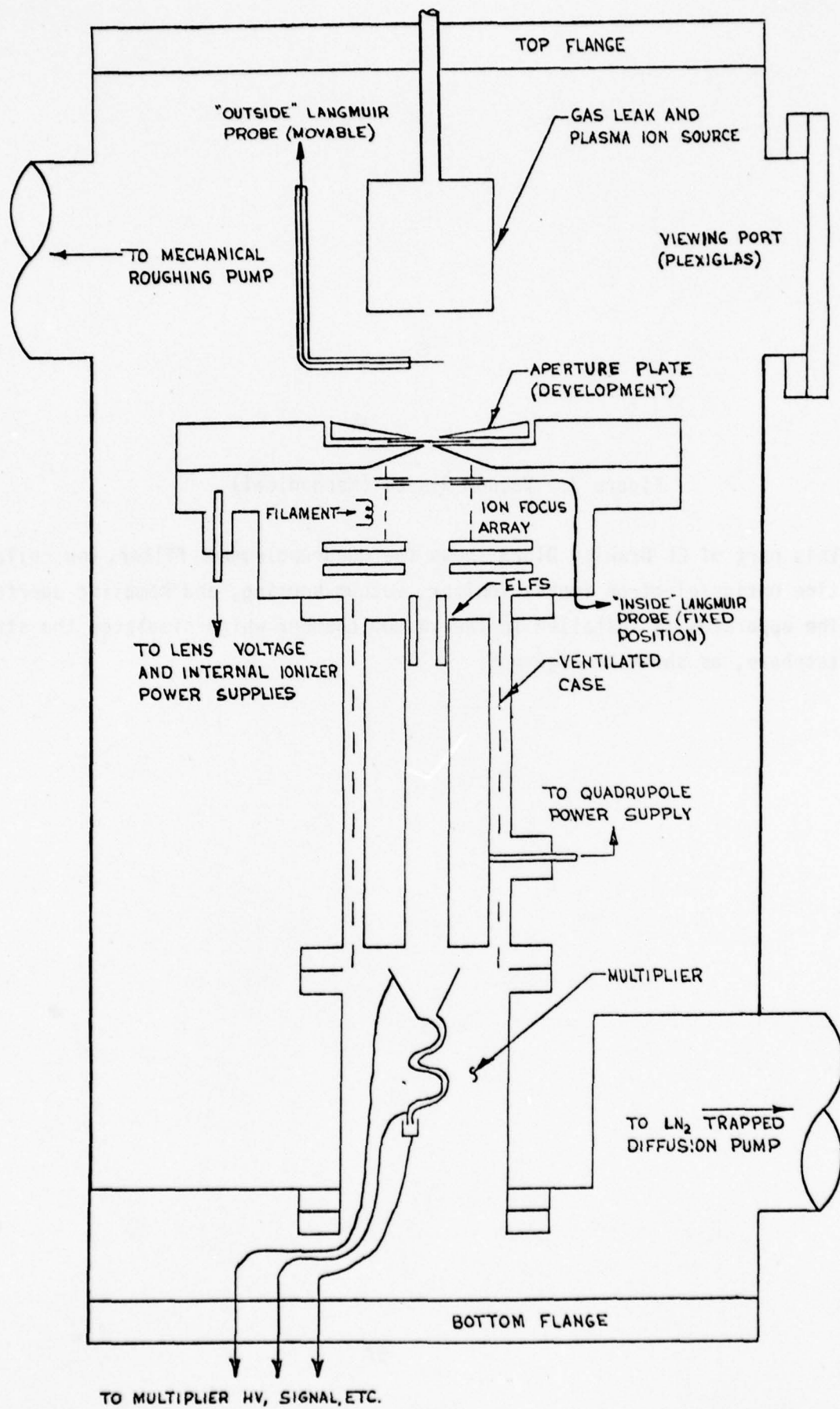


FIGURE 8

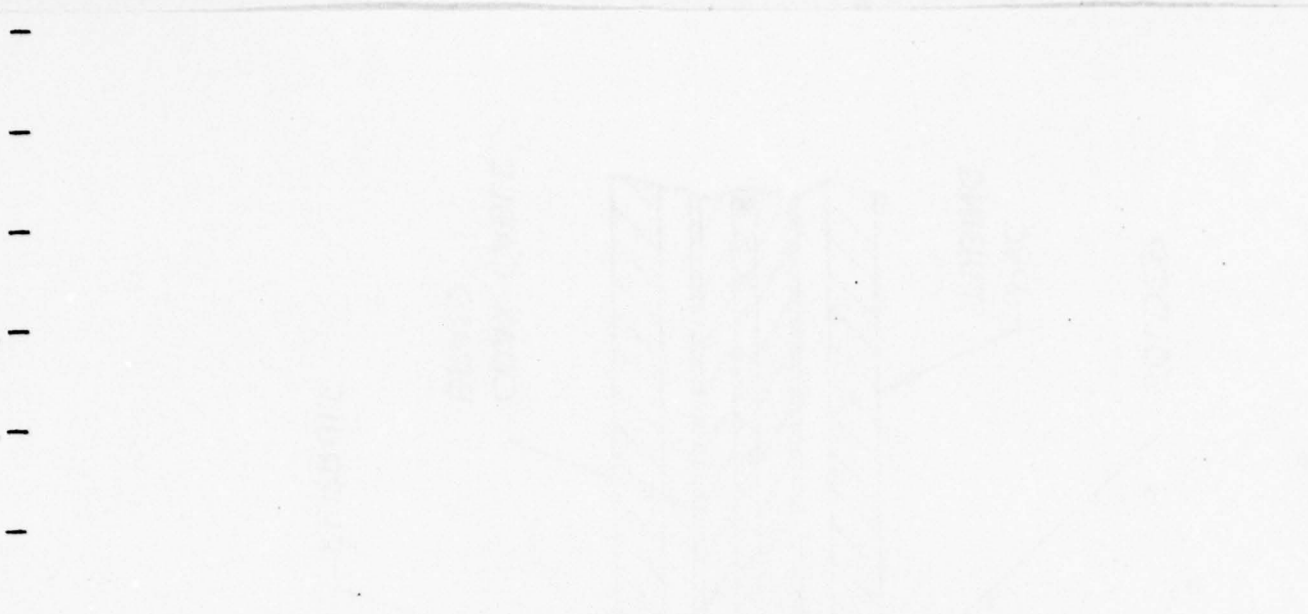


Figure 8: Vacuum System (Schematic)

This figure shows the installation of the ion sampling package, Figure 7, in a vacuum chamber simulating the stratosphere. Parts represented include plasma ion source, movable ("outside") Langmuir probe, fixed ("inside") Langmuir probe, pumping ports, and viewing port.

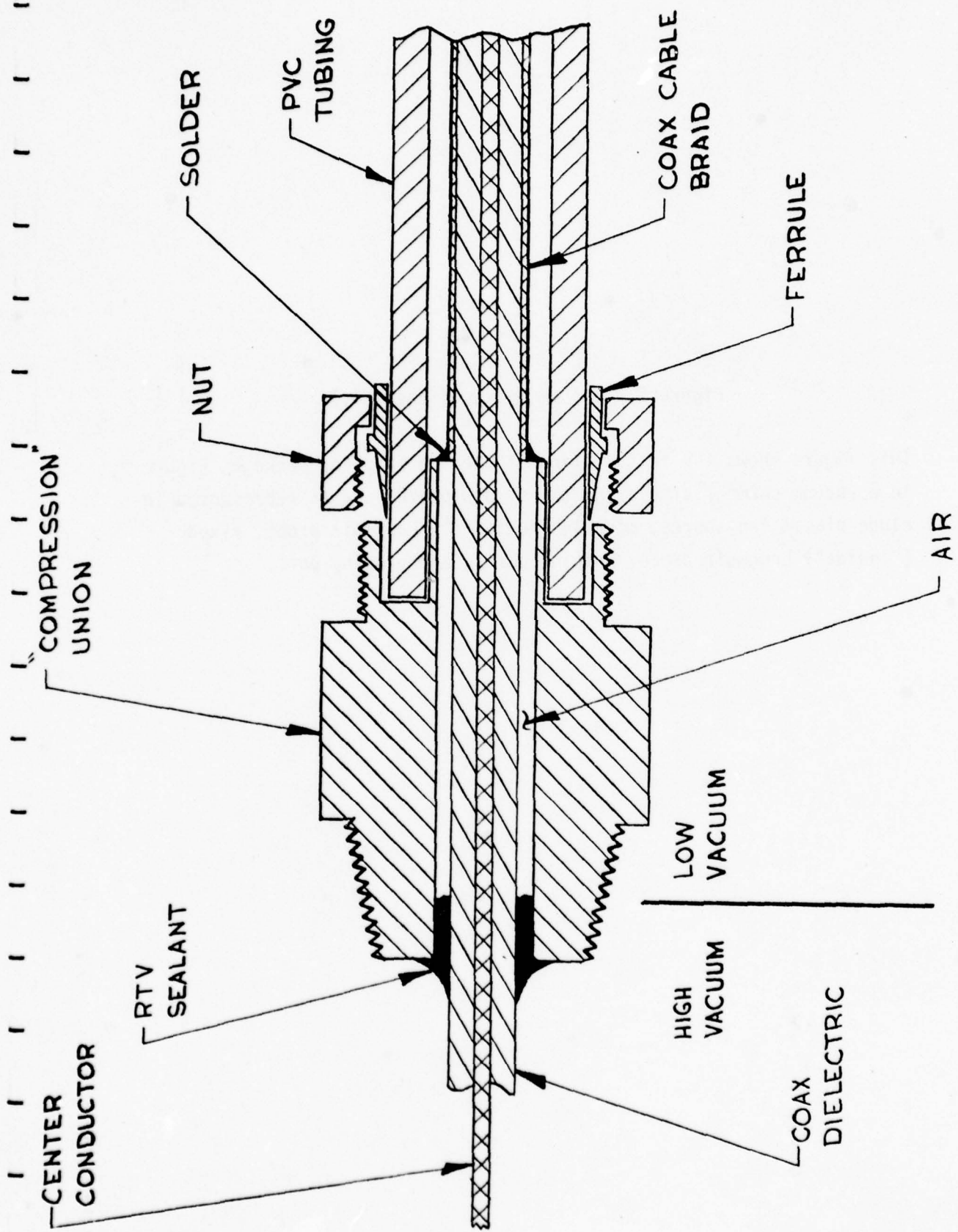


FIGURE 9

Figure 9: RF Feedthru for Use at Approximately One Torr

This design made it possible to lead the quadrupole RF cables through the simulated stratosphere without inducing electrical discharge; the RF cables are effectively jacketed by several millimeters of air at one atmosphere, until they penetrate the high vacuum, where discharge cannot occur.

The ion optics are designed so that they can also be used as an electron impact ionizer so the quadrupole performance can be checked on the background gas, or on intentionally introduced test compounds.

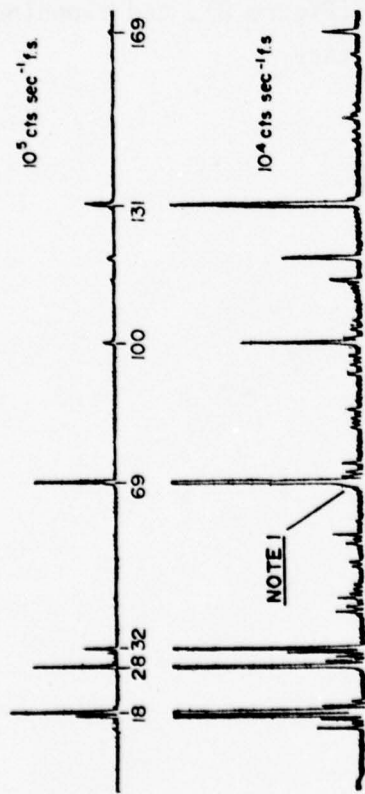
All data taken on this instrument are obtained via a 4501-type counting Channeltron^R on axis, a discriminator/amplifier, and a ratemeter/scaling amplifier driving a two-pen chart recorder, usually with a factor of ten sensitivity difference between the two pens. Mass peak intensities are marked in equivalent counts/second.

Figures 10, 11, and 12 characterize the performance of the mass spectrometer instrument using the electron impact ionizer incorporated in the ion collection optics (275-N2).

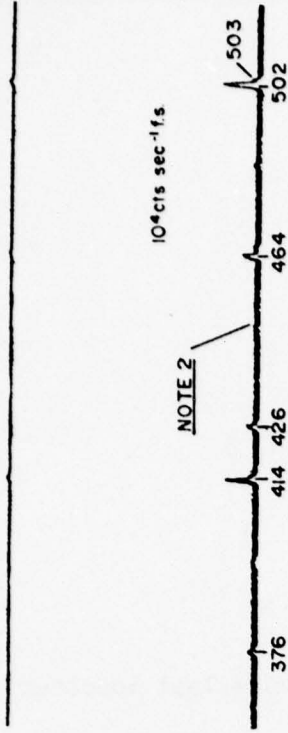
Figure 10 demonstrates the resolution and transmission capability of the instrument from 0 to over 500 amu, using the test compound perfluorotributylamine (PTA, also called FC-43). High mass resolution has been intentionally degraded in favor of sensitivity, so the 502 peak and its ¹³C isotope at 503 are only partially resolved. The instrument is capable, at reduced transmission, of completely resolving these peaks. These data were collected by removing the aperture-holding flange and flooding the vacuum chamber with PTA vapor to a pressure of approximately 10⁻⁵ torr.

In Figure 11 we further illustrate the resolution and transmission characteristics of the mass filter, again using the 275-N2 ion collection and focus optics as an electron impact ionizer. Again, the aperture-holding plate was removed, and the chamber flooded with air at approximately 10⁻⁵ torr. The "integral" spectra demonstrate excellent transmission with only the rudimentary kind of mass resolution available in the operating mode in which the DC voltage is removed from the poles. Comparing the "integral" and resolved spectra provides a measure of the cost, in transmission, of mass resolution. In the very low mass regime this cost is low (about a factor of two here), but at higher masses it is considerable (about a factor of five around 40 amu), and based on experience with similar instruments we believe it to be 10³ or more at very high masses (e.g., over 500 amu).

In Figure 12 we examine in more detail the relationship between transmission and resolution under conditions similar to those described for Figure 11. We show in Figure 12 repeated traces of the 28-32 amu region at



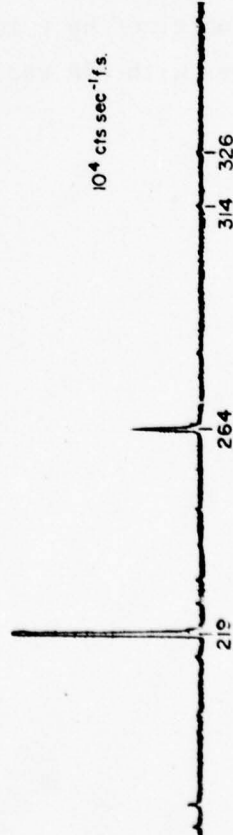
10⁵ cts sec⁻¹/s



10⁵ cts sec⁻¹/s



10⁴ cts sec⁻¹/s



NOTE 1 BROADENING OF LOW MASS SIDE OF 69 PEAK IS DUE TO VIOLENT KINEMATICS OF CF₃* DISSOCIATION FROM PTA MOLECULE; THIS IS NORMAL.

NOTE 2 SEPERATE MEASUREMENTS SHOW > 90% OF BACKGROUND NOISE LEVEL IS DUE TO THE ION GAUGE.

NOTE 3 IONIZING ELECTRONS ~ 10 uA @ 100 eV.

FIGURE 10

Figure 10: Perfluorotributylamine Test Spectrum

PTA spectrum on electron impact using the EI ionizer capability of the 275-N2 ion collection and focusing optics. These spectra illustrate the performance of the instrument in the electron impact ionization mode, particularly with regard to its ability to adequately resolve high masses. Spectra were obtained by removing the Aperture Plate (Figure 8), and flooding the chamber with PTA vapor at approximately 10^{-5} torr.

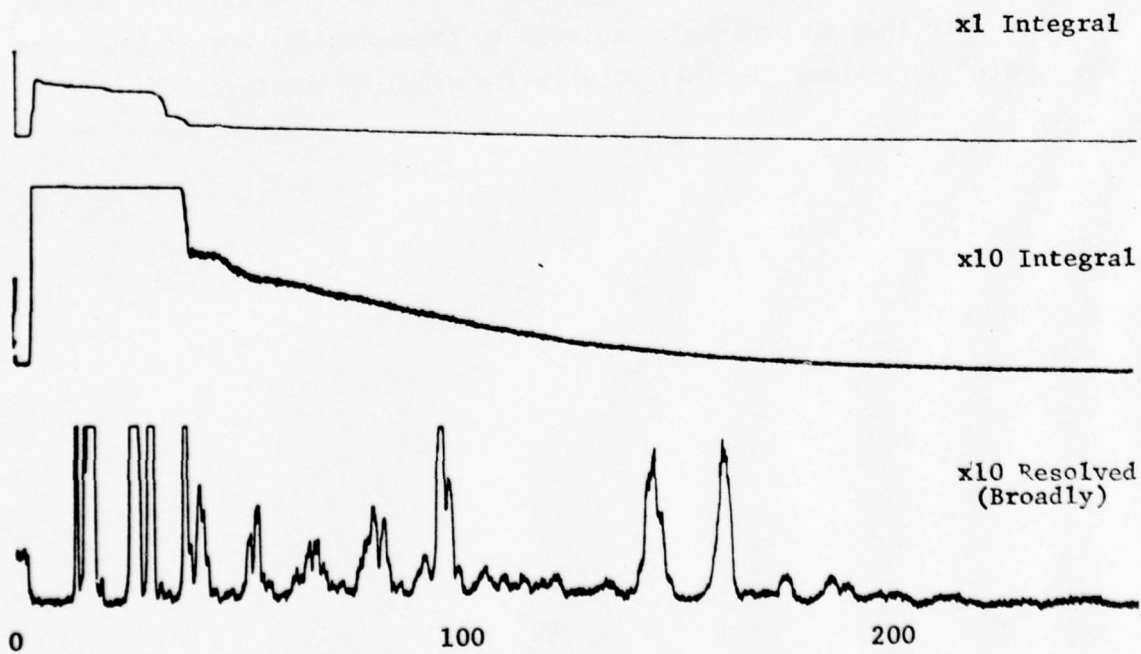
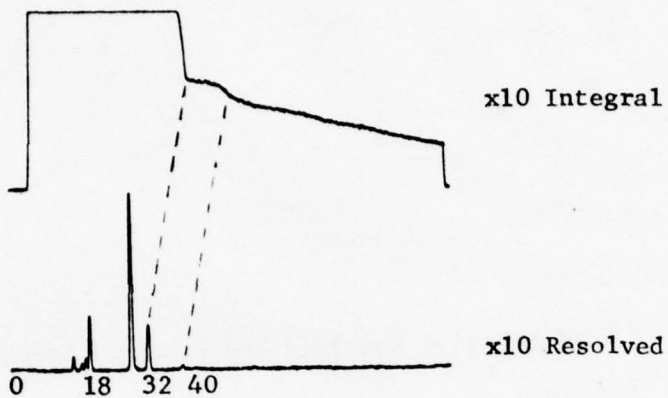
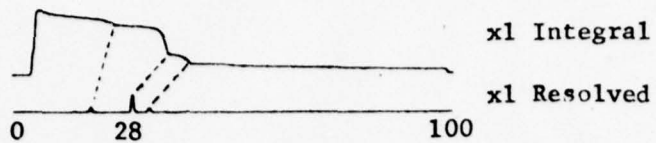


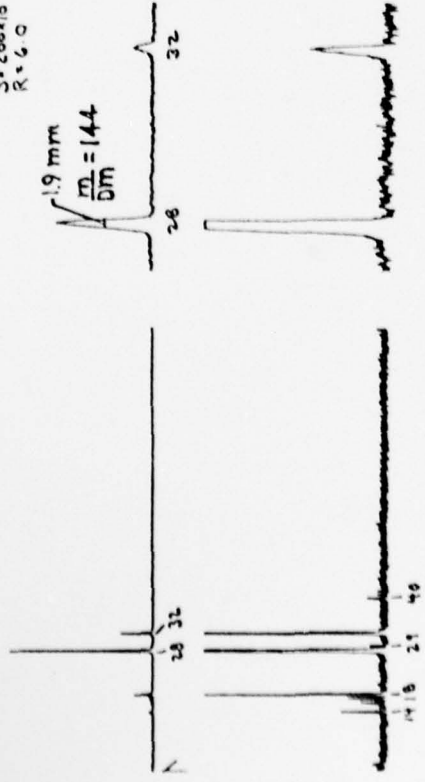
FIGURE II 65

Figure 11: Resolved and Integral Spectra

Further illustrating (see Figure 10) the resolution and transmission characteristics of the mass filter, this figure uses the 275-N2 ion collection and focusing optics as an electron impact ionizer with an air sample. The Aperture Plate (Figure 8) was removed, and the test chamber flooded to approximately 10^{-5} torr. The "integral" spectra demonstrate excellent transmission with only a rudimentary kind of resolution; this mode of operation is well known. It is seen that at low masses the "price" of resolution is modest, i.e., no more than an order of magnitude in transmission, but at high mass the "price" is severe. Further details are given in the text.

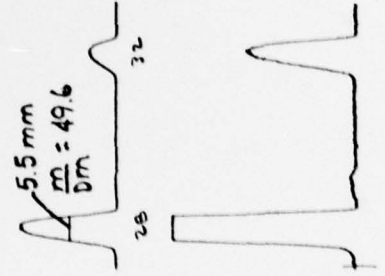
S = 200x10
R = 6.0

1.9 mm
 $\frac{m}{Dm} = 144$



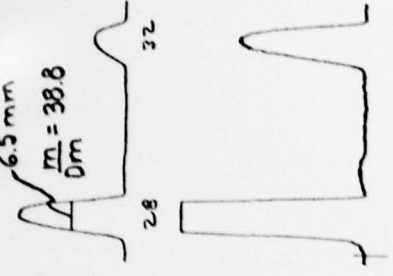
S = 1000x10
R = 4.0

5.5 mm
 $\frac{m}{Dm} = 49.6$



S = 1000x10
R = 3.5

6.5 mm
 $\frac{m}{Dm} = 38.8$



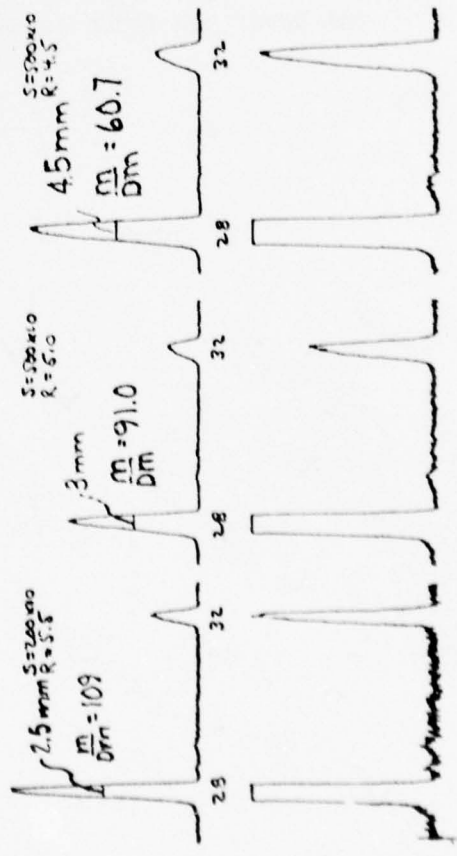
2.5 mm
 $\frac{m}{Dm} = 109$

S = 500x10
R = 6.0

3 mm
 $\frac{m}{Dm} = 91.0$

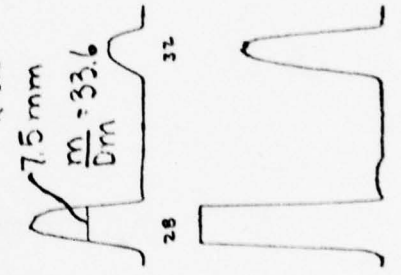
S = 500x10
R = 4.5

4.5 mm
 $\frac{m}{Dm} = 60.7$



S = 1000x10
R = 3.0

7.5 mm
 $\frac{m}{Dm} = 33.6$



S = 1000x10
R = 2.5

9 mm
 $\frac{m}{Dm} = 30.33$

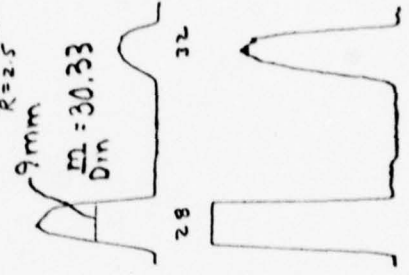


FIGURE 12

Figure 12: Transmission vs. Resolution

Under conditions similar to those in Figure 11, the transmission/resolution tradeoff is here examined experimentally. A series of mass scans of the region including the N_2^+ (23 amu) and O_2^+ (32 amu) air peaks are made at various resolution control settings. Each lower pen trace represents 4x the upper pen trace sensitivity. The results are plotted in Figure 13.

various resolution settings, and in Figure 13 graphically display the result. Note that a resolution ($m/\Delta m_{1/2}$) of about 50 is sufficient to completely separate $^{14}\text{N}^{14}\text{N}^+$ from $^{14}\text{N}^{15}\text{N}^+$, with the advantage that at this low resolution the peaks are approximately flat topped rather than assymmetrically triangular. Flat topped peaks are more suitable for making stable intensity measurements, especially in apparatus electronically programmed to examine ion signals at specific masses without recording complete spectra.

Details of how to operate the ion optics package as an electron impact ionizer are not given here because the 275-N2 and L2 Instruction Manual (deliverable item) covers this topic. The actual mounting structure of the AFGL device differs from the standard N2 package because of AFGL's unique pumping requirements, but ion optically AFGL has been supplied with the latest version of the 275-N2 device.

To demonstrate the functioning of the 275-N2 ion optics package as a collector of ions emerging from a small differential pumping aperture, we show Figures 14 and 15. Each of these uses a 275-N2 package in a differentially pumped vacuum system. Figure 14 shows ions emerging from a 0.002" aperture sampling an atmospheric pressure plasma produced by a ^{63}Ni β -ray source in clean, dry nitrogen, and Figure 15 shows ions emerging from an approximately 0.020" aperture sampling an approximately 1 torr plasma produced by a 2450 MHz microwave discharge in research grade helium with 1.02 ppm H_2 added.

In Figure 14, the sampled plasma is formed at approximately one atmosphere in clean, dry nitrogen at about 200°C; excitation is with 1 mCi ^{63}Ni . The two spectra illustrate the effect of slightly changing the trace water concentration. The excellent performance of the apparatus under these conditions leads us to expect similarly excellent performance in the simulated stratospheric sampling configuration (Figure 8). Further details concerning the experimental conditions and apparatus which generated these data are given in Reference 14.

In Figure 15, the sampled plasma is formed by a 2450 MHz discharge in helium at several torr, i.e., in the range of atmospheric pressures of

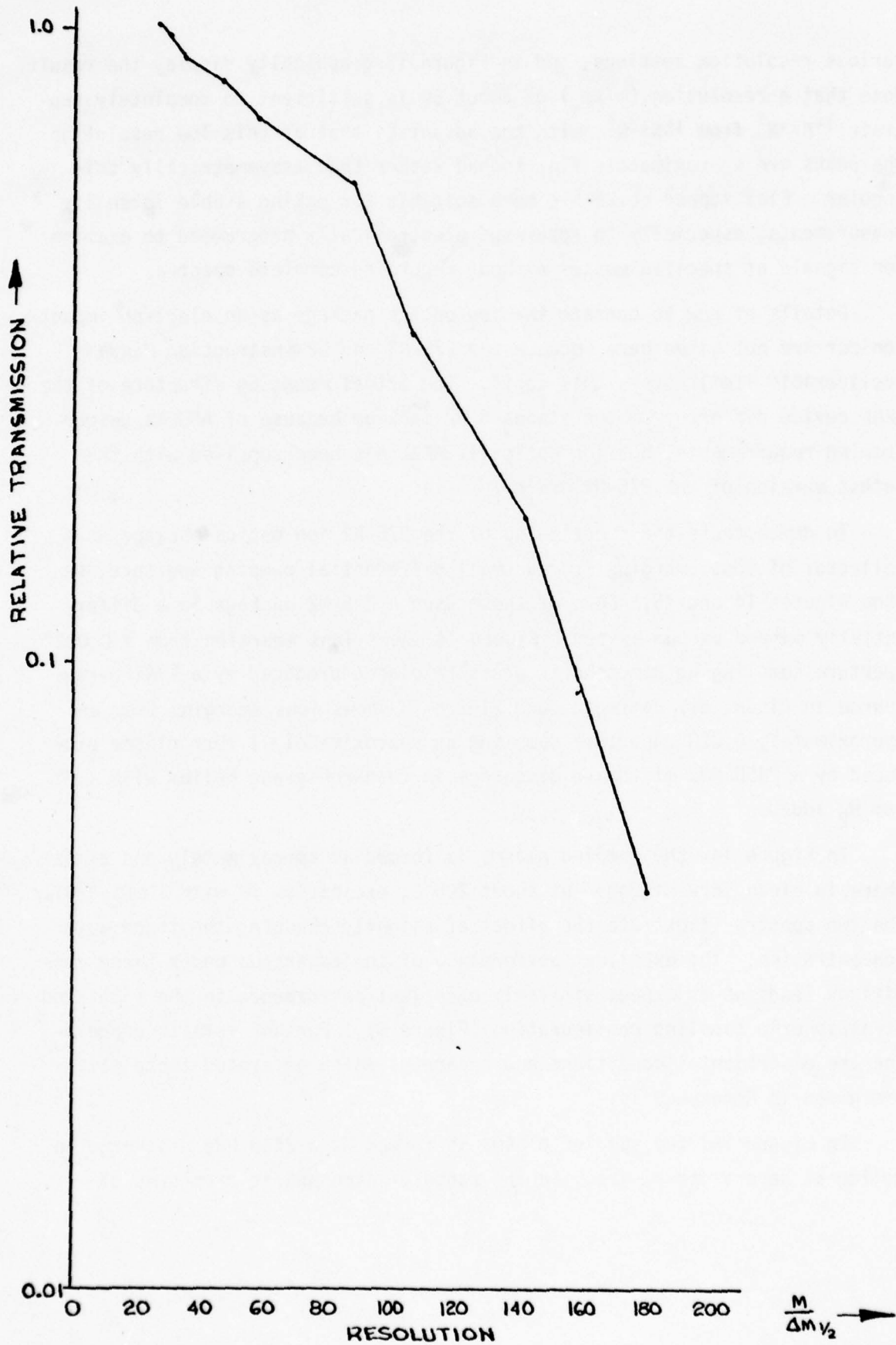


FIGURE 13

Figure 13: Transmission Vs. Resolution

This graph summarizes the data shown in Figure 12. The resolutions ($m/\Delta m_{1/2}$) are calculated on the N_2^+ peak in each case. It is seen that the price of additional resolution is indeed high, and best experiment designs will involve operating at the lowest resolution providing acceptable separation. Furthermore, at lower resolution the peak shape is more flat topped than at higher resolution, where peaks are asymmetrically triangular. Flat topped peaks are more suitable for intensity measurements, especially in apparatus electronically programmed to examine ion signals at specific masses without recording complete spectra.

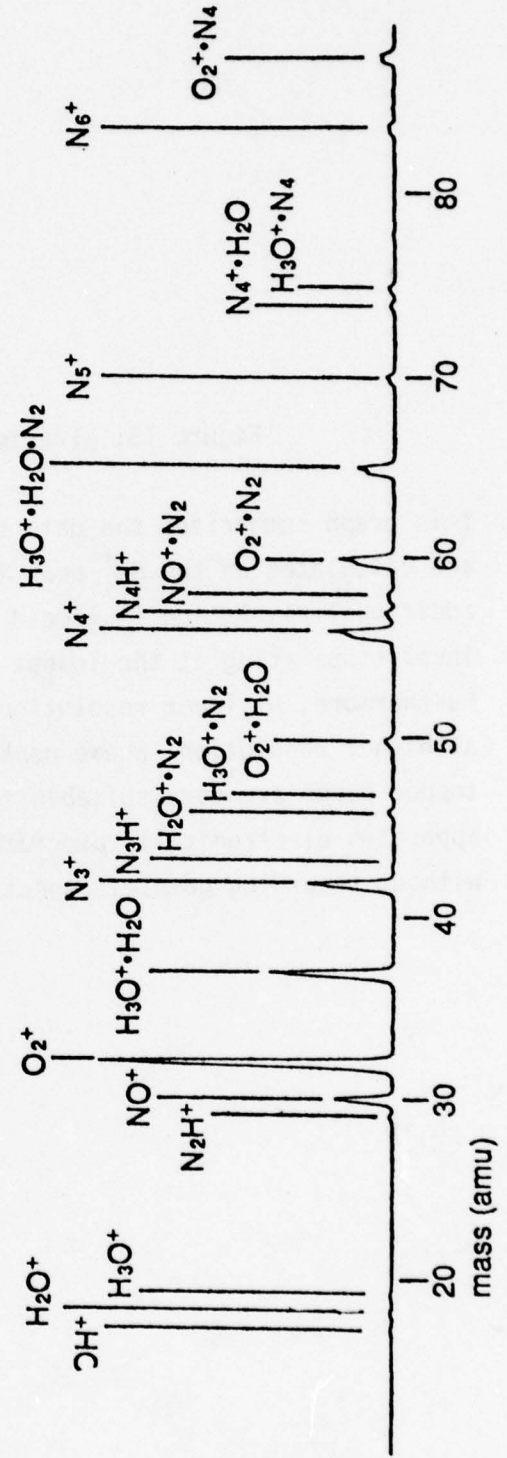
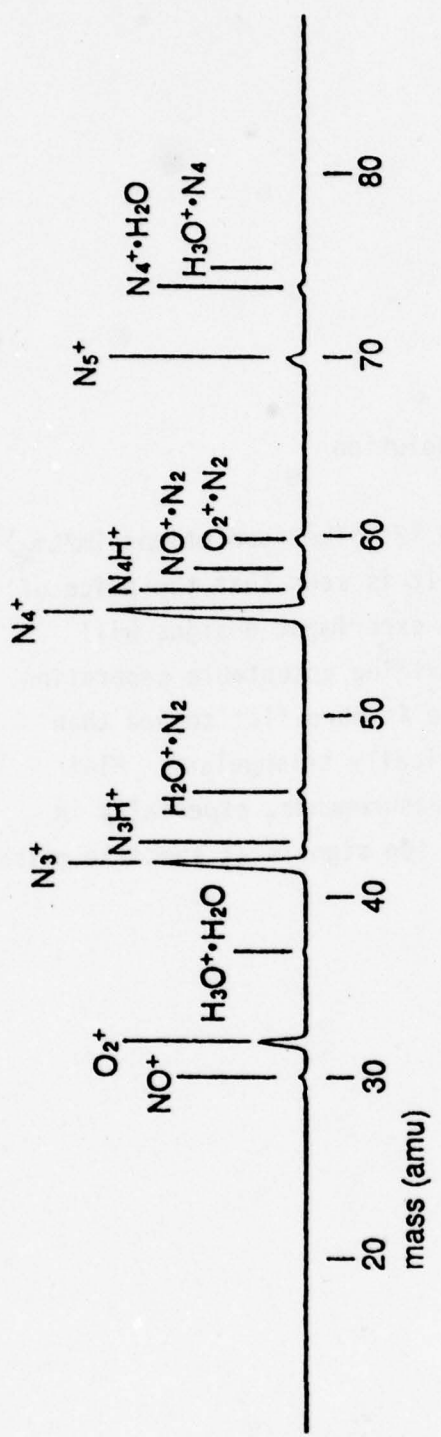


FIGURE 14
72

Figure 14: API Spectrum

This illustrates the use of the 275-N2 ion collection and focusing assembly to analyse ions from a weak atmospheric pressure plasma. The ion focusing optics used to collect these data are identical to those installed in the AFGL instrument, and the ion sampling aperture is very similarly located with respect to the ion optics. The sampled plasma is formed at approximately 1 atmosphere, in clean, dry nitrogen at about 200°C; excitation is with 1mCi ^{63}Ni . The two spectra illustrate the effect of slightly changing the trace water concentration. The excellent performance of the apparatus under these conditions leads us to expect similarly excellent performance in the simulated stratospheric sampling configuration (Figure 8). Further details concerning these spectra are given by M. W. Siegel and W. L. Fite, "Terminal Ions in Weak Atmospheric Pressure Plasmas -- Applications of Atmospheric Pressure Ionization to Trace Impurity Analysis in Gases", J. Phys. Chem. 80 2871-81 (1976).

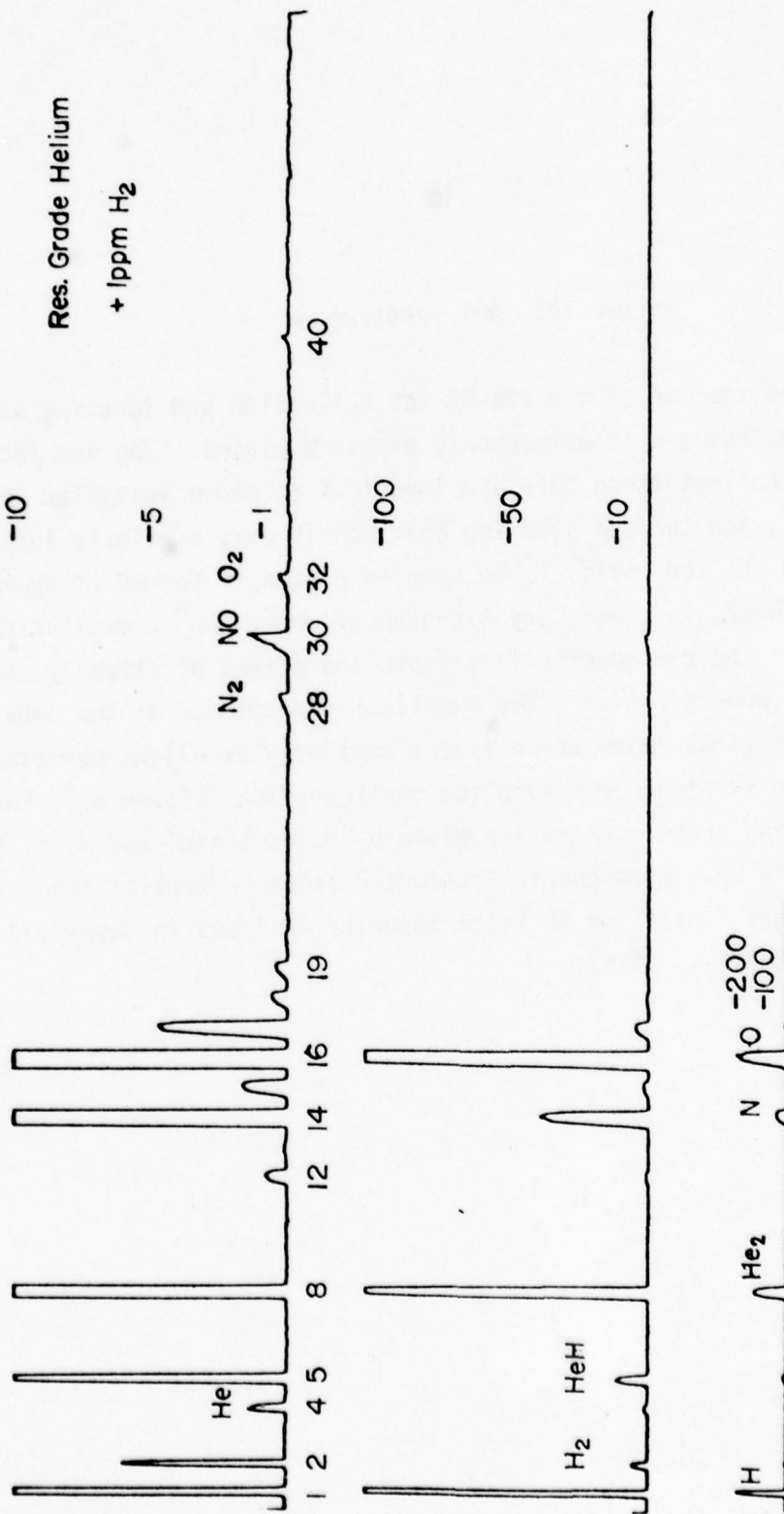


FIGURE 15

Figure 15: Microwave Discharge Spectrum

This illustrates the use of the 275-N2 ion collection and focusing assembly to analyze ions from a plasma at several torr, i.e., in the range of stratospheric pressure of interest to AFGL. Ion densities are higher here, the plasma being excited by approximately 1 watt/cm³ of microwave power at 2450 MHz. Signal-to-noise ratios here are, however, very large, and extrapolation of these results to the lower ion density regimes to be encountered in simulated or real stratospheric ion sampling appears entirely justifiable. Note that, as expected, the ion spectra are dominated by the effect of trace impurities, the pseudo-primary ions He₂⁺ accounting for only about 25% of the total ion current. In this apparatus, the discharge was confined by a quartz tube with a sampling aperture located, relative to the 275-N2 optics, in about the same place as the sampling aperture used in the simulated stratospheric measurements (Figure 8). The excellent performance of the apparatus in this configuration leads us to expect similarly excellent performance in the stratospheric sampling configuration.

interest to AFGL. Ion densities are higher here, the plasma being excited by approximately 1 watt/cm³ of microwave power; signal-to-noise ratios are, however, very large and extrapolation of these results to the lower ion density regimes to be encountered in simulated or real stratospheric ion sampling appears entirely justifiable. The again excellent performance of the apparatus in this second configuration further leads us to expect similarly excellent performance in the stratospheric sampling configuration.

V - ANCILLARY APPARATUS

In this section we discuss several additional items which were constructed for use in the test program.

1. Atmospheric Pressure Ion Source

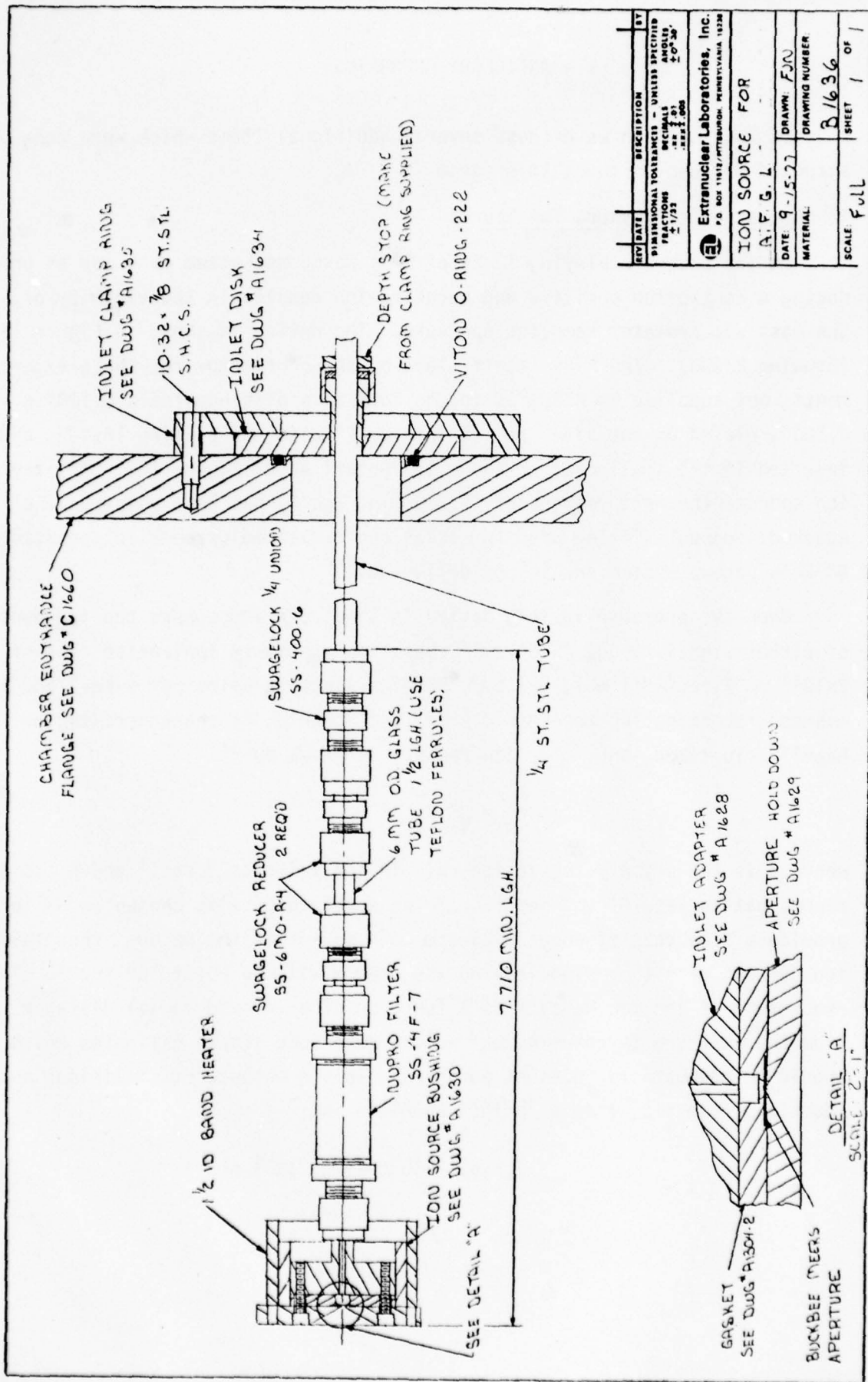
An ion source employing 1 mCi of ^{63}Ni was constructed as a way of producing a controlled positive and negative ion density in the vicinity of the mass spectrometer sampling aperture. The device is shown in Figure 16, (Drawing B1636). The ^{63}Ni itself (lent by the contractor for these experiments, not supplied to AFGL) is in the form of a platinum foil, 0.100" x 0.500", plated on one side, rolled into a "C" with the plating inside, and inserted in the small chamber shown in "Detail A" of Figure 16. Only the ion source (the part designated "7.710 min. lgh.") has been shipped. The quick-disconnect fitting used for axial and radial adjustment is specific to EL's vacuum system and is non-deliverable.

When the pressure in this device is about one atmosphere the ion density of either sign is about $4 \times 10^8 \text{ cm}^{-3}$, based on a primary ionization rate of $2 \times 10^{11} \text{ cm}^{-3} \text{ sec}^{-1}$ (1 mCi, 0.1 cm^3 , 500 ion-electron pairs per β -ray) and an assumed recombination rate of $10^{-6} \text{ cm}^3 \text{ sec}^{-1}$, which is characteristic of heavily clustered ions. The ion density is given by⁽¹⁴⁾

$$n_0 = \sqrt{S/R_0}$$

where S is the primary ionization rate in ion pairs $\text{cm}^{-3} \text{ sec}^{-1}$ and R_0 is the recombination rate of $\text{cm}^3 \text{ sec}^{-1}$. If the aperture size is chosen so as to provide a flow rate of about $0.25 \text{ atm-cm}^3\text{-sec}^{-1}$ into the vacuum, then the ion current of either sign leaving the source will be about 10^8 sec^{-1} . The exact form of the ion density as a function of axial and radial distance from the aperture is unknown, but we can make some simple estimates which should be adequate for present purposes. In the absence of collisions and reactions, the flux from a "point" aperture is

$$j(r, \theta) = 10^8 \cos \theta / \pi^2 \text{ cm}^{-2} \text{ sec}^{-1}$$



REV	DATE	DESCRIPTION	BY
		DIMENSIONAL TOLERANCES - UNLESS SPECIFIED FRACTIONS DECIMALS ANGLES	
		1/32 .001 1/16 .002 1/8 .003 1/4 .005 3/8 .007 1/2 .010 3/4 .015 1 .020 1 1/4 .030 1 1/2 .040 2 .060 2 1/2 .080 3 .100	
Extranuclear Laboratories, Inc. P. O. BOX 11812, PITTSBURGH, PENNSYLVANIA 15228			
ION SOURCE FOR A.P.G.L.			
DATE 9-15-77		DRAWN: FJN	
MATERIAL:		DRAWING NUMBER	
		B/1636	
SCALE: Full		SHEET 1 OF 1	

FIGURE 16 78

CHAMBER ENTRANCE FLANGE SEE DWG # C1660

10-32 x 7/8 ST. STL. S.H.C.S.

INLET CLAMP RING SEE DWG # A1635

INLET DISK SEE DWG # A1634

DEPTH STOP (MAKE FROM CLAMP RING SUPPLIED)

VITON O-RING - 222

1/4 ST. STL. TUBE

7.710 MIN. LGH.

1/2 ID BAND HEATER

ION SOURCE BUSHING SEE DWG # A1630

SS-4 F-7

NUPRO FILTER

SS-6 MO-R-4 2 REQ'D

SWAGELOCK REDUCER

6 MM OD GLASS TUBE 1/2 LGH. (USE TEFLON FERRULES)

SS-400-6

SWAGELOCK 1/4 UNION

INLET ADAPTER SEE DWG # A1628

APERTURE HOLD DOWN SEE DWG # A1629

GASKET SEE DWG # A1628

BUCKBEE MEERS APERTURE

DETAIL "A"

SCALE 2-1"

Figure 16: API Source Assembly (Mechanical)

The depicted atmospheric pressure ion source was constructed to produce appropriately low ion densities in the vicinity of the sampling aperture (Figure 8). Provision is made for translation along the axis and for limited transverse motion. The electrical isolation ("6 mm O.D. Glass Tube") allows the ion source to be biased with respect to the sampling apparatus. Functional details of this source are similar to those in the API source used to obtain the data shown in Figure 14. This ion source was delivered to AFGL for further tests as may be deemed appropriate.

and the corresponding density is

$$\rho(r,\theta) = 10^8 \cos\theta / \pi r^2 v \text{ cm}^{-3}$$

where v is the ions' thermal velocity, i.e., $\approx 5 \times 10^4 \text{ cm sec}^{-1}$. It follows that on axis the ion density drops to 10^4 cm^{-3} in 2.5 mm, and to 10^2 cm^{-3} in 2.5 cm. In the presence of collisions the problem is more difficult, but qualitatively we expect the ion density to drop more slowly because the thermal velocity is replaced by the smaller bulk flow velocity. Recombination, diffusion, and essentially hydrodynamic effects complicate the problem.

It would nevertheless appear that within a reasonable range of working distances this ionizer should produce in the region of the mass spectrometer sampling aperture an ion density in the range anticipated for the stratosphere, and that the ion density at the sampling aperture should be effectively controllable by simply moving the source.

2. Corona Discharge Ion Source

A corona discharge source (Figure 17) was constructed to provide higher ion density than that available from the atmospheric pressure ion source. This source was constructed from stock parts to fill an immediate need and no formal design drawing was made. Its form is a grounded mesh cage surrounding a tungsten needle at an appropriate high voltage. It was convenient and perhaps advantageous to make the gas feed coaxial with the needle.

The ion density in the cage can be very roughly estimated by considerations similar to those used for the atmospheric pressure ion source, above. The corona current was typically the order of $10 \mu\text{A}$ at a voltage the order of 3kV, so the primary energy deposition rate was the order of 0.03 watts or roughly $2 \times 10^{17} \text{ eV/sec}$. At a mean ion pair production rate estimated by the W-value⁽¹⁵⁾ of one ion pair/35 eV, it follows that we produce the order of $5 \times 10^{15} \text{ ion pair/sec}$. The active volume is the order of 15 cm^3 (as determined by the visible glow), so in the above formulation

$$S \approx 3 \times 10^{14} \text{ cm}^{-3} \text{ sec}^{-1}$$

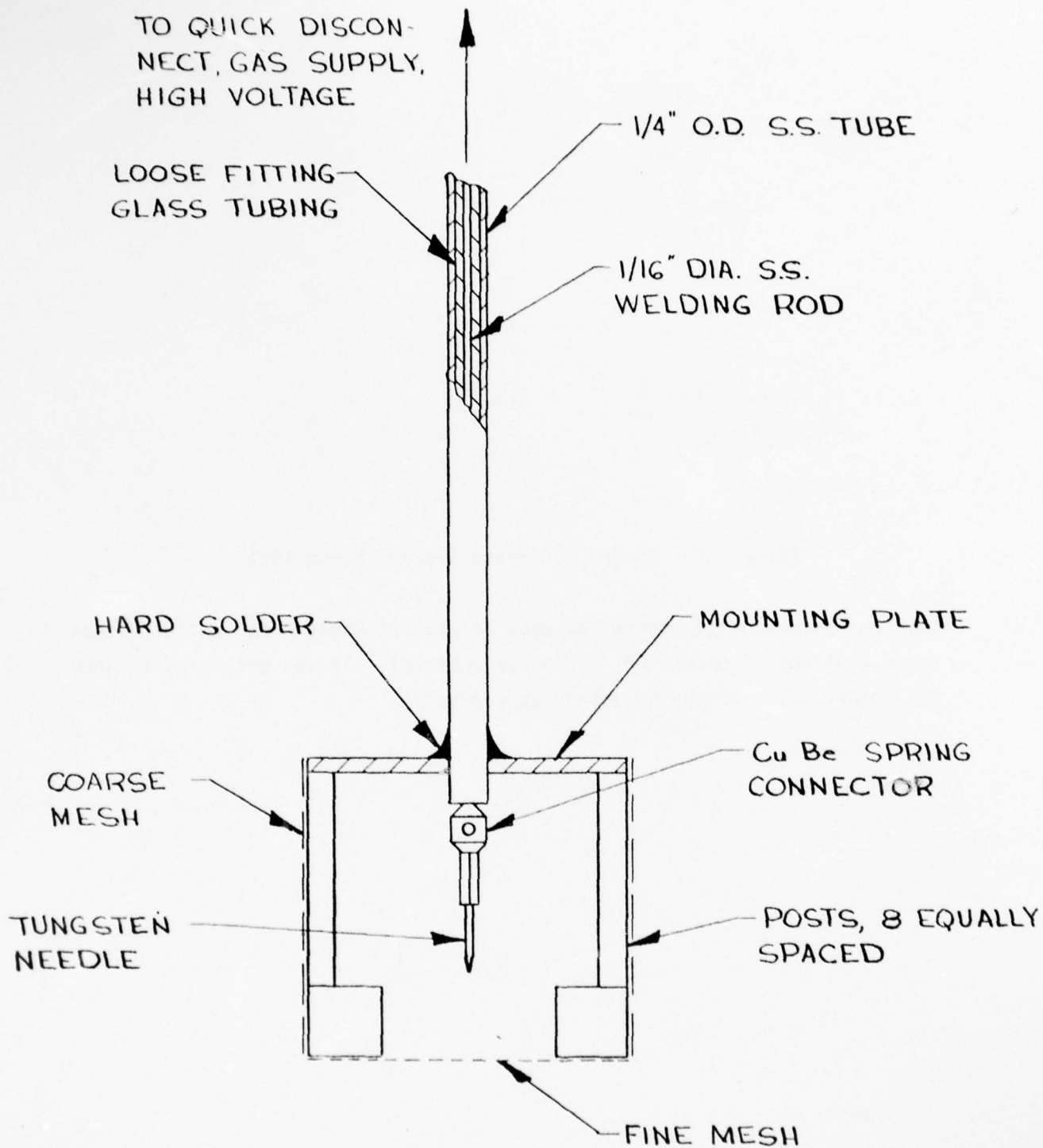


FIGURE 17

Figure 17: Corona Discharge Source (Schematic)

This corona discharge source was used to produce higher ion densities than those available from the API source (Figure 16). It was delivered to AFGL for further tests as may be deemed appropriate.

and

$$n_0 \approx 2 \times 10^{10} \text{ cm}^{-3}$$

with an assumed recombination rate of $10^{-6} \text{ cm}^3 \text{ sec}^{-1}$. Because of the square root, this number is relatively insensitive to S.

To estimate the ion density as a function of distance from this source, we can assume field free conditions (so ion motion is diffusive and ambipolar), and uniform planar geometry as would apply if the distance to the plane of the sampling aperture were a small fraction of the cage diameter. Ions are destroyed by recombination according to

$$\dot{n} = -Rn^2$$

or

$$n^{-1} = n_0^{-1} + Rt$$

where t is the "age" of the recombining plasma, n is the instantaneous density, and n_0 is the initial density. The translation from age to position is given by

$$t \approx d^2/D$$

where d is the distance from the planar source and D is the diffusion constant. It thus follows that

$$n^{-1} = n_0^{-1} + \frac{Rd^2}{D}$$

This function, for $n_0 = 2 \times 10^{10} \text{ cm}^{-3}$, $R = 10^{-6} \text{ cm}^3 \text{ sec}^{-1}$, and $D \approx 100 \text{ cm}^2 \text{ sec}^{-1}$ at about 1 torr, is plotted in Figure 18. While the approximations are very crude, and the planar approximation is certainly invalid at distances greater than one or two centimeters, the qualitative behavior shown here is expected to be valid. That is, the very high ion density at the source is expected to drop by several orders of magnitude very quickly, then to change relatively slowly in the range of practical working distances.

3. Prototype External Ion Collection Array

An experimental ion collection array of the type discussed in the design evaluation report was constructed as sketched in Figure 19. Its construction

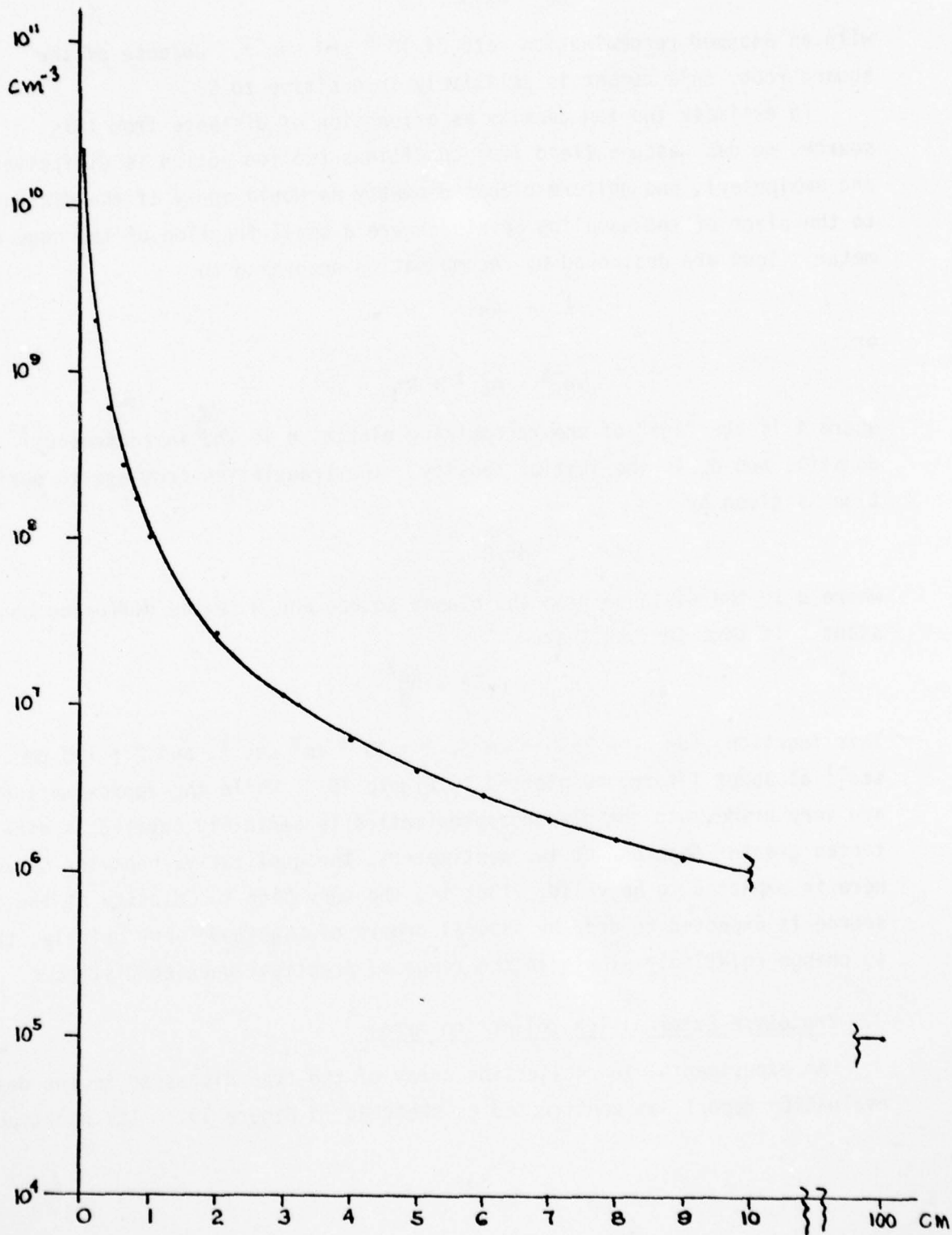


FIGURE 18

Figure 18: Estimated Ion Density vs. Position

As discussed in the text, this figure graphically displays the calculated estimated ion density vs. position delivered by the corona discharge ion source of Figure 17. Calculations are based on the plane-parallel plate approximation.

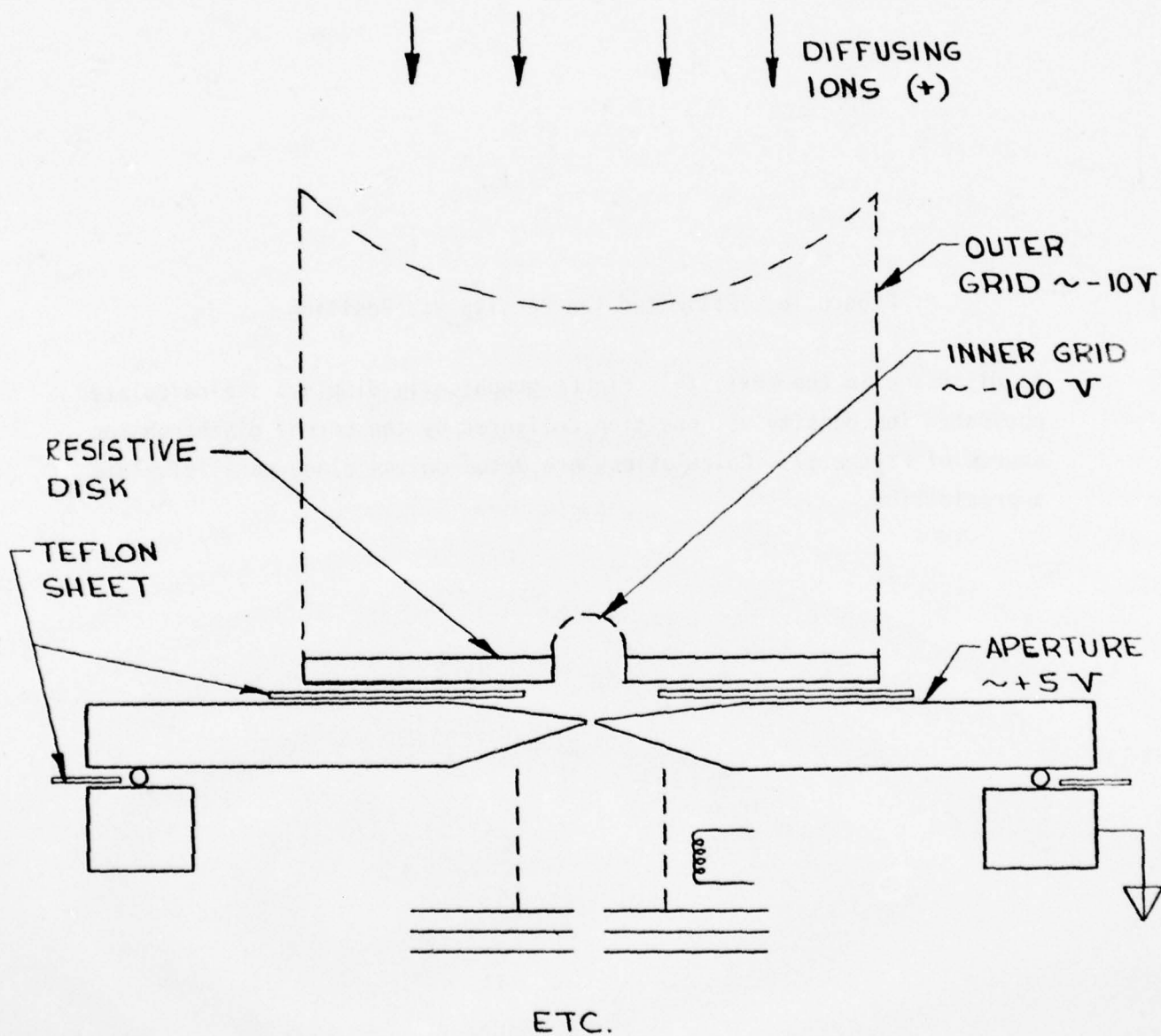


FIGURE 19

Figure 19: External Ion Collection Array

Based on the principles developed in Section III.9 (Figures 4, 5, and 6), an experimental "external ion collection array" was constructed as sketched. Potentials shown correspond to the discussion in Figure 20. Incomplete understanding of the density and energy distribution of the ions made by the corona discharge source (Figure 17) made it impossible to develop a good understanding of the potential value of this device. It has been preserved for future experiments.

was adequate for the tests, but too crude a design to be suitable for shipment to AFGL. It has been preserved and may be used for further tests in the future.

The theory of the device rests on the realization that ion mobilities at about 1 torr are only a few (cm/sec)/(volt/cm), while thermal velocities are the order of 5×10^4 cm/sec. Thus even fairly strong fields of the order of a few hundred volt/cm can perturb, but not dominate ion motion. Under these circumstances, unconventional ion-optical potential distributions can be used. As a specific example, in Figure 20 we show a possible set of potentials which might be applied to the array of Figure 19 and the corresponding ion speeds. For simplicity, potential gradients are represented as linear, and electric fields as, therefore, constant.

The interesting thing to note is that in a vacuum, ions would be forbidden to traverse the region between the inner grid and the aperture, but at high pressure the bulk gas flow dominates their motion and the retarding effect of the reversed field is only a perturbation.

It is thus intended that, biased approximately as shown, the array will urge distant ions into the large volume inside the outer grid, then direct them towards the inner grid where they will be caught up in the increasingly rapid fluid motion and carried through the aperture into the vacuum.

It is to be reiterated, as discussed in the original proposal and in Section III, that this part of the project was undertaken as a "long shot". Our general feeling about any external ion collection array is that it is unlikely to work, and if it does work it is likely to induce undesirable effects such as unnatural ion chemistry, mass discrimination, and de-clustering. The main reason for our pessimism is the fruitlessness of trying to induce charge imbalances of any significant magnitude: the electrostatic forces resulting from such imbalances will act to balance and cancel the external fields imposed by the apparatus.

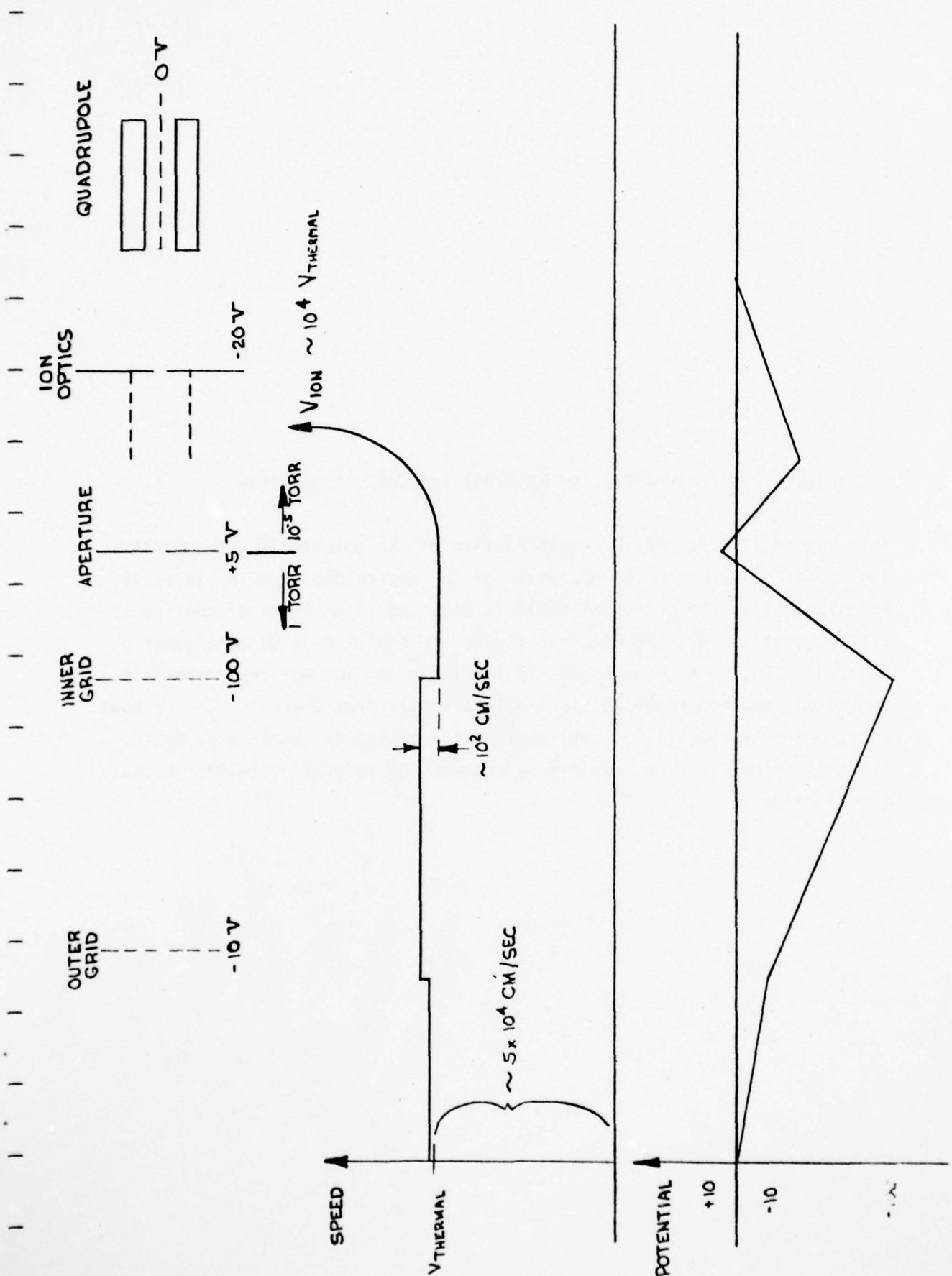


FIGURE 20

Figure 20: Potentials for External Ion Collection Array

This figure is a schematic representation of the potentials and expected ion speeds relevant to the operation of the device depicted in Figure 19. For simplicity, the potential field is depicted as a series of continuous line segments, i.e., the electric fields are depicted as discontinuously constant. In the high pressure (~ 1 torr) region, ion motion is mobility dominated, and ion speeds differ only slightly from thermal. In the mass spectrometer vacuum (10^{-5} torr) region, ion motion is accelerated by the ion collection field and rapidly approaches the several eV ($\sim 10^4 \times$ thermal speed) range.

Movable Langmuir Probe

To facilitate ion density measurements in the simulated stratosphere, a Langmuir probe was constructed in such a way that measurements could be made as a function of position along the instrument axis, and as a function of radial position from the axis. The device is non-deliverable, but we report its design both for future reference and also because AFGL may find it useful in later tests. The design is shown in Figure 21.

Fixed Langmuir Probe

As depicted in Figure 8, a probe was installed in the "basket" of the ion focus array to facilitate ion density measurements between the sampling aperture and the mass filter entrance. It was a very simple design, a length of 0.020" teflon coated wire (0.014" wire diameter) with the insulation removed from about 3 mm at a location a few cm from one end. The wire was threaded through the basket and the stripped part roughly centered. The sampled current was led out through the spare feedthrough in the mass spectrometer test housing.

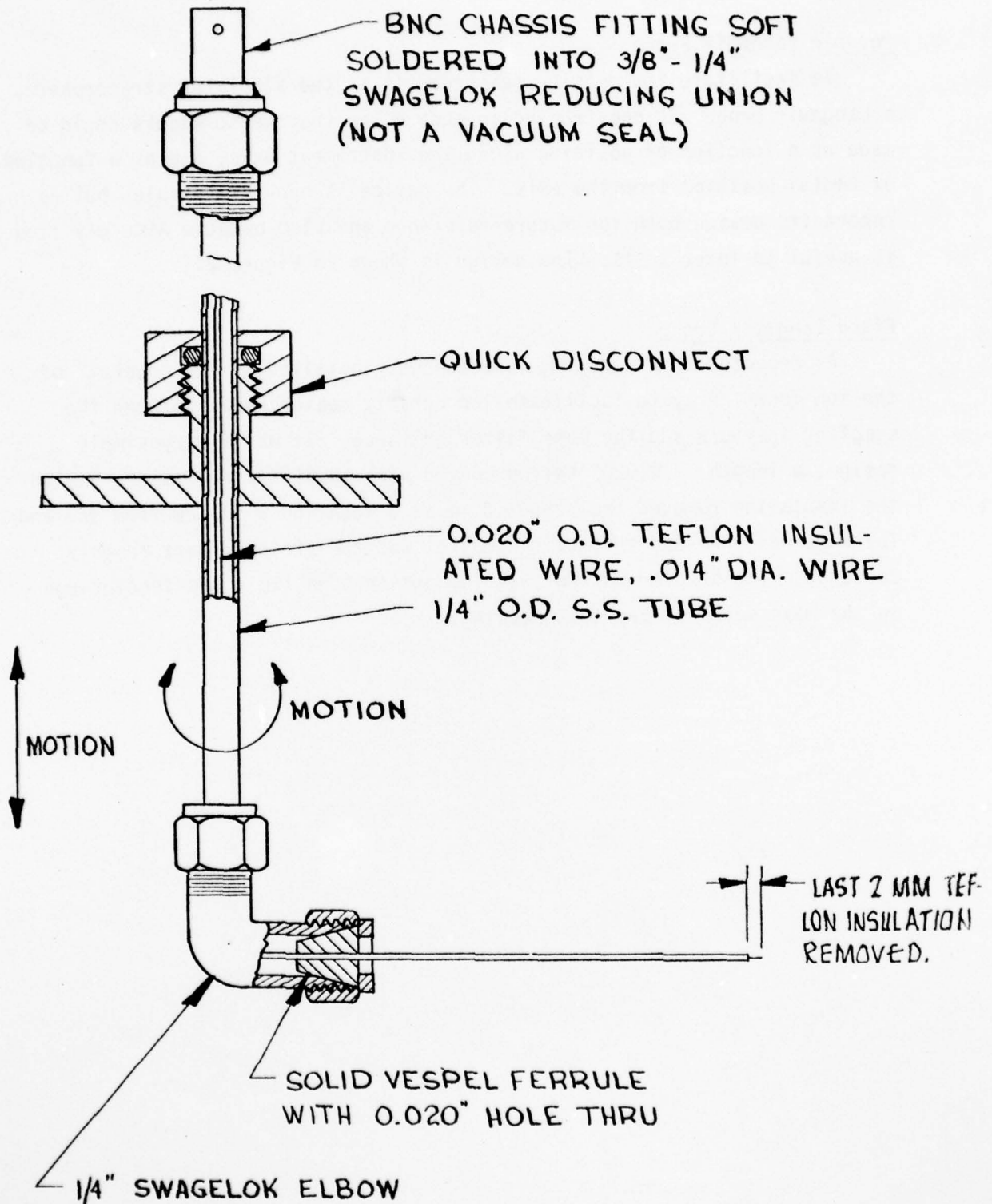


FIGURE 21

Figure 21: "Outside" Langmuir Probe

A simple Langmuir probe provided with axial and rotational movement allows mapping of the ion density in all regions of interest. Some measurements with this probe are shown in Figure 27.

VI - EXPERIMENTAL PROGRAM AND RESULTS

Figure 22 serves to define the external constraints on the program by showing, as a function of altitude, the pressure, density, temperature and approximate mean free path. The stratosphere is defined as the region between 20 and 50 km, with a corresponding pressure range of 38 to 0.61 torr. AFGL has informed us that the altitude limit of balloons capable of carrying instruments of the type we are discussing is about 45 km, but that the practical limitation for the presently contemplated AFGL project will probably be about 40 km, where the pressure is slightly over 2 torr. It is intended that the instrument continue to operate at as low an altitude as possible, limited by the gas load handling capability of the cryopump. Because of pumping speed limitations in the test apparatus, much of the laboratory work was done at somewhat lower pressures with the intent of scaling the results. These limitations were described in the original proposal for this work, and are quantified below.

In the free molecular flow regime, the pumping speed of an aperture of negligible thickness is given by

$$S = A\bar{v}/4$$

where A is the aperture area and \bar{v} the mean molecular speed. If the distribution is Maxwellian

$$\bar{v} = \sqrt{\frac{8}{\pi} \frac{kT}{m}}$$

In actuality contemplated apertures are sufficiently large compared to the mean free path at stratospheric pressures that flow begins in the viscous region, enters the transition region somewhere in or beyond the aperture, and is described by free molecular flow only some distance into the mass spectrometer vacuum. Ignoring these complications, which we will do for simplicity, is generally known to introduce errors which rarely exceed a factor of two and are thus acceptable for the following discussion.

Figure 23 shows the relationship between aperture diameter, acceptable inside pressure, flight package pumping speed, and minimum working altitude.

AD-A069 726

EXTRANUCLEAR LABS INC PITTSBURGH PA

F/G 14/2

STUDIES OF THE BALLOON-BORNE MASS SPECTROMETER PROBLEM. (U)

AUG 78 M W SIEGEL, W L FITE

F19628-77-C-0183

UNCLASSIFIED

AFGL-TR-78-0220

NL

2 OF 2

AD
A069726



END
DATE
FILMED
7-79
DDC

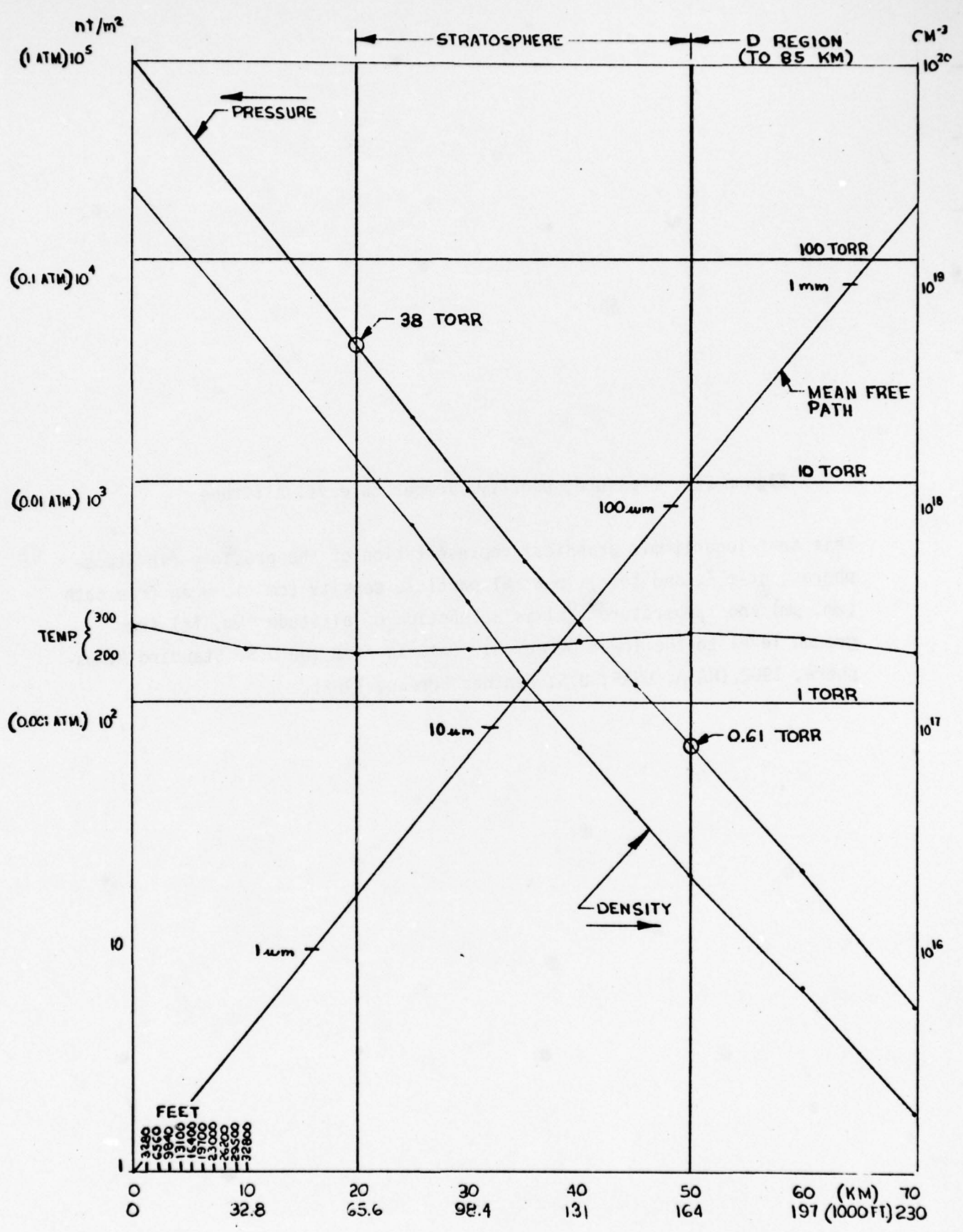


FIGURE 22

Figure 22: Pressure, Density, Temperature vs. Altitude

This semi-logarithmic graphical representation of the pressure (in atmospheres, nt-m^{-2} , and torr), neutral particle density (cm^{-3}), mean free path (mm, μm) and temperature ($^{\circ}\text{K}$) is a function of altitude (km, ft) from ground level to the lower D-region. Data is from the U.S. Standard Atmosphere, 1962 (NASA, USAF, U.S. Weather Bureau, 1962).

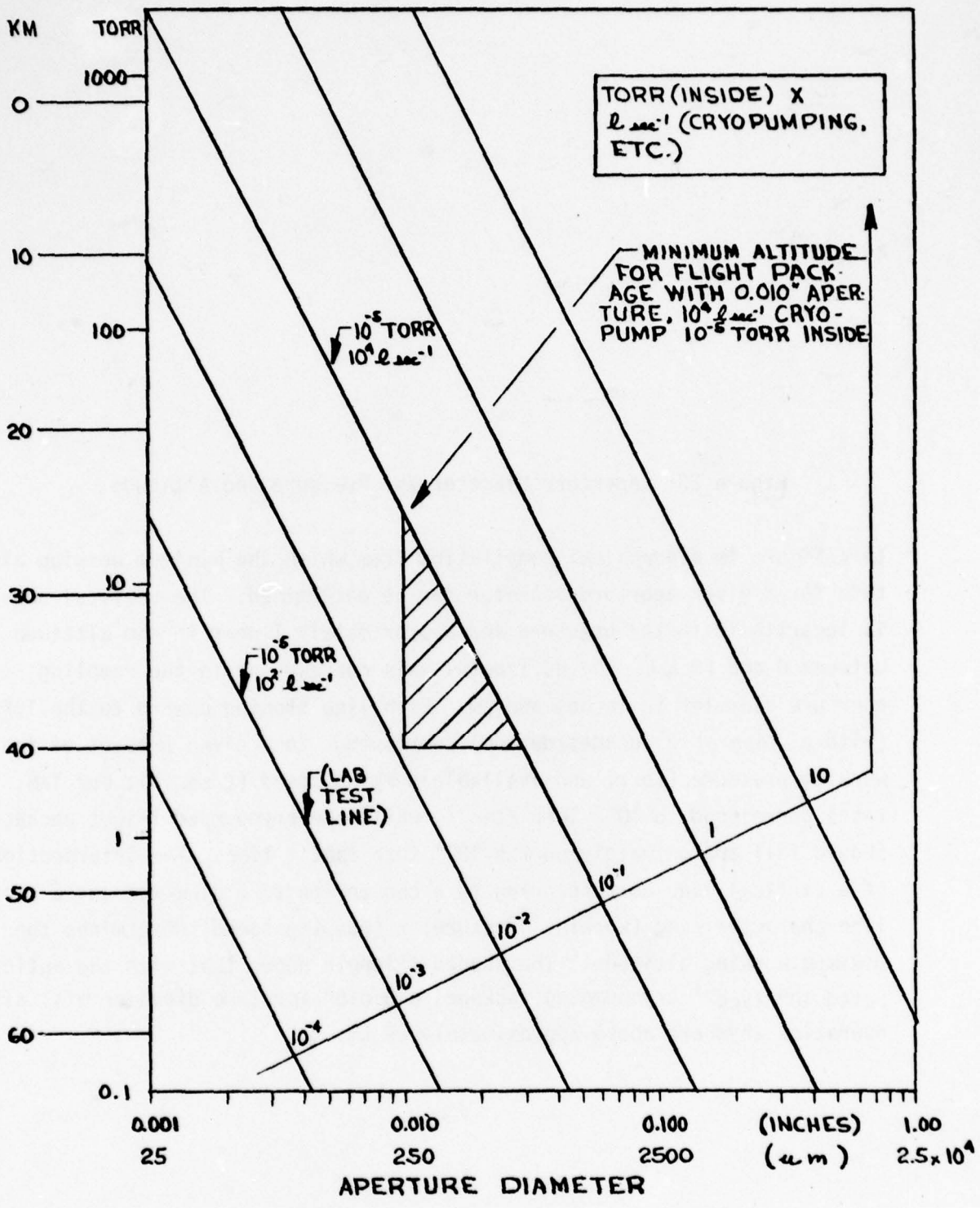


FIGURE 23

Figure 23: Aperture Diameter Vs. Pressure and Altitude

This figure is a graphical compilation from which the minimum working altitude for a given aperture diameter can be determined. The vertical axis is logarithmic in the pressure and approximately linear in the altitude between 0 and 60 km. The horizontal axis corresponds to the sampling aperture diameter in inches and μm . Each line sloping upward to the left (with a slope of -2 decades/decade) corresponds to a given product of inside working pressure (torr) and available pumping speed ($\ell \text{ sec}^{-1}$); our lab tests correspond to 10^{-3} torr $\ell \text{ sec}^{-1}$, while the cryopumped flight package should fall approximately on the 10^{-1} torr $\ell \text{ sec}^{-1}$ line. The intersection of a vertical line corresponding to a chosen aperture diameter and a sloping line characterising (working pressure) \times (pumping speed) determines the minimum working altitude. The shaded triangle shows that with the anticipated 10^4 $\ell \text{ sec}^{-1}$ cryopumping package, a 0.010" aperture diameter will allow operation anywhere above approximately 25 km.

Each sloping line corresponds to a given gas handling capacity (inside pressure times cryopump speed, in torr-ℓ-sec⁻¹); the minimum working altitude is given by the intersection of the vertical line corresponding to aperture diameter and the sloping line corresponding to pump load in torr-ℓ-sec⁻¹. Thus for a 10⁻¹ torr-ℓ-sec⁻¹ load into a 10⁴ ℓ-sec⁻¹ pump with a 10⁻⁵ torr maximum tolerable working pressure, a 0.010" aperture will allow descent to the 18 torr regime (~25km), while a 0.030" aperture will allow operation only at the upper limit of the balloon's altitude capability.

In the laboratory tests the pumping speed is two orders of magnitude smaller than in the proposed flight package. The corresponding simulated altitude range requires aperture diameters an order of magnitude smaller, i.e., 0.001" to 0.003". As an alternative to using very small apertures in the laboratory tests, some tests were done with larger apertures at higher simulated altitudes, i.e., the 0.1-1 torr regime.

Figure 24 shows a plot of the inside pressure vs. the outside (simulated stratosphere) pressure over several decades. The leveling off at low pressure is, of course, a measure of the system base pressure. The aperture size was approximately 0.017" (0.015-ℓ-sec⁻¹) during the preliminary tests plotted here. From this and the slope of the linear portion, we conclude that the available pumping speed is about 227-ℓ-sec⁻¹. The ion gauge is, however, below the aperture-lens-quadrupole-multiplier assembly, and the actual pumping speed in the lens region is at least a factor of two less.

Initial tests with the API ion source showed that the observed ion signals were smaller than expected. For example, with the source aperture placed 2 cm from the sampling aperture, a sampling aperture of about 0.017", and an "outside" pressure of 0.1 torr, it was possible to see a definite ion signal in the "total ion" (DC pole voltage off) mode only when the source was biased approximately 90 V positive with respect to the sampling aperture. In another early test a 1 mCi ⁶³Ni foil rolled into a "C" and placed so that it surrounded the sampling aperture was found to yield a somewhat more intense ion signal, so that a mass spectrum with a resolved peak at 19 amu (H₃O⁺)

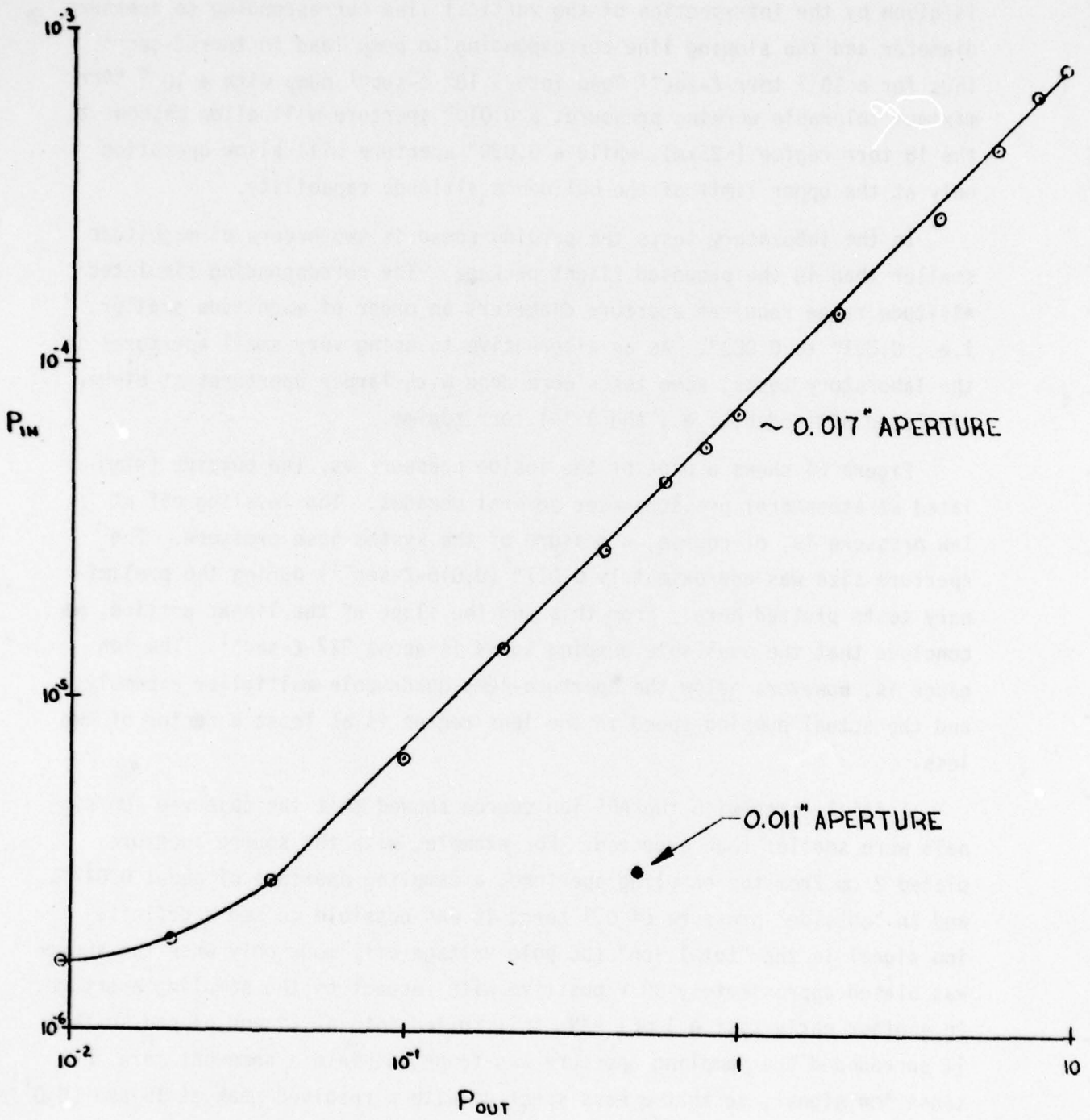


FIGURE 24

Figure 24: Inside vs. Outside Pressure

This is an experimental determination of the inside (mass spectrometer) pressure vs. the outside (simulated stratosphere) pressure, confirming the expected pumping speeds of the sampling aperture and pumping system. Measurements made with Bayard-Alpert type ion gauge inside, thermocouple gauge outside.

could be discerned. However, neither of these two signals were deemed sufficiently intense to provide a basis for optimization of the instrument. We therefore proceeded to work on developing a somewhat more intense ion source in the expectation that we could use it to optimize the instrument parameters to the point where the less intense sources would be useful. This source is of relevance not only for the tests, but for the information it provides about how the external ionizer should be designed and constructed.

The source depicted in Figure 17 was constructed in several steps, each some improvement on the last. For example, the first attempt had a corona point, but no surrounding cage; this led to the observation of ions of such high energy that the ion optics had little or no effect, and only very high retarding values of the pole bias gave spectra with acceptable mass resolution. In several iterations the cage structure with very fine mesh facing the sampling aperture was developed.

A grid (more or less in the form of the "outer mesh" of Figure 19) was effective in reducing high energy ions and increasing the observability of low energy ions. This method was not further pursued because it told us more about the ion source than about the stratospheric ion sampling problem. In this mode, with N_2 (not air) being leaked into the outer chamber, we observed mass spectra in which H_2O^+ , OH^+ , N_2H^+ , and traces of many other ions were observed at more-or-less thermal energies, while copious quantities of N^+ continued to be observed with much higher energies. It was at about this point in the experimental work that the modifications to the aperture holding flange were made, as described in Figure 7 and in the accompanying text. The aperture size was also decreased to enable operation in more appropriate pressure regimes.

After these modifications, the prototype external ion collection array (Figure 19) was constructed to see whether it would function and whether it could thus be used to improve ion collection and make it possible to return to the API source. The results of these tests were surprising. For example, a mass spectrum obtained with this arrangement is shown in Figure 25; this

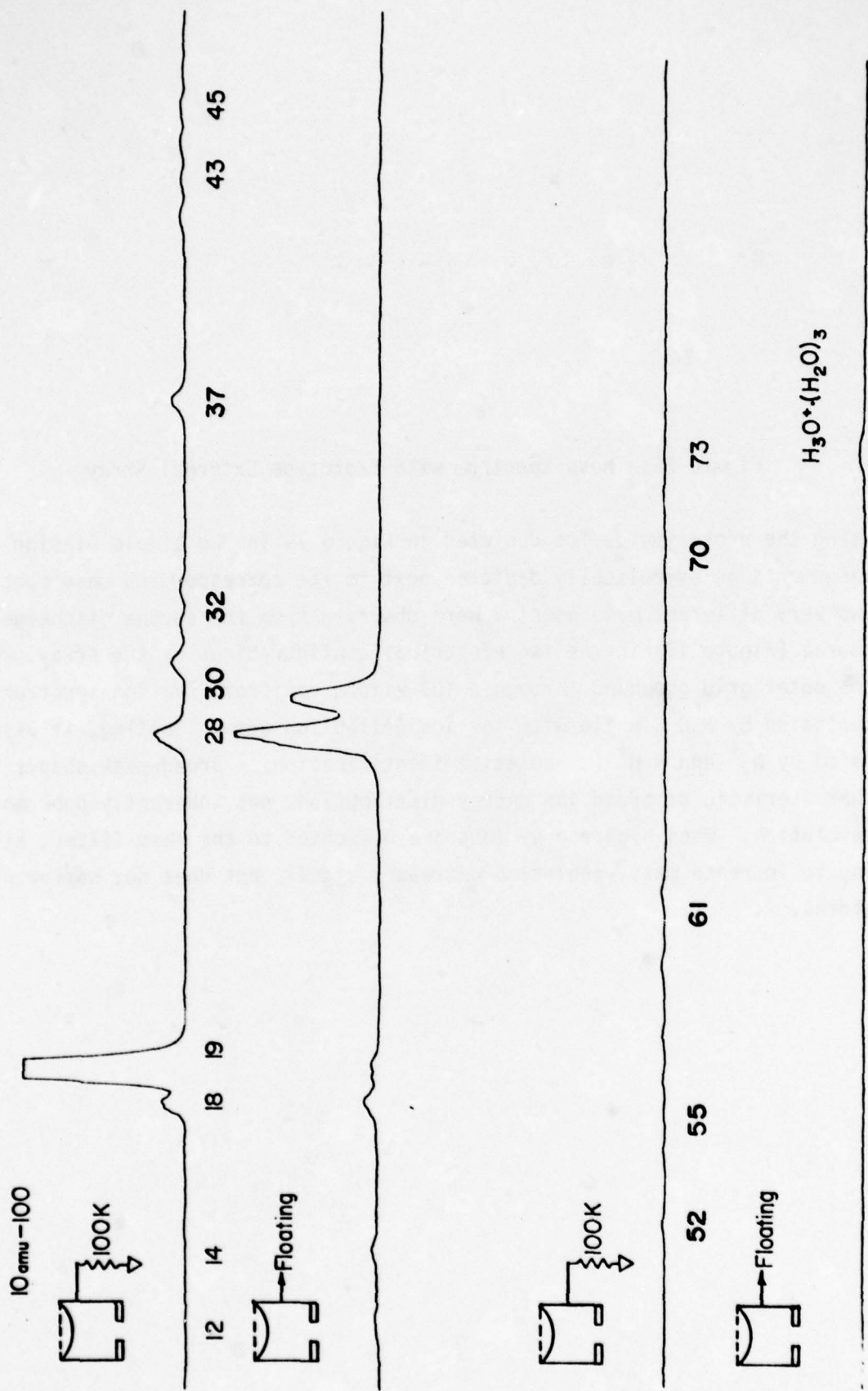


FIGURE 25

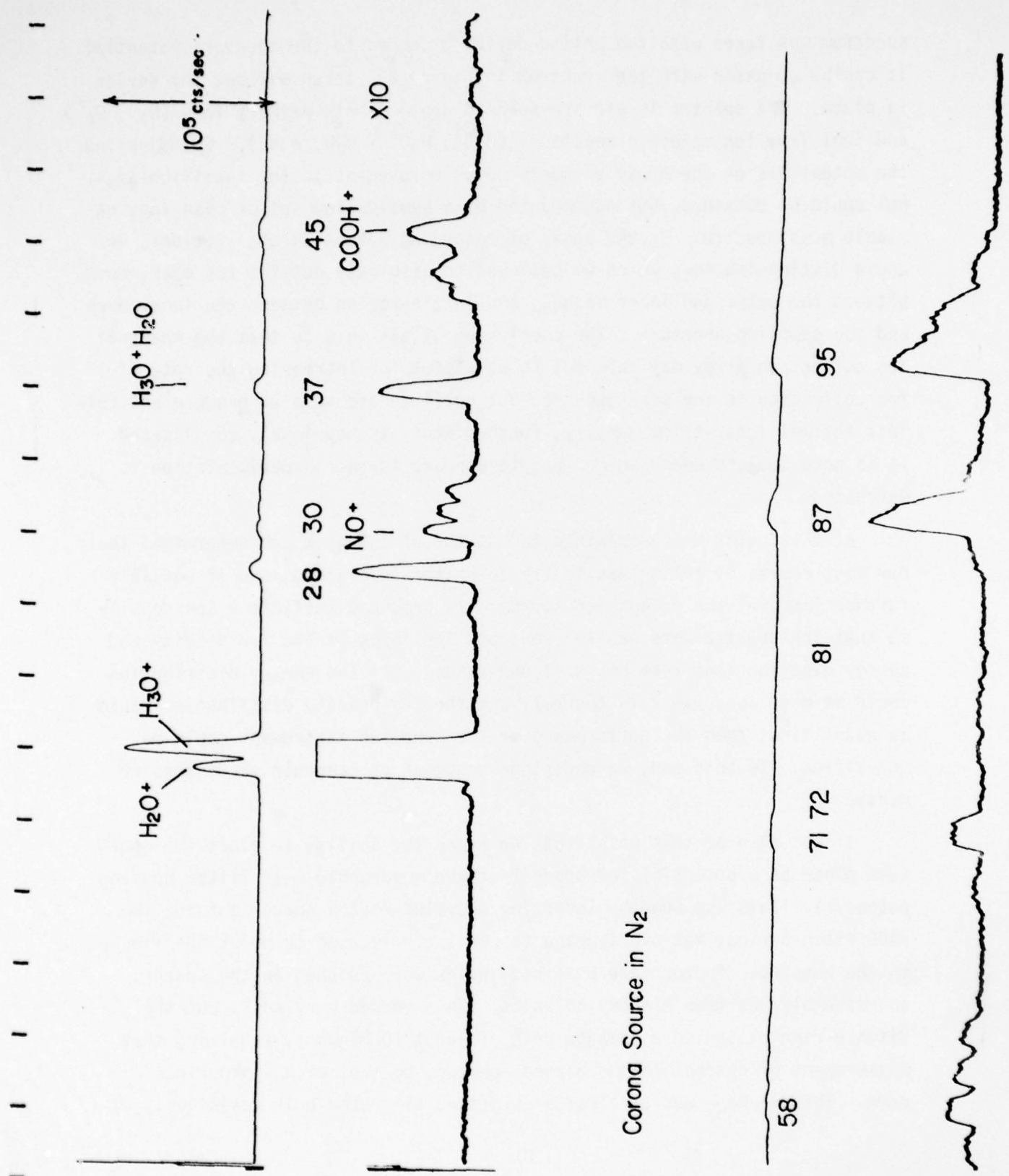
Figure 25: Mass Spectrum with Prototype External Array

Using the prototype device depicted in Figure 19 in two simple biasing arrangements as symbolically depicted next to the corresponding mass spectra. Two very different mass spectra were observed from the corona discharge ion source (Figure 17) in the two electrical configurations of the array. With the outer grid grounded through a 100 kilohm resistor, the ion spectrum was dominated by H_3O^+ , while with the ion collection array floating, it was dominated by N_2^+ and N_2H^+ (speculative identification). Broad peak shapes are characteristic of broad ion energy distribution, not inherently poor mass resolution. When high energy ions are presented to the mass filter, attempting to increase mass resolution decreases signal, but does not narrow peak widths.

spectrum was taken with the entire device grounded to the aperture potential. It can be compared with the spectrum in Figure 26, taken without the device in place. The spectra in air are seen to contain both primary ions (N_2^+ , O_2^+) and ions from ion molecule reactions (H_3O^+ , $H_3O^+ \cdot H_2O$, etc.). By adjusting the potentials on the array elements some improvement in the total ion signal could be obtained, but accompanied by a bewildering set of changing, unstable mass spectra. On the basis of retarding potential observations, we could distinguish ions which we believed to originate outside the outer mesh, between the outer and inner meshes, and in the region between the inner mesh and the sampling aperture. The conclusion of all this is that the external ion collection array may turn out to be useful for increasing the rate of ion collection in the stratosphere, but until we are able to produce and collect thermal ions at low density, further study is hopelessly complicated. It is nevertheless encouraging that it appears further experimentation is warranted.

At this point we re-examined the status of the work and determined that our best course of action was to try to better understand, and if possible further improve, the corona ion source. It produced sufficient ion density so that ion spectra were easily seen, but the forms of the ion density and energy distributions were not well understood. If the energy distribution could be made approximately thermal, and the ion density distribution could be quantified, then the performance of the sampling instrument could be quantified. To this end, we undertook a number of Langmuir probe measurements.

It was also at this point that we added the ability to float the aperture plate at a potential independent of the quadrupole mass filter housing potential. This was done by inserting a 0.010" Teflon spacer outside the #166 Viton o-ring, but overlapping the bolt circle used to mount the flange to the housing. Appropriate bolt body holes were punched in the spacer, and assembly was made with nylon bolts. This worked very well, but the Viton o-ring presented a leakage path of about 10 Megohms, requiring that measurement of current to the biased aperture be made with appropriate care. This leakage was at first a surprise, since the bulk resistivity of



Corona Source in N_2

FIGURE 26
106

Figure 26: Ion Spectrum Without External Array

Shows an ion spectrum between 0 and 100 amu without the external ion collection array used in Figure 25. The resolution at high mass has in this case been intentionally degraded to improve transmission. The ion spectrum is dominated by H_2O^+ and H_3O^+ , and their clusters.

the Viton is obviously very high; in the o-ring configuration; however, it presents a very high ratio of contact area to leakage length, and a correspondingly low resistance.

The character of the external probe measurements is illustrated by Figure 27. The inset illustrates the geometry employed, with the probe deployed approximately on the sampling system axis at a continuously variable position between the corona discharge cage and the sampling aperture. The negatively signed current collected by a positive probe voltage was essentially independent of probe location, and its shape was similar to the expected sigmoidal. The positively signed current collected by negative probe voltage showed a strong position dependence, falling off sharply with distance in qualitative agreement with Figure 18. The shape of the positive ion characteristics was unexpected, failing to show the anticipated sigmoidal shape seen on the negative ion side; rather there appeared to be a qualitatively exponential increase of current with voltage. This is perhaps an indication of incipient breakdown due to electron emission by the probe. Recall that classical probe theory explicitly assumes the probe to be incapable of "cathodic" behavior. We regard the external probe observations as incompletely understood, but sufficient to make certain useful comparisons as developed below.

The character of the internal probe measurements is illustrated by Figure 28. The probe leakage current, shown as a straight line with a slope of approximately $(2 \times 10^{12} \text{ ohms})^{-1}$, was subtracted from the raw data to produce the plotted result. It appears from these data that the probe is seeing a reasonably normal plasma composed primarily of positive and negative ions; that some electrons are also present is evidenced by the negative saturation current being somewhat greater than the positive saturation current.

It is of interest to note that the ratio of inside probe current to outside probe current is the order of 10^{-6} . At the time these measurements were made the aperture diameter was 0.011", or about 10^{-2} the "planar" source diameter; thus in a simple geometrical picture we expect the total

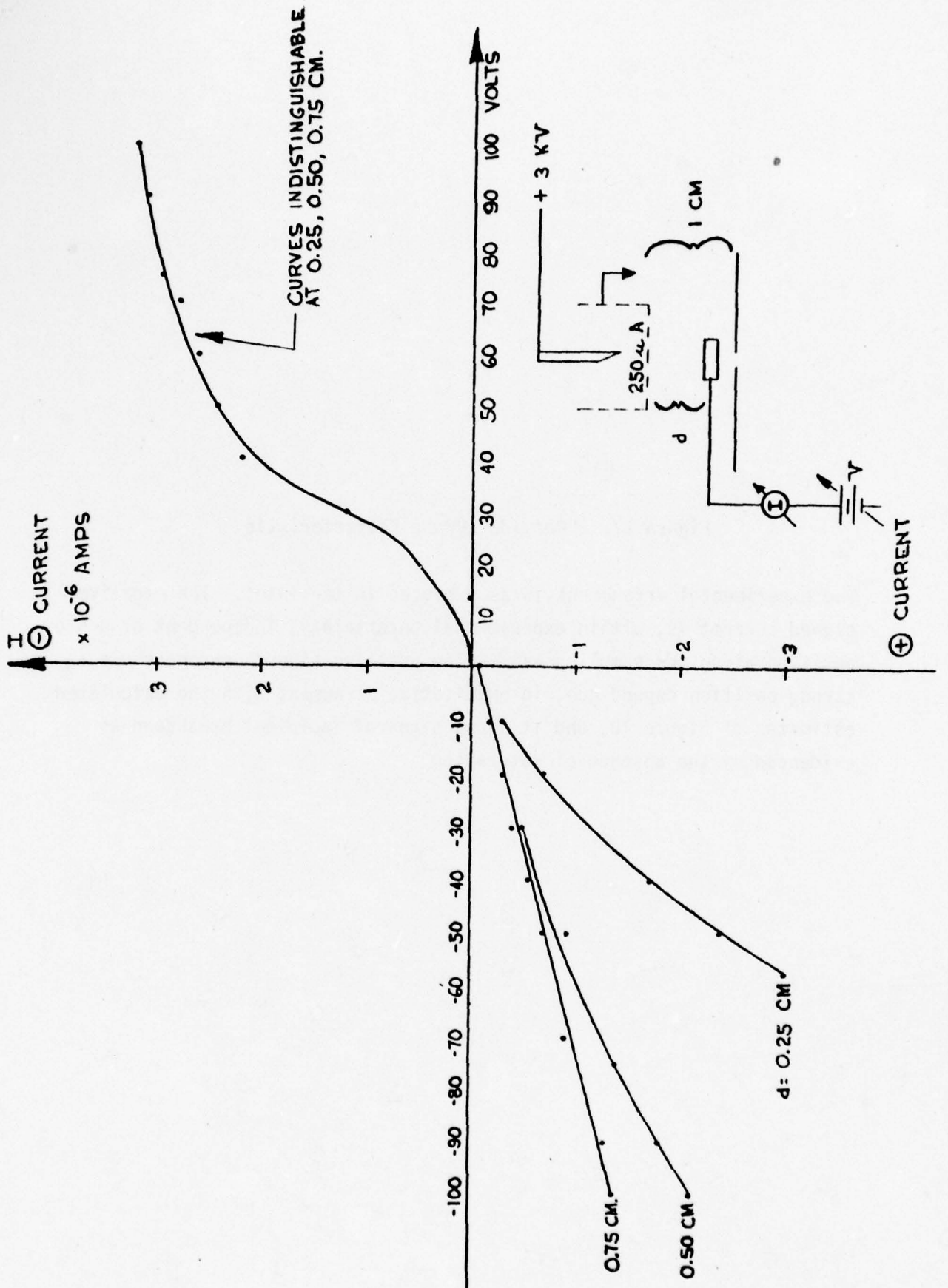


FIGURE 27




Figure 27: "Outside" Probe Characteristic

The experimental arrangement is as depicted in the inset. The negative signed current is, within experimental uncertainty, independent of probe position along the sampling axis. The positive signed current shows a strong position dependence, in qualitative agreement with the calculated estimates of Figure 18, and it shows signs of incipient breakdown as evidenced by the absence of saturation.

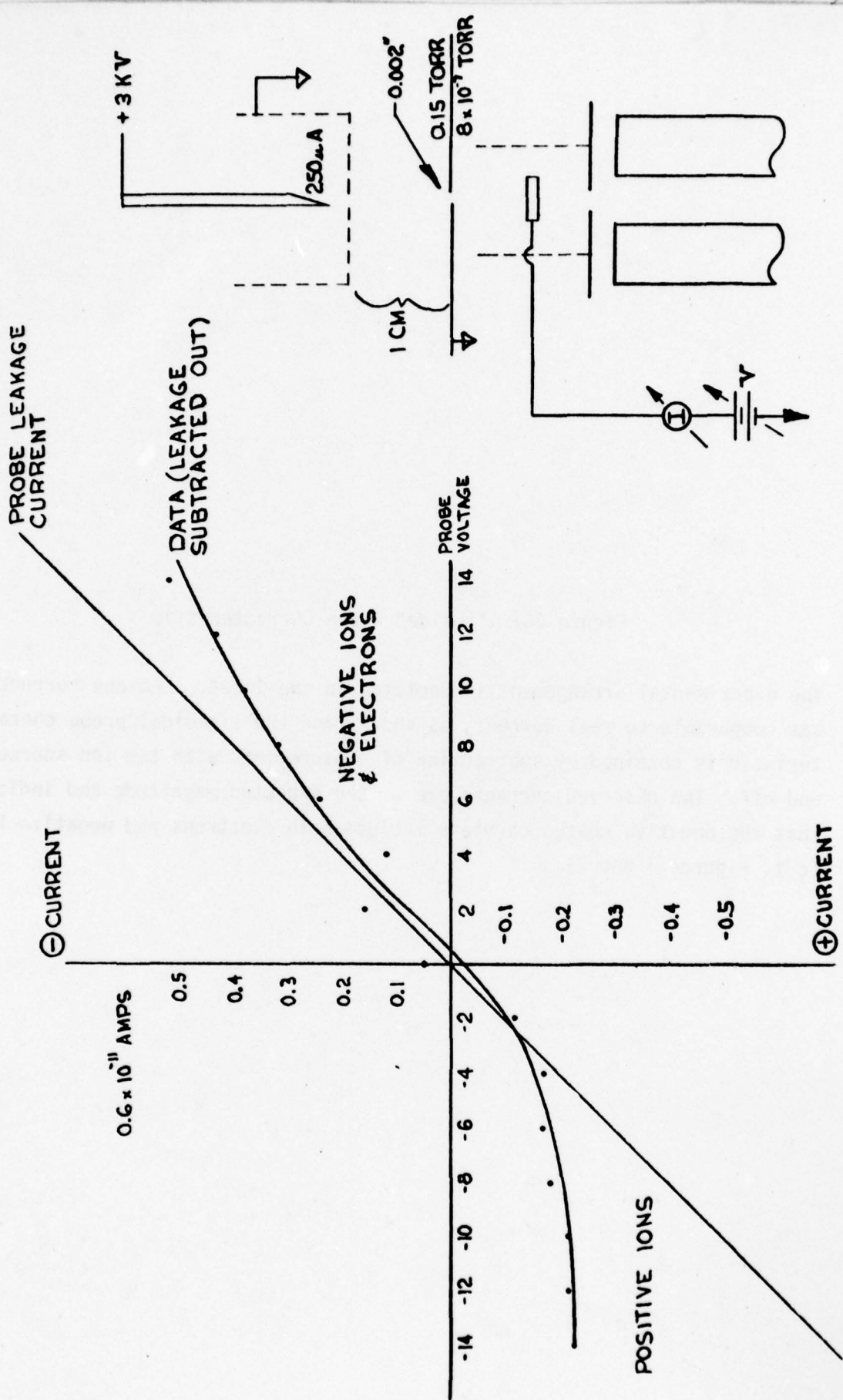


FIGURE 28

Figure 28: "Inside" Probe Characteristic

The experimental arrangement is depicted in the inset. Leakage current was comparable to real current, as shown, and the sigmoidal probe characteristic is obtained by subtraction of measurements with the ion source on and off. The observed currents are of the expected magnitude and indicate that the negative charge carriers include both electrons and negative ions (c.f. Figures 1 and 2).

inside current to be the order of 10^{-4} of the outside current. How much of this can be collected by the inside probe is difficult to estimate, but the observed 10^{-2} seems reasonable.

Under these conditions, the mass spectrometric measurements continued to be confusing. Observed total and resolved ion currents were anomalously small compared with the inside probe current, and the ion optics (which we reiterate we have used in a wide range of apparently similar applications, e.g., Figures 14 and 15) behaved quite unconventionally. There were unusual memory effects in several of the ion optical potentials, most notably the sampling aperture flange potential. Dramatic hysteresis effects were observed as these potentials were varied; for example, the total ion current might rise smoothly as a voltage was raised to some well-defined value, where it would drop very suddenly and be recoverable only by decreasing the voltage to zero and repeating the process.

The contractual time and funding limitations required us to cease further experimental work before we could reach an understanding of these phenomena.

VII - CONCLUSION AND RECOMMENDATIONS

We recall that the project required: (1) theoretical study of the problem; (2) construction of a test chamber; (3) construction of mass spectrometric apparatus deliverable to AFGL; (4) construction of prototype ion sampling apparatus; and (5) experimental studies. The theoretical studies yielded a Design Evaluation Report and literature search; the Design Evaluation Report included the conclusions of detailed calculations based on models of the ion sampling problem, which to the best of our knowledge have not been considered by previous investigators in parameter regimes relevant to the stratosphere. The test chamber was constructed as defined by the original proposal, and it performed as expected. The mass spectrometric apparatus was manufactured, tested to specifications, used in the experimental studies and has since been packaged and delivered, with appropriate instruction manuals, to AFGL. Prototype ion sampling apparatus was constructed, used in the experimental studies, and where suitable has been delivered; where unsuitable for delivery, it has been described herein and preserved by the contractor for possible future studies. The experimental program proved to be significantly more complex and technically difficult than we anticipated, with the result that no single clear conclusion was reached within the allotted time and funding limits; we can identify the reasons for these difficulties and will in this section suggest specific ways in which this line of research can be productively resumed in the future.

On the strength of our best judgment, based on our experience with approximately ten different apparatuses presenting ion sampling problems apparently very similar to those presented here, we proposed a test configuration which we believed would be adequate for the job, without being lavish. Because an existing differentially pumped vacuum chamber was available in EL's inventory and could be loaned to AFGL gratis, the expense of test chamber construction was minimized. The time price of this cost minimization was an experimental configuration less conducive to quick and easy modification than turned out to be desirable. In retrospect, manufacturing cost was exchanged for labor cost. At the outset we recognized that this

might happen, but we believed the experimental work would go so smoothly as to make the tradeoff reasonable.

To summarize the experimental work actually completed, we have succeeded in mass spectrometrically sampling ions from a fairly weak plasma in the pressure regime approximately characteristic of the stratosphere, but have obtained clear mass spectra only at ion densities probably higher than those expected to be ambient in the stratosphere. Attempts to quantify the ion density actually produced in the simulated stratosphere led to difficult-to-interpret results, and this activity occupied more time than planned. Our difficulty may have important implications with respect to the practicality of equipping the balloon package with an in-flight ionizer designed to increase ambient ion densities while insofar as possible maintaining ion chemistry characteristic of the region. Measurement of the ion density delivered to the ion focusing package in the mass spectrometer high vacuum led to results consistent with the apparent external ion density and expected ion collection processes. The mass spectrometric ion signal accompanying this measurement of ion density in the high vacuum was anomalously low. This measurement was made in the final days of the experimental program and could not be subjected to systematic analysis; it is now our belief that the problem was largely due to an inefficient particle multiplier, possibly damaged by operation at an excessively high pressure.

At the conclusion of these experiments, it is our opinion that if this line of laboratory research is continued, it should be with mass spectrometric apparatus and a vacuum system effectively equivalent to the apparatus which will be flown in the balloon program. Our ability to obtain meaningful results was severely hampered by the lack of pumping speed available; this limited our ability to use large sampling apertures characteristic of anticipated flight conditions, provided a less than favorable particle multiplier environment so detection system noise was worse than might be desirable, and the multiplier may have been degraded as well. A desirable system would include an essentially flight-worthy mass spectrometer system, ion focus package, multiplier, and cryogenic pumping housing equipped with a versatile sampling aperture flange which can be easily modified to allow optimization

of gas and ion flow, closure mechanism, and external ion collection array if such proves worthwhile. This system would be enclosed in a large, easily accessible vacuum chamber capable of simulating stratospheric pressure, and in which the problem of simulating stratospheric ion density could be approached with suitable instrumentation. Techniques developed in connection with this latter activity would naturally carry over into the development of a meaningful in-flight ionizer. This revised experimental approach would involve little additional expense in the context of the total program leading to actual balloon flight of an ion-sampling mass spectrometer; it would involve a rescheduling of spending in that a suitable cryopump would be built before rather than after the experimental work was completed.

REFERENCES

- (1) Defense Nuclear Agency Reaction Rate Handbook, Second Edition (March 1972), M.H. Bortner and T. Bauer, Editors-in-Chief, Chapter 2; The Natural Atmosphere: Atmospheric Structure, K.S.W. Champion, Editor.
- (2) R.S. Narcisi and A.D. Bailey, AFGL, private communication.
- (3) E. Arijs, J. Engels, and D. Nevejans, *Nature* 271 642-4 (1978), and references 7-11 therein.
- (4) McDaniel, E.W., Collision Phenomena in Ionized Gases (Wiley, New York, 1964), Appendix I, p. 693.
- (5) Mitchner, M. and C.H. Kruger, Jr., Partially Ionized Gases (Wiley, New York, 1973) p. 49.
- (6) Ref. 1, Chapter 17 (A.V. Phelps, Ed.), especially Table 17-5.
- (7) Ref. 1, Chapter 16 (M.A. Biondi, Ed.), especially Table 16-1.2.
- (8) Ref. 4, p. 49.
- (9) Ref. 5, p. 140 ff.
- (10) Ref. 5, pp. 146, 7.
- (11) E.U. Condon, Ed., Handbook of Physics (McGraw-Hill, New York, 1958), Section 8, Chapter 5, R.J. Maurer, ed., p. 8-66.
- (12) D.E. Gray, Ed., American Institute of Physics Handbook, (McGraw-Hill, New York, 1972), Section 6, B.H. Billings, Ed., Table 6k-19, p. 6-220.
- (13) E.Ya. Zandberg and N.I. Ionov, Surface Ionization (Israel Program for Scientific Translation Ltd., Keter Press, Jerusalem, 1971) p. 261.
- (14) M.W. Siegel and W.L. Fite, *J. Phys. Chem.* 80 2871-81 (1976).
- (15) Ref. 12, Section 8, J.B. Marion, Ed., Table 8i-1, p. 8-296.

APPENDIX I - DELIVERABLE ITEMS

Identification

Tag

Description and References

- A Spare quadrupole entrance plate with ELFS (EL Patent #3867632). This item is provided as a "spare" should AFGL elect to operate the quadrupole (L) without the attached ion optics/electron impact ionizer. In assembly (L) the ELFS is installed in a specially designed endplate on which the ion optics/EI ionizer are mounted. See Figure 7.
- B Set of instruction manuals for Alcatel 2008 and 2012 mechanical forepumps and for Varian M-4" diffusion pump stack.
- C Varian M-4" diffusion pump stack, including liquid nitrogen trap, gate valve, and manual valves for fore line, roughing line, and air vent.
- D Corona discharge source. This is further described in the text and is sketched in Figure 17.
- E Assembly rods, multiplier case-to-quadrupole case. These rods run between the sampling aperture flange at the top of the quadrupole vacuum case and a special clamping flange at the top of the multiplier vacuum case. In a vertical configuration their use is optional as the connection between the two cases is self-aligning and vacuum tight without additional loading. The rods and clamping flange are provided for additional security or for use if the apparatus is installed in a non-vertical arrangement. See Figure 7.
- F Spare metal o-rings. These pressurized metal o-rings gasket the multiplier case to the differential pumping wall in the test vacuum chamber. See Figure 1.
- G Multiplier case. See Figure 7. (N.B. - Multiplier not supplied).
- H ^{63}Ni ion source (radioactive material removed - device tested for radioactive contamination and found to be uncontaminated - copy of leak test certificate 1241 attached). This source produces ions at approximately atmospheric pressure, from which they may be carried by gas flow into a lower pressure region. It is further described in the text and Figure 16.

- J Multiplier housing clamp. See (E).
- K Instrument housing and aperture plate. This is the vacuum chamber in which the low pressure ion optics, quadrupole (in specially vented case), etc. are housed. It is provided with an aperture plate for ion sampling experiments. See Figure 7.
- L Ion optics and quadrupole. See Figure 7. Instruction manuals for quadrupole assemblies and for 275-N2 API Focusing Lens Assembly and 275-L2 API Focus Control (275-L2 not provided) and an instruction manual for quadrupole power supplies are provided under separate cover.
- M Alcatel 2008 pump with zeolite trap. See (B).
- N Alcatel 2012 pump with zeolite trap. See (B).



HEALTH PHYSICS inc.

2986 Industrial Blvd. • Box 197 • Bethel Park, Pa. 15102 • Phone 412 • 563-2242

CERTIFICATE OF LEAK TEST

NO. 1241

This is to certify that the source indicated below was leak testing using an approved method. The leak test was performed by Dr. M. W. Siegel,
Extranuclear Laboratories on 5-16-78.

SOURCE DESCRIPTION:

<u>Radioisotope</u>	<u>Activity</u>	<u>Model No.</u>	<u>Serial No.</u>	<u>Manufacturer</u>
Ni-63	1 mCi	NER9991	305-69-1	NEN

INSTALLED IN:

<u>Device</u>	<u>Model No.</u>	<u>Serial No.</u>	<u>Manufacturer</u>
-	Removed from AFGL test source and returned to storage.		

LOCATION:

<u>Company</u>	<u>Company Address</u>
Extranuclear Laboratories, Inc.,	P.O. Box 11512, Pittsburgh, PA 15238

Analysis of the leak test specimen, No. A918, By Applied Health Physics, Inc. indicated the presence of <0.005 microcurie of Beta activity on 5-18-78.

Pursuant to the results of this leak test, the following action is recommended:

Analysis indicated 0.005 microcurie or more of radioactivity on the leak test specimen. Immediately withdraw the source from use. Decontaminate and repair it or conduct disposal in accordance with applicable regulations. Also, file a report with the regulatory agency within the time period prescribed - if required.

Analysis indicated less than 0.005 microcurie of radioactivity on the leak test specimen. The sealed source may be used as authorized. This source must be leak tested again, on or before 11-16-78 or within any other such time period required by the regulatory agency.

This certificate is an essential record and should be maintained for inspection by the regulatory agency.

APPLIED HEALTH PHYSICS, Inc.

BY: Thomas F. Stacy

Thomas F. Stacy

DATE: 5-18-78

APPENDIX II - ANNOTATED BIBLIOGRAPHY

The following articles are of interest to the problems faced in this contract. References found in each of these articles may be of further interest.

The most useful work here, in our opinion, is the one by J. B. Hasted as it thoroughly considers various hydrodynamic and ion-optical aspects of the sampling problem, although incompletely in the parameter regime appropriate to the stratospheric ion sampling problem.

Arijs, E., Effusion of Ions Through Small Holes, Vacuum 24 (1974) 341-5. Derives a modification to the usual free molecular flow formula for effusion of ions through an aperture of zero thickness, taking aperture thickness and wall neutralization into account. Useful only for case where mean free path exceeds aperture diameter, i.e., well above the stratosphere.

Arijs, E., Ingels, J., and Nevegans, D., A Balloon-Borne Quadrupole Mass Spectrometer for the Determination of the Ionic Composition of the Atmosphere, Technology of Scientific Space Experiments (Conference), Paris, 26-30 May 1975, CNES.

A cryopumped quadrupole system designed to operate above 35 km. Good experimental details. Laboratory tests described.

Arijs, E., Ingels, J. and Nevejan, D., A Balloon Borne Mass Spectrometer for the Measurement of Ion Densities in the Lower Ionosphere, Aeronomica Acta C-39-1974.

A quadrupole system for altitude above 35 km. A multiple (800) hole sampling aperture is employed, for reasons which are unclear. Many electronic details.

Arijs, E., Ingels, J., and Nevegans, D., Mass Spectrometric Measurement of the Positive Ion Composition in the Stratosphere, Nature 271 (1978) 642-4.

Arnold, F., Kissel, J., Krankowsky, D., Wieder, H., and Zähringer, J., Negative Ions in the Lower Ionosphere: A Mass Spectrometric Measurement, J. Atmospheric and Terrestrial Physics 33 1169-75 (1971).

Describes observations of negative ions in the D region, above 71 km, at night. The instrument is a cryopumped quadrupole, but minimal apparatus details are given.

Arnold, F., Krankowsky, D., and Marien, K. M., First Mass Spectrometric Measurements of Positive Ions in the Stratosphere, Nature 267 (1977) 30-32.

Data obtained during downleg of rocket flights. A brief report with few experimental details.

Bailey, A. D., and Narcisi, R. S., Instrumentation Paper 95, AFCRL-66-148 (1966).

This paper, and others of similarly limited distribution, are frequently referenced as containing more experimental details than are given in the journal and conference publication literature. Other limited distribution works by the same authors include Environmental Research Paper 82, AFCRL-65-81 (1965) ("includes discussions and calculations of the aerodynamic and plasma phenomena..."), and AFCRL-72-04-74 (1972), AFCRL-73-03-50 (1973), and AFCRL-66-33-9 (1966). Also in this category is the University of Illinois Aerospace Report #48 (1973).

Balsiger, H., Eberhardt, P., Geiss, J., and Kopp, E., A Mass Spectrometer for the Simultaneous Measurement of the Neutral and the Ion Composition of the Upper Atmosphere, Rev. Sci. Instruments 42 (1971) 475-6.

A magnetic instrument in which the shift in mass scale between ion and neutral observation could be used to deduce the vehicle potential with respect to the surroundings.

Bering, E. A., Properties of the Wake of Small Langmuir Probes on Sounding Rockets, J. Atmos. and Terrestrial Physics 37 (1975) 119-29.

Includes observations concerning the effect of magnetic fields and of vehicle charge on photoemission.

Danilou, A. D., Ionization-Recombination Cycle of the D-Region, J. Atmos. and Terrestrial Physics 37 (1975) 885-94.

Considerations of positive ion, electron and negative ion chemistry in upper and lower D-regions.

Dorman, F. H. and Hamilton, J. A., Double Probes in a Slightly Ionized Collisional Plasma, Int. J. Mass Spec. and Ion Physics 20 (1976) 411-24.

Considerations of relationships between probe current and plasma density in the 1-10 torr range, but "slightly ionized" means 10^{10}cm^{-3} and so is heavily ionized in the context of the stratospheric problem.

Hasted, J. B., Mass Spectrometric Monitoring of Ions in Plasmas and Swarms, Int. J. Mass Spec. and Ion Physics 16 (1975) 3-14.

Of particular interest to the problem of sample aperture biasing and its effect on the spatial region sampled. Considers both plasma effects and ion optical effects. Probably the most useful reference encountered.

Kendal, B. R. F. and Weeks, J. O., Bonded Electrodes for Use on the External Surfaces of Spacecraft, Rev. Sci. Instrum. 46 (1975) 1123-5.

A perhaps useful technique employing a polyimide material and glass beads.

Krankowsky, D., Arnold, F., Wieder, H., and Kissel, J., The Elemental and Isotopic Abundance of Metallic Ions in the Lower E-Region as Measured by a Cryogenically Pumped Quadrupole Mass Spectrometer, Int. J. Mass Spec. and Ion Physics 8 (1972) 379-390.

Useful for experimental details. Unusually high pressure (2×10^{-4} torr) was maintained in the quadrupole region. These are rocket measurements.

Milloy, H. B. and Elford, M. T., Mass Discrimination in Ion Sampling from Drift Tubes, Int. J. Mass Spec. and Ion Physics 18 (1975) 21-31.

Theoretical and experimental examination. Concludes that low gas pressure and small sampling apertures minimize mass discrimination. General quantitative criteria was not stated.

Narcisi, R. S., and Bailey, A. D., Mass Spectrometric Measurements of Positive Ions at Altitudes of 64-112 km, J. Geophys. Res. 70 3687 (1965).

Describes a rocket-borne cryopumped quadrupole system for positive ions at 50 km and higher.

Narcissi, R. S., and Roth, W., The Formation of Cluster Ions in Laboratory Systems and in the Ionosphere, in Advances in Electronics and Electron Physics, L. Marton (ed.) 29 79-113 (1970) (Academic Press, NY).

A review, including a summary of experimental and observational details reported earlier. An excellent starting point for getting into the field.

Narcisi, R. S., Bailey, A. D., Della Lucca, L., Sherman, C., and Thomas, D. M., Mass Spectrometer Measurements of Negative Ions in the D- and Lower E-Regions, J. Atmos. and Terrestr. Physics, 33 1147-59 (1971).

Rocket measurements on two flights. Many details of mechanical and electrical steps taken to optimize ion collection in a region of high electron density.

Narcissi, R. D., Bailey, A. D., Wlodyka, L. E., and Philbrick, C. R., Ion Composition Measurements in the Lower Ionosphere During the November 1966 and March 1970 Solar Eclipses, J. Atmospheric and Terrestrial Physics 34 647-658 (1972).

Describes rocket flights over Brazil (1966) and Virginia (1970). The apparatus is similar to that described elsewhere.

Narcisi, R. S., Philbrick, C. R., Ulwick, J. C., Gardner, M. E., Mesospheric Nitric-Oxide Concentrations During a PCA, J. Geophys. Res. 77 1332 (1972).

Three rocket measurements in D and E regions during PCA, using cryopumped quadrupoles; Langmuir probes for total charge. Ions were NO^+ and O_2^+ rather than $\text{H}^+(\text{H}_2\text{O})_n$, above 77 km. Few experimental details.

Narcisi, R. S., Sherman, C., Wlodyka, L. E., and Ulwick, J. C., Ion Composition in an IBC Class II Aurora: 1. Measurements, J. Geophys. Res. 79 2843 (1974).

Describes a rocket-borne instrument with no vacuum pump, for altitudes above 100 km. A companion article describes results.

Olsen, J. R., Amme, R. C., Brooks, J. N., Murcray, D. A., Steffen, R. E., Sturm, R. E. and Keller, G. E., Balloon-Borne Ion Sampling Package, Rev. Sci. Instr. 49 (1978) 643-9.

Preliminary results shown. An aperture 0.3 mm (0.012") in diameter with a unique shape giving it very small central thickness is employed.

Parker, L. W. and Whipple, E. C. Jr., Theory of Spacecraft Sheath Structure, Potential, and Velocity Effects in Ion Measurements by Traps and Mass Spectrometers, J. Geophys. Res. Space Physics 75 (1970) 4720-33.

Computational technique for predicting ion collection compared with some experimental results. Concludes that concentrations inferred either with large draw-in potentials or under large Debye-length conditions must be corrected for electric field effects.

Rosen, A., (editor), Spacecraft Charging by Magnetospheric Plasmas, MIT Press (Cambridge, Mass., 1975).

Seguin, J. G., Dugan, C. H., and Goodings, J. M., Plasma Sampling Diagnostics Using Ion Kinetic Energy Distributions, Int. J. Mass Spec. and Ion Physics 9 (1972) 203-213.

Relatively high density plasmas (10^9 - 10^{10} cm⁻³) with relatively high electron temperatures (~1e V) are sampled and energy and mass analyzed. At pressures of interest, mobility considerations dominate the sampling problem.

Sugimura, T., Prediction of Positive Ion Collection by a Rocket-Borne Mass Spectrometer, Rarefied Gas Dynamics, Progress in Astronautics and Aeronautics, 51 (1977) 959-74.

Primarily applicable to rocket sampling at altitudes above 70 km.

Walters, R. L. Jr. and Walters, J. P., Device for Stroboscopic Extraction of Atmospheric Pressure Species into Regions of High Vacuum, Rev. Sci. Instru. 48 (1977) 643-6.

Primarily applicable to neutral sampling with modest vacuum systems. Allows "gulping" relatively large samples at times known to be interesting (e.g., after a spark) while maintaining only a small time average gas load.

Woods, R. O. and Devlin, T. L., A Cryopumping System for Balloon-Bourne Mass Spectrometers, Rev. Sci. Instrum. 45 (1974) 136-7.

Some possibly useful techniques discussed.

Zbinden, P. A., Hidalgo, M. A., Eberhardt, P. and Geiss, J., Mass Spectrometer Measurements of the Positive Ion Composition in the D- and E-Regions of the Ionosphere, Planet. Space Sci. 23 (1975) 1621-42.

Heavy on observational data, light on experimental details, many additional references.